ANALYSIS OF ENERGY PRODUCTION BY SALINITY EXCHANGE IN POROUS ELECTRODES

Programa Oficial de Doctorado en Física y Ciencias del Espacio

TESIS DOCTORAL 2017

MARÍA DEL MAR FERNÁNDEZ MARTÍNEZ-REY

DIRECTORES

ÁNGEL V. DELGADO MORA

GUILLERMO R. IGLESIAS SALTO

Departamento de Física Aplicada

Grupo de Física de Interfases y Sistemas Coloidales

Universidad de Granada

Editor: Universidad de Granada. Tesis Doctorales
Autora: María del Mar Fernández Martínez-Rey
ISBN: 978-84-9163-519-2
URI: http://hdl.handle.net/10481/48310

La doctoranda / The *doctoral candidate* **María del Mar Fernández Martínez-Rey** y los directores de la tesis / and the thesis supervisor/s: **Ángel V. Delgado Mora y Guillermo R. Iglesias Salto.**

Garantizamos, al firmar esta tesis doctoral, que el trabajo ha sido realizado por la doctoranda bajo la dirección de los directores de la tesis y hasta donde nuestro conocimiento alcanza, en la realización del trabajo, se han respetado los derechos de otros autores/as a ser citados/as, cuando se han utilizado sus resultados o publicaciones.

/

Guarantee, by signing this doctoral thesis, that the work has been done by the doctoral candidate under the direction of the thesis supervisors and, as far as our knowledge reaches, in the performance of the work, the rights of other authors to be cited (when their results or publications have been used) have been respected.

Granada, a 27 de enero de 2017.

Directores de la Tesis / *Thesis supervisors;*

Ángel V. Delgado Mora Guillermo R. Iglesias Salto

Doctoranda / *Doctoral candidate*:

María del Mar Fernández Martínez-Rey

A mi padre y a mi madre,
*por ser un **mar** infinito de amor que nos abraza.*

A El Salvador,
*por ser un **río** que empuja, con fuerza, a la esperanza.*

Contents

1

Introduction

1.1. Introduction: renewable energy challenge

Electrical energy has become a basic need akin to water or food, which further conditions access to other essential services such as sanitation, healthcare and education. It has become virtually essential to contemporary human survival. Electricity cooks food, powers household appliances, supports a healthy temperature, provides clean water (by powering pumps or desalination treatment), and enables proper health care (refrigerated vaccines, operating theatres, life support systems, electroshock therapy, emergency treatment, or intensive care). Electricity enables agricultural production, processing, and marketing (thereby ensuring food security), provides educational aids (computers, printers and photocopiers) and encourages social cohesion (participation in cultural productions, entertainment, or recreation). The United Nation Development Program (UNDP) concluded that "energy is central to the satisfaction of basic nutrition and health needs" [1, 2].

The United Nation Development Program (UNDP) concluded that energy is central to the satisfaction of basic nutrition and health needs

However, the most basic energy services are far from being a resource for the benefit of all. The World Energy Outlook 2015 [3] has published databases on electricity access in 2013: an estimated 1.2 billion people (17% of the global population) did not have access to electricity and more than 2.7 billion people (38% of the world's population) are estimated to have relied on the traditional use of solid biomass for cooking, which causes harmful indoor air pollution. Many more suffer from electric supply that is of poor quality. More than 95% of those living without electricity are in countries in sub-Saharan Africa and Asia, and they are predominantly in rural areas (around 80% of the world total).

On the other hand, there is no doubt that our world is currently facing a multiplicity of linked ecological crises. While the most discursively visible of these it is the climate crisis, which has been principally caused by the traditionally industrialized countries [4], we are at the same time facing an **energy crisis**. Supplies of fossil fuels, on which the global economy

has been based for some 250 years, are less and less able to match demand, which will, in medium term, lead to drastic increases in energy process and escalating conflicts over energy security. Moreover, problems with energy supply and use are related to many environmental concerns as air pollution, acid precipitation, ozone depletion, forest destruction, and emission of radioactive substances [5]. In addition, we are at the same time facing a drastic reduction of biodiversity, desertification, a fresh-water crisis, overfishing and several more: together they constitute a **biocrisis**, a crisis of human life on this planet.

In the scientific context, renewable energy research is generally assumed as one of the main routes to overcome these ecological crises. Although there is no doubt that renewable energy production will definitely reduce pollution, carbon dioxide emissions and fossil energy usage, a deeper analysis, linking the environmental situation that the planet is facing with the economic system in which our society is based, is needed [6, 7]. Renewable energy challenge should always be accompanied by three other major changes: **energy savings on the demand side**, **efficiency improvements in the energy production** and **energy resources for the benefit of all** [8, 9]. With these aims, a social change is also needed if we want that renewable energy challenge would properly contribute to a more sustainable, fair and humane world.

Renewable energy technologies use the energy inherent in sunlight and its direct and indirect impacts on the Earth (photons, wind, hydropower, photosynthetic energy stored in biomass), gravitational forces (tidal energy), and the heat of the Earth's core (geothermal) as the resources from which they produce energy. Therefore renewable energy technologies turn these natural energy sources into touchable forms of energy: electricity, heat and fuels. These resources represent a massive energy potential which dwarfs that of equivalent fossil resources. In fact, as Fig. 1.1 squematically shows, renewable energy sources have the potential to provide 3078 times the current global energy needs [10].

So far, the global renewable energy share stands at 18.3% of the global total final energy consumption (which is the energy delivered to the consumer), increasing by 0.15% per year during the 2010/2012 period [8, 9].

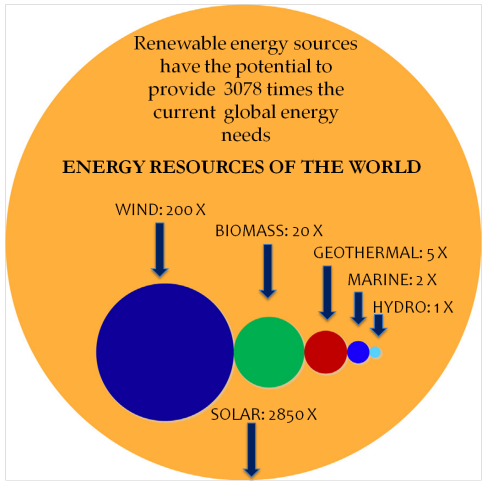

FIGURE 1.1: Energy resources of the world.

Following this tendency, renewable means of producing and storing electricity are expected to be increasingly important in the future and might play a significant role in the replacement of fossil fuels [11] which will be an important step towards overcoming world energy crisis. In fact, global electricity generation from renewable energy sources is expected to grow 2.7 times between 2010 and 2035 [10].

However, renewable energies are generally diffuse and not fully accessible, some are intermittent, and all have distinct regional variability. Such aspects of their nature give rise to difficult, but solvable, technical, political and economical challenges inherent to the development and use of renewable energy resources. Despite having such difficulties and challenges, the research and development on renewable energy resources and technologies has expanded during the past two decades [5, 10]. In fact, given the recent strides in condensed-matter physics and materials technology, renewable energies have been optimized and have considerably reached existing technologies standards: for instance, solar and wind energy are outstanding among all renewable energies in terms of efficiency. However, scientific research has also worked on finding new energy sources. In the recent past, other renewable energy alternatives have been growing in importance. Concretely, scientists have been increasingly looking at the

massive amounts of energy stored in the ocean.

1.2. Salinity difference energy

Oceans and seas have the potential to play a significant role in providing energy. Apart from the fossil organic fuels that the ocean sediments may hold, the seas of this planet are collectively a broad and important realm that must be considered in assessing future power sources and power generation. Sources of marine renewable energy can be classified as mechanical (waves and swell, tides, and currents), chemical (salinity gradients and biomass), and thermal (temperature gradients, including ice). Tidal energies rely on the gravitation attraction of the Earth-Moon-Sun system whereas the others all rely on solar energy. Table. 1.1 shows various of these marine energy sources and their power potential. Although some of these resources necessarily present some challenges, much of the infrastructure and knowledge necessary to generate energy from the ocean already exists [12, 13] and marine currents energy might become the most promising candidate for some particular sites. However, it will be critically important to ensure that the development of new ocean energy technologies does not harm the marine environment, which is already subject to multiple threats such as overfishing, pollution, habitat loss, and climate change, special effort should be done to understand the ecological implications of altering the hydrodynamics of the marine environment [14].

TABLE 1.1: Marine Renewable Resources [15].

Resources	Power (TW)
Ocean Currents	0.05
Ocean Waves	2.7
Tides	0.03
Thermal gradient	2.0
Salinity difference	2.6

One of the most powerful marine renewable resources shown in Table 1.1

is **salinity difference energy**, also termed osmotic power or **blue energy**. The concept of salinity difference energy has been known for a long time, as described in detail by G.L. Wick [16] regarding the first studies of R.E. Pattle in 1954 [17]. Salinity energy source exists everywhere in nature and they are associated to the release of the Gibbs free energy of a system when two liquids or gases containing different compositions are mixed without chemical reactions.

Salinity energy sources are associated to the release of the Gibbs free energy of a system when two liquids or gases containing different compositions are mixed without chemical reactions

Salinity difference energy is particularly concentrated where fresh water rivers flow into the ocean. In fact, in river mouths, the mixing of a certain volume of low salinity water concentration (expressed as c_1) with a much larger volume of salt water (c_2 concentration) is continuously taking place. According to thermodynamics, the spontaneous mixing of ions of sea water and river water produces an entropy increase and hence, a free energy decrease. In other words, the rise in concentration of the fresh water in the process results in an increase, Δp, of its osmotic pressure up to the sea water value, $\Delta p = (c_2 - c_1)RT$, which amounts to 10 atm per type of ion (about 20 atm for NaCl solutions). This pressure is equivalent to a 200 m water head. One may conceptualize it as a 200 m waterfall at the mouth of every river. According to Norman [18]: *the tremendous energy flux available in the natural salination of fresh water is graphically illustrated if one imagines that every stream and river in the world is terminated at its mouth by a waterfall*. Additionally, Ramon et al. [19] refers to river mouths as *silent waterfalls*. Therefore, the energy loss (which we partially aim to use) would be ΔpV or ≈2 MJ for one cubic meter of water mixture. If we focus on El Guadalquivir, the largest river of our region, Andalucía, and assume that the whole river volume flow (on average 164 m^3/s) could be employed for this purpose, the available power would be more than three times the Granada power consumption which is around 100 MW (<www.junta de andalucia.es>). Similarly, for the whole planet, it is estimated that the total available power from blue energy sources would be ≈ 2.6 TW, which roughly coincides with the

annual electricity demand [20].

Salinity difference energy is completely renewable and sustainable due to water evaporation by the sun and subsequent precipitation. It is a limitless supply (if river and seawater are used). In principle, there is no fuel cost and it produces no pollutants, like NO_x, CO_2 emissions or other significant effluents [21] that may produce climate change, no thermal pollution, no radioactive waste and no daily fluctuations in production due to variations in wind speed or sunshine. Basically, it is clean and green. Probably, inefficient extraction may occur but it should be acceptable as long as there is an adequate compensation on energy extraction. Concluding, there is no doubt that salinity difference energy will have an important role as a recently emerged renewable energy source taking part in a more sustainable energy system for our planet.

Nowadays there are two main challenges for blue energy: to **find suitable locations for salinity difference energy** and to **develop a suitable technique for the conversion of blue energy into usable energy**. The first challenge has been focused in calculating the ecological potential for blue energy plants. These studies allow a more realistic assessment of the exploitable potential for salinity difference plants. The calculation of the ecological potential is based on the amount of usable water which is limited due to ecological constraints, for instance, the ecological stability of the river considering the annual variability [22, 23].

1.2.1. Blue energy production techniques

The objective of our research is the second one: developing efficient blue energy techniques. Remarkable advances in fundamental studies, experimental investigations and field demonstrations have been carried out towards finding efficient methods in the past decade. Among them, the membrane-based techniques are the most advanced ones: **pressure retarded osmosis** (PRO) and **reverse electrodialysis** (RED). As it will be further explained, they have different working principles, operating considerations and membrane properties [19, 24]. PRO generates an osmotic pressure difference between two chambers in order to produce pressur-

ized water to generate electricity through a hydro-turbine, as it shown in Fig. 1.2 left. RED, on the other hand, creates an electrical potencial difference between the electrodes of a cell where dilute and concentrated solutions flow separated by cationic and anionic exchange membranes alternatively (see Fig. 1.2 right). Despite the considerable progress made in those techniques [25], these are mostly at laboratory scale. Furthermore, they have some disadvantages that should still be solved to move towards commercialization, particularly in relation to membranes performance and cost in the case of RED, and the need to use electromechanical converters, like dynamos or turbines in PRO.

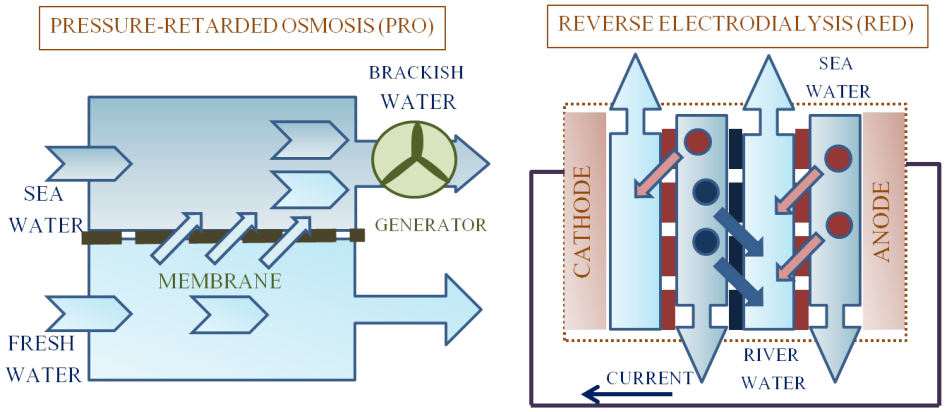

FIGURE 1.2: Sketch of the membrane-based techniques PRO (left) and RED (right).

A recent approach, called **capacitive mixing (capmix)**, comprises a group of techniques which are based on the variation of the potential difference between two porous electrodes by exchanging the ionic contents of the solution in contact with them [26]. An important difference with respect to the previous technologies is that here the two solutions do not flow simultaneously, but alternatively through the same compartment, which is a cell made of two oppositely faced activated carbon electrodes.

The three already mentioned techniques: PRO, RED and Capmix are the power generation processes analog to desalination processes: reverse osmosis, electrodialysis and capacitive deionization, respectively [27–29]. Whereas energy is consumed in the separation processes to desalinate salty

feed streams, the reverse operation produces energy by controlling mixing of solutions of different concentrations.

We would like to add that although research to date has tended to focus on the natural process of mixing river water with seawater in river mouths as the main source of salinity difference energy, other salinity difference sources have also grown in importance within the recent past. Concentrated brine water from desalination plants can be paired with waste water from a treatment facility, reducing desalination energy cost [30]. The latest researches have also led to a new interest in low temperature (<80°C) waste heat and waste water from the industrial sector to convert it into useful work. For instance, waste heat can be used to generate low and high concentration solutions for salinity difference energy either by membrane distillation process [31] or by using thermolytic solutions [32]. As an interesting alternative, it has been recently shown that mixing solutions with different dissolved CO_2 concentration is a related method which can be used to harvest energy from gas emissions [33, 34].

Blue energy efficiency

As mentioned above, the power available by salinity gradient method is very significant. However, only part of this might eventually be actually used, considering the efficiency attainable by existing methods. This can be defined using different concepts. The more general definition, the **fuel efficiency**, η_{fuel}, is defined as the fraction of the free energy of mixing 1 m^3 of fresh water with unlimited amount of salt water, that is:

$$\Delta g = \Delta G/V \approx 2.3 MJ/m^3 \tag{1.1}$$

that might be converted into useful work. It can be written in terms of power as:

$$\eta_{fuel} = \frac{< VI >}{\Delta g J} \tag{1.2}$$

where $< VI >$ is the average power, and J is the flow rate of solutions through the cell.

Similarly, the **cycle efficiency** is the relation between the average energy extracted as compared to the total energy that could have been extracted in an ideal theoretical cycle of the specified salinity different method with the same amount of solution. In later phases of the development, the *free energy efficiency*, in which energy cost like pumping energy and others, should be also taken into account. However, in a labscale performance, such definition is not useful, since pumping and pre-treatment are not optimized. In other cases, the emphasis is on economic costs, and hence, the efficiency can be calculated in terms of the power extracted per unit gram of material or surface area of electrode.

1.2.2. Pressure-retarded Osmosis

Sidney Loeb [35] was the first author to recognize Pressure-retarded Osmosis (PRO) as a source of energy. The driving mechanism for the production of electric power is osmosis: the spontaneous fluid flow phenomenon induced when two solutions of different concentrations are placed in contact through a barrier which is permeable to the solvent but impermeable to solutes. Following this principle [16], seawater is pumped into a chamber where the pressure is lower than the osmotic pressure difference between fresh water and seawater. This produces a fresh water flow through a semipermeable membrane increasing the pressure within the salty chamber as it is schematically shown in Fig. 1.2 left; this pressurized solution is split into two streams, where one is depressurized by a hydropower turbine to generate power and the other one passes through a pressure exchanger in order to pressurize the incoming sea water. Hence, PRO converts chemical energy into mechanical work by controlled mixing of waters of different salinities. The key components in a traditional PRO plant are the membranes and their performance is very important for PRO energy cost. Thus a big effort has been devoted to finding appropriate fouling-resistant and solutes-impermeable membranes with tailored surface properties and membrane modules with improved hydrodynamic mixing to

mitigate fouling [32, 36, 37].

The Norwegian state power company Statkraft SF, a company with a strong tradition in hydropower, was engaged in the PRO technology development aiming at cost-effective power productions. The world's pioneering salinity difference energy demonstration plant was inaugurated in November 2009- testament of the techno-madurity of the method. However, the pilot plant generated roughly 1 W/m^2 using commercial membranes and, in December 2013, Statkraft announced the discontinuation of the work in PRO, including shuttering the demonstration plant. The reason cited was the updated cost forecast which made PRO energy uncompetitive in the power market. This fact underlines the already mentioned need on further research and development of effective and inexpensive membranes [38].

1.2.3. Reverse Electrodyalisis

Reverse Electrodyalisis (RED) is another membrane-based technology, but ion exchange membranes are applied instead of semipermeable membranes. Moreover, this technique can convert the free energy generated by the mixing of two aqueous solutions into electrical power directly with no other auxiliary equipment. Thus, as Fig. 1.2 shows, seawater and freshwater are pumped into stacks of alternately arranged anion and cation exchange membranes. The former one contains positive charges and the reverse happens to the cation exchange membrane. The difference in chemical potential between two water streams is the driving force for this ion transport. Electro-neutrality is maintained by redox reactions at the electrodes at the end of the stack.

Investigation into the use of RED as a salinity gradient technology emerged in the early 1950s when Pattle constructed a small stack that produced a maximun electromotive force of 3.1 V [17]. This approach was further developed by Weinstein and Leitz [39] and later by Lacey [40]. Similar to PRO, the major constraint in RED is the need of ion exchange membranes with required properties such as high-selectivity, low resistance and low cost [32]. In this sense, over the past decades, new materials and improved

fabrication methods resulted in important advances towards RED membranes optimization as shown in the following reviews [41, 42].

RED also underwent parallel advacements in terms of field demonstration. In November 2014, a RED pilot plant began operation in the Afsluitdijk, in the Netherlands, where salt and fresh water are separated by a 90 m wide dike [38, 43]. During this crucial pilot phase, Redstack engineers confronted RED technology in the real world, outside of the laboratory environment in order to reach the 50 kW capacity aimed for by this pilot.

Recently, Yip and Elimelech [24] compared the efficiencies and power densities achievable with RED and PRO. Regarding efficiency, the method used for its calculation involves comparison of the actual useful work with the Gibbs free energy of mixing known proportions of solutions with different concentrations [44–46]. Typical results indicate fuel efficiencies (Eq. 1.2) in the order of 54 % (38 %) for PRO (RED) when combining 600 mM-1.5 mM NaCl solutions.

1.2.4. Capmix techniques

Alternative approaches which aim to take advantage of salinity energy sources have recently emerged, in particular those presented in this thesis and called capmix techniques. Their development would not have been possible without the great progress of the electrochemical science in the past century [47]. In particular, the progress made toward energy storage science and concretely, the development of the fundamentals of the electrical-double layer capacitor (a type of supercapacitor), has made possible the emergence of the capmix techniques. Electrical double layer capacitors (EDLC) differ from conventional electrostatic capacitors in that they store charge in the form of ions, rather than electrons, on the surface of materials with high specific area (m^2/g). EDLC are usually made by two faced electrodes which are prepared as compacts of finely-divided porous carbon providing a much greater charge density that is possible with non-porous, planar electrodes. In this sense, the capmix cell, the cell used for capmix energy extraction procedure, is deeply inspired on the EDL capacitor structure.

Capmix technologies comprise a novel and promising group of techniques whose energy extraction procedure involve the use of electrical double layer capacitors.

Capmix techniques perform the mixing process of the two solutions with different ionic concentration (for instance, seawater and river water) in a controlled way, that is, the two solutions flow alternatively through the same compartment which is a cell made of two oppositely faced electrodes which constitutes basically a EDL capacitor. There are principally three capmix techniques, known as **capacitive energy extraction based on double layer expansion** (CDLE), **capacitive energy extraction based on Donnan potential** (CDP) and the most recent one, **soft electrode technique** (SE). CDLE was the original capmix technology, demonstrated for the first time by Brogioli in 2009 [48] and later extended to lab-scale experiments [49–51]. Afterwards, in 2010, the CDP method was elaborated by Sales et al. [52]. The newest research on capmix techniques was carried out by Ahualli et al. [53] in 2014. They developed the final method, which combines aspects of both CDLE and CDP original technologies, namely soft electrode technique.

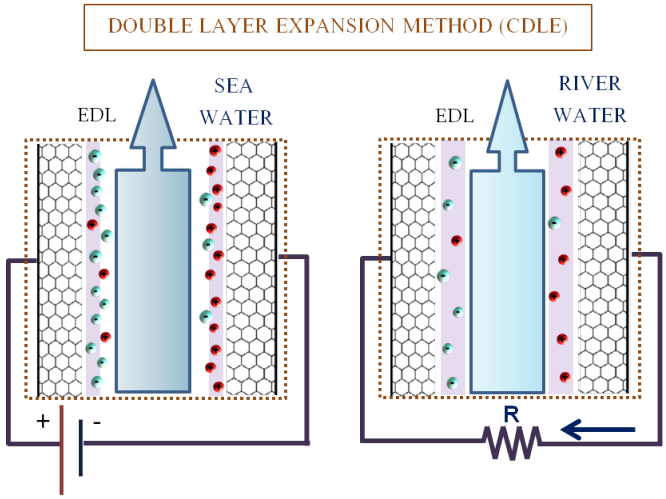

FIGURE 1.3: Sketch of the working principle of the CDLE capmix technique.

The starting point is the consideration that the electric potential at the

solid/ionic solution interface increases (if charge is constant) when decreasing the ionic strength of the medium. This property is widely known in the science of colloidal systems and interfaces and is due to the characteristics of the electrical double layer (EDL) (see section 2.1). Based on this principle, a cell made of two oppositely faced activated carbon electrodes through which seawater and river water may flow is used for energy extraction. Electrodes made of nanoporous carbon particles are chosen in order to increase charge transfer. In Fig. 1.3, it is shown a sketch of the working principle of CDLE. Initially, ions are stored on the electrodes of the CDLE cell by means of an external voltage source or battery. After introducing fresh water in the capmix cell, voltage increases between the electrodes, and an electrical current can spontaneously flow in closed circuit conditions. Since this transfer is performed at a higher potential, we obtain more energy than that initially extracted from the battery, resulting in a positive balance of energy. Hence, the result is that electrical work is made available, without use of any kind of either selective membranes or electromechanical converters. Within this frame, a lot of theoretical [54–56] and experimental work has been done [49–51]. In principle, the CDLE approach would be very cheap and easy to implement because of the absence of membranes. Despite this, the problems of self-discharge of the cell have prevented real progress of this technique [57].

A different approach is that of the Capacitive energy extraction by Donnan Potential (CDP). In this case, the method is self-sufficient, meaning that it works without the need of external power sources since the origin of the voltage difference is the Donnan potential of the membranes separating the solution from the carbon particles. Placing one electrode in contact with a cationic membrane and the other with an anionic one produces a voltage difference between both electrodes. This method relies on the change of the Donnan potential with the salinity of the solution. If an external load is connected to the electrodes, current will flow through it in both steps, although in opposite directions. Hence, energy will be obtained every time the water is exchanged.

Fig. 1.4 shows the electrostatic potential profile inside the CDP cell. Let us assume that initially the whole cell is bathed in the fresh water solution

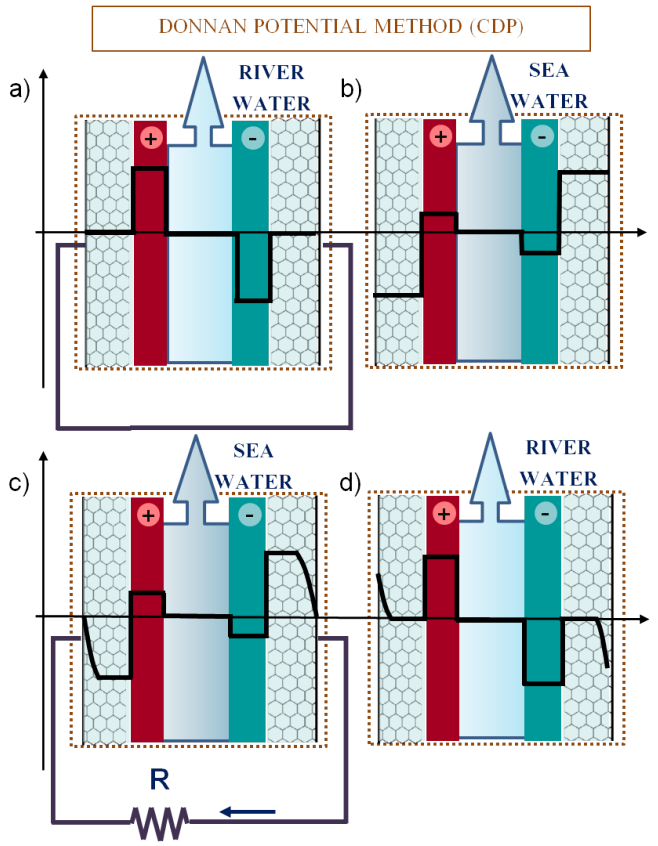

FIGURE 1.4: Schematics of the CDP methodology. Electrostatic potential profile when a): fresh water flows through the spacer between anion and cation exchange membranes, with short-circuted electrodes; b): salt water flows under open circuit conditions; c): the electrodes are connected by means of a load resistance, and the electrode potential decreases as charging proceeds; d): fresh water is pumped in open circuit, leaving the cell ready for stage a) again.

on both side of the membranes, with short-circuited terminals (Fig. 1.4a). If any cell potential is generated because of small concentration differences between both sides of any of the membranes, this would be compensated by electrode charge. If now sea water is allowed in the spacer (Fig. 1.4b) under open circuit conditions, a membrane potential will be generated: the anionic membrane let anions through itself, that is, it is positively charged, whereas the cationic membrane will be negatively charged. As a result,

a potential difference will be measured (positive at the anionic membrane side and negative at the cationic one). If a load is connected to the cell, current will flow externally until the electric potentials at both electrodes are equal, building EDLs at both solid solutions interfaces (Fig. 1.4c), and hence electric energy is extracted during this stage. The potential difference between the electrodes will be zero, but charge has been transferred from one to the other, both being charged in consequence. The circuit is opened and fresh water is pumped again, with the result that the membrane potential goes to zero again and the electrodes gain potential due to the transferred charge obtained in the previous step (Fig. 1.4d). If the external load is connected, current flows in the opposite direction, returning the previously stored charge, and work is extracted again, the system going back to step Fig. 1.4a. Since no external source is necessary, leakage is a secondary problem and very promising results have been already obtained [58–62]. In this case, the most important challenges come from the cost and fouling and bio-fouling problems that prevent a long use of the membranes [41].

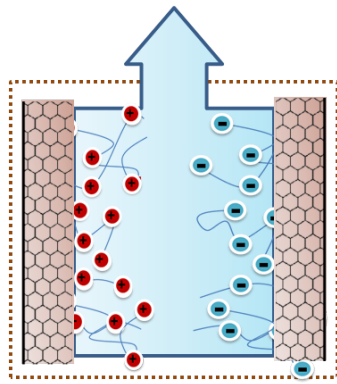

FIGURE 1.5: Sketch of the capmix cell for the soft electrode method.

Finally, the soft electrode method is a promising one developed in this work. It is based on conductive electrodes made of an activated carbon core with a polyelectrolyte layer either cationic or anionic on each electrode respectively (Fig. 1.5). The core of the SE approach is the spontaneous generation of charge on the electrodes, without the use of either membranes or

a power supply, allowing the generation of electrical energy due to changes in both the EDL capacitance of the carbon electrodes and the Donnan potential of the polyelectrolyte layer when solutions are exchanged. Thus this method has a large number of advantages as it reduces CDLE losses problems and avoids the use of ion exchange membranes resulting in a reduction of costs [53, 63].

Note that not all of these methods are capable of producing the same amount of power. Table 1.2 summarizes typical values for the three main capmix methods. Fuel efficiency (Eq. 1.2) is also included. It should be noted that, at the moment, the highest reported fuel efficiency value is for CDP, which reaches approximately 13 % [58], whereas CDLE and SE method show lower efficiency values (0.4 and 1 %, respectively). Despite this, aspects related to cost production and cell assembly are more advantageous for CDLE and SE methods.

TABLE 1.2: Capmix techniques characteristics and current power and energy values.

Capmix Methods	Charging electrode method	Power (mW/m^2)	Efficiency
CDP	Membranes	100-300	13 %
SE	Polyelectrolyte layer	30	1 %
CDLE	Power supply	5-10	0.4 %

It should be recalled that all the techniques described require forcing the solutions through the cell, whatever the design. This means that pumping energy or hydraulic losses should be considered when establishing the net power achievable with the device. However, this is not possible to take into account yet. Only for large scale setups can we expect that the obtained energy outbalances the pumping energy.

1.3. Objectives and thesis outline

The objectives of this thesis can be summarized as follows:

a. Find the fundamentals of the capmix methods, answering questions

as: *which are the processes by which EDLs acquire charge?; how much of this charge can be effectively recovered in the external circuit?; what are the maximum energy and power reasonably to be expected?; how does the nature of the solutions affect the whole energy harvesting process?*

b. Setup experimental methods for extracting energy. Find the optimum working conditions.

c. Describe and evaluate the use of polyelectrolyte-coated or *soft* electrodes for the capmix purpose.

d. Explore the possibility of approaching *real world* implementation, such as up-scaling, use of natural waters, use of real river mouth locations, etc.

Keeping in mind these objectives, the thesis is arranged as follows. In Chapter 2 we give an exhaustive account of EDL processes in capmix methods. The charging processes in the double layer, and the physical parameters of the porous medium will be analyzed. The experimental details concerning materials, measurement cells and procedures are described in Chapter 3, and Chapter 4 is devoted to the detailed description of the results that can be obtained when the techniques are performed under different options. Chapter 5 is exclusively dedicated to the soft electrode technique and finally Chapter 6, followed by the conclusions section, contains our approximation to *real world* applications (natural waters from the Mediterranean sea and the Pacific ocean, scaling up, mixed solutions...).

2

Fundamentals of capacitive double layer extraction method

The capacitive double layer extraction (CDLE) method derives from the fact that electrical double layers (EDLs) can accumulate a large amount of charge because the interfacial area is usually high, and that the capacitance of the EDL depends very significantly on the ionic contents of the medium. In this chapter we analyse the principles of this technique, which is part of the capmix methods.

2.1. Electrical Double Layer at equilibrium

Let us consider an approximately planar interface where the solid particle bears a uniform charge density and is in contact with an ionic solution. The net surface charge of the particle must be compensated for by ions around it so as to maintain the electroneutrality of the system. Both the surface charge and its compensating countercharge in solution form the **electrical double layer** (EDL) [64]. In spite of the traditional and simple use of the word "double", its structure can be very complex, not fully resolved in many instances, and it may contain three or more layers, extending over varying distances from the solid surface.

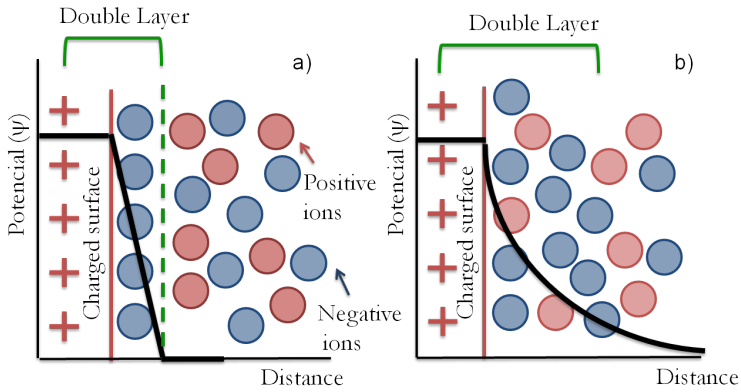

FIGURE 2.1: Schematic representation and potential as a function of time of the electrical double layer according to the Helmholtz model (a) and according to Gouy-Chapman model (b).

Throughout history, many models have been proposed towards the correct description of the structure of the interface at electrodes surfaces [65].

The original approach adopted by von Helmholtz to describe the double layer corresponds to a model consisting of two layers of opposite charges, separated by a small distance (of the order of atomic dimensions) and facing each other, as the plates of a typical capacitor. This model is illustrated in Fig. 2.1a where, as it can be observed, the potential as a function of distance linearly decreases from the solid to the end of the EDL.

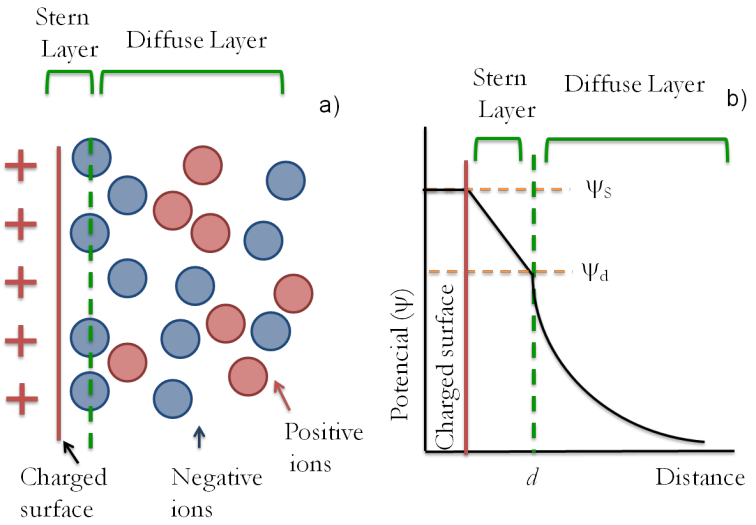

FIGURE 2.2: The electrical double layer according to the Stern model: a) an schematic representation and b) the electric potential profile as a function of the distance.

Lately, it became realized that ions on the solution side of the double layer would not remain static in a compact array as Fig. 2.1a shows. On the contrary, they would be subjected to the effects of thermal fluctuations as is illustrated in Fig. 2.1b. Thus, these surrounding ions are able to move by Brownian motion so that the region of charge imbalance, due to the presence of the particle, can be quite extended, forming the *diffuse layer* where the potential profile progressively decreases. For our 100 nm diameter particle, this diffuse layer can stretch out to several diameters [66]. The theory of such a diffuse layer was developed independently by Guoy and Chapman in the early 1900s and is based on the following premises [67]:

i) ions are point charges.

ii) they are influenced by the local electrostatic potential and by diffusion.

iii) the solvent is a structureless continuum, affecting the distribution only through its macroscopic dielectric permittivity $\epsilon = \epsilon_0\epsilon_m$ where ε_0 and ε_m are the electric permittivity of vacuum and the relative electric permittivity of the solvent, respectively.

In 1924, Stern realized that the main drawback of Guoy-Chapman model treatment was the overestimation of the capacitance of the EDL. Therefore, he proposed a model which overcomes this problem assuming finite ions size. That is, in real system, ions can approach a surface to a distance not less that their radii. And thus, the electrical double layer should have an inner region, known as the Stern layer, that is empty and is approximately one hydrated ion radius thick. As Fig. 2.2a illustrates, the centers of any ions attached to the surface are located within the Stern layer and they are considered to be immobile. Ions whose centers are located beyond the Stern layer form the diffuse (mobile) part of the electrical double layer. The electric potential shown in Fig. 2.2b linearly changes from the surface to the end of the Stern layer located at the so-called Stern plane or outer Helmholtz plan. This marks the beginning of the diffuse layer, beyond which the potential decays to zero in an approximating exponential function [68]. The potential profile $\Psi(\mathbf{r})$ in this layer (Fig. 2.2b) is given by Poisson's equation:

$$\varepsilon_0\varepsilon_m\nabla^2\Psi(\mathbf{r}) = -\rho(\mathbf{r}) = -\sum_{i=1}^{N} z_i e c_i \tag{2.1}$$

where $\rho(\mathbf{r})$ is the volume charge density at position $\mathbf{r}$, e is the electron charge and z_i and c_i are the valences and number concentrations of ions of type i (there are N ionic species in the solution).

The number concentrations of ions of each type, c_i, in a given position is related to the electric potential in that position by the Boltzmann equation:

$$c_i = c_{i0}\exp\left[-\frac{z_i e\Psi(\mathbf{r})}{k_B T}\right] \tag{2.2}$$

being c_{i0} its bulk concentration far from the particle surface, k_B the Boltzmann constant and T the absolute temperature. From this, **Poisson- Boltzmann equation** will be read:

$$\varepsilon_0 \varepsilon_m \nabla^2 \Psi(\mathbf{r}) = -\sum_{i=1}^{N} z_i e c_{i0} \exp\left[-\frac{z_i e \Psi(\mathbf{r})}{k_B T}\right] \tag{2.3}$$

The total charge per unit area of surface, σ, is obtained by assuming the volume charge density through the whole electrical double layer:

$$\sigma = -\int_{EDL} \rho(\mathbf{r})\, d^3\mathbf{r} \tag{2.4}$$

This equation can be simplified in cases of high symmetry, for instance, if an interface is planar (x perpendicular to the plane). Moreover, taking into account that the Stern layer of Fig. 2.2 was described as free of ions due to finite ion size, the previous integral of the volume charge density can be just calculated from the beginning of the diffuse layer $x = d$ to the bulk solution. Thus, it can be obtained:

$$\sigma = -\int_{d}^{\infty} \varepsilon_0 \varepsilon_m \frac{d^2\Psi}{dx^2} dx = \varepsilon_0 \varepsilon_m \left.\frac{d\Psi}{dx}\right|_{x=d} \tag{2.5}$$

and for cylindrical coordinates (considering a cylindrical pore with radius R which volume is occupied by the solution):

$$\sigma = -\varepsilon_0 \varepsilon_m \left.\frac{\mathrm{d}\Psi}{\mathrm{d}r}\right|_{r=R^-} \tag{2.6}$$

In both cases, it is assumed that the derivative of the potential is zero at large distance from the interface.

The surface which envelopes each particle and which marks the region where the liquid first begins to move with respect to the solid is called the **surface of shear** or, in the case of large flat surface, the **slipping plane**.The electrostatic potential in this plane, relative to the potential in the bulk solution, is called the **zeta potential** ζ. Its position is not fully established, but for all practical purposes it may probably be identified with the start of the diffuse layer. By electrokinetic methods it is possible to obtain the point

where $\zeta = 0$ so no charge is measured because the diffuse charge is zero. This is called the **isoelectric point** (i.e.p.) and it will be a experimental variable in this thesis. The reason is that it is one way to examine the existence of adsorbed charge in the fixed layer. We can also define the **point of zero charge** (p.z.c.) or pH where $\sigma = 0$ [67].

A useful approximation for Poisson-Boltzmann equation (Eq. 2.3) can be made when the electrical energy is small compared with the thermal energy of ions ($|z_i e\Psi| < k_B T$). This is known as the **Debye-Hückel approximation**. Let us consider the one-dimensional case ($\Psi = \Psi(x)$) with binary and symmetrical electrolytes ($N = 2$ and $z_+ = -z_- = z$) with bulk concentration c. Expanding the exponential in Eq. 2.2 and neglecting all but the first two terms and applying electroneutrality ($\sum_{i=1}^{2} z_i e c_{i0} = 0$), we get:

$$\varepsilon_0 \varepsilon_m \frac{d^2\Psi}{dx^2} = -\rho \approx \frac{2z^2e^2c}{k_B T}\Psi \tag{2.7}$$

Eq. 2.7 can be easily solved for the diffuse layer assuming the boundary conditions specified in Fig. 2.2b: $\Psi(x = d) = \Psi_d$ and $\Psi(x \to \infty) = 0$ to give:

$$\Psi(x) = \Psi_d \, e^{-\kappa x} \tag{2.8}$$

It provides a useful parameter called Debye-Hückel parameter κ. It plays an important role in the theory of the double layer. The quantity $1/\kappa$ is often referred to as the **thickness of the double layer**:

$$\kappa = \sqrt{\frac{2e^2z^2c}{\varepsilon_0 \varepsilon_m T k_B}}$$

Fig. 2.3 shows the potential profile deduced from Eq. 2.8 for two different ionic concentrations: 20 mM (typical river water ionic strength) and 500 mM (common sea water value) of sodium chloride concentration in *a* and *b*, respectively. It is easy to observe how the thickness of the double layer κ^{-1} is strongly ionic concentration dependent. Indeed, if the ionic concentration increases (decreases), the thickness of the double layer decreases

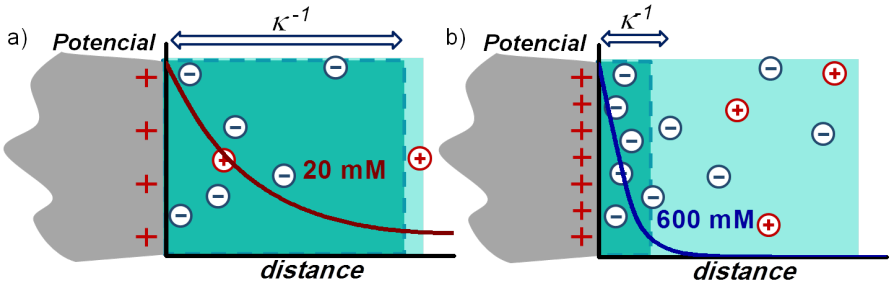

FIGURE 2.3: Electric potential profile in the EDL at 20 mM (a) and 500 mM (b) sodium chloride concentration.

(increases). This process is usually referred to as **compression (expansion) of the double layer**.

Unfortunately, for our case, the assumption $|z_i e\Psi| < k_B T$ does not hold. Although capmix experiments are always carried out for potentials below 1.2 V to avoid faradaic reactions, the previous assumption is only valid for Ψ smaller than 25 mV. Fortunately, Poisson-Boltzmann equation can be still easily solved if we particularize for the case considered:

$$\varepsilon_0 \varepsilon_m \frac{d^2\Psi}{dx^2} = 2zec \sinh \frac{ze\Psi}{k_B T} \tag{2.9}$$

We can calculate the total charge, σ. With this aim, firstly, Eq. 2.9 is integrated, obtaining [66]:

$$\frac{d\Psi}{dx} = -\sqrt{\frac{8ck_B T}{\varepsilon_0 \varepsilon_m}} \sinh \frac{ze\Psi}{2k_B T} \tag{2.10}$$

Finally, using Eq. 2.5 and assuming that the surface Ψ_S and the diffuse potential Ψ_d are very similar: $\Psi_S \approx \Psi_d$, we get:

$$\sigma = \sqrt{8\varepsilon_0 \varepsilon_m c k_B T} \sinh \frac{ze\Psi_S}{2k_B T} \tag{2.11}$$

As mentioned, the EDL constitutes a **microscopic** (or nanoscopic) **capacitor** precisely because of this capability of charge accumulation. One of the plates of the capacitor is the particle surface, and the other is distributed

in a diffuse region (with thickness equal to the Debye length, κ^{-1}). Finally, from Eq. 2.11, it can be easily obtained that the **EDL differential capacitance** per unit area is:

$$C_d = \frac{d\sigma}{d\Psi_S} = \varepsilon_0 \varepsilon_m \kappa \cosh \frac{ze\Psi_S}{2k_B T} \tag{2.12}$$

In the CDLE process, a change in the capacitance of the EDL is produced by changing the salinity of the solution in contact with the interface. Additionally, modifications can be produced by changing the permittivity of the solution, by, for instance, increasing or reducing its temperature.

2.2. How can energy be extracted from EDLs

If we connect a capacitor to a battery through a resistor, the capacitor will store some energy (U=$\frac{1}{2}QV$) because positive and negative charges will be kept separated on the plates. If the circuit is open, hence the charge does not change, and we decrease somehow the capacitance (for instance, by increasing the distance between the plates), the voltage between the plates, and hence, the energy increases. Physically, the work of separating the charges produces an increase of their potential and hence, an increase of the stored energy. After that, if the circuit is connected again, there will be a spontaneously discharging current to the battery, which can be used to extract energy, in an amount larger than that used for charging. This process has been called **capacitive energy extraction** [48].

Key property of EDLs
If sea water is substituted by fresh water in open circuit conditions (i.e. the surface charge density at the wall does not change) the electric potential increases.

The Capmix cell, as it has been explained in section 1.2.4, consists of a couple of porous electrodes with high surface area (activated carbon, typically used in supercapacitors, is a good possibility) that are facing each other at a certain distance, enabling water to flow in between them. Fig. 2.4 left is a detailed view of one electrode of the cell. Let us imagine that this electrode has been initially charged at a certain potential in salt water (500 mM ionic concen-

tration). Afterwards, this salt water is exchanged for fresh water (20 mM) as the case may be in a river mouth, and in open circuit conditions. Since the surface charge density at the wall (σ) does not change, the electrical potential slope at the surface should remain (following Eq. 2.5) while charge will be redistributed in a thicker space (which is similar to the increase of the distance between the plates of a common capacitor as it has been already mentioned), bringing about an EDL expansion and an increase of the surface potential ($\Delta\Psi$) as it is shown in Fig. 2.4 left.

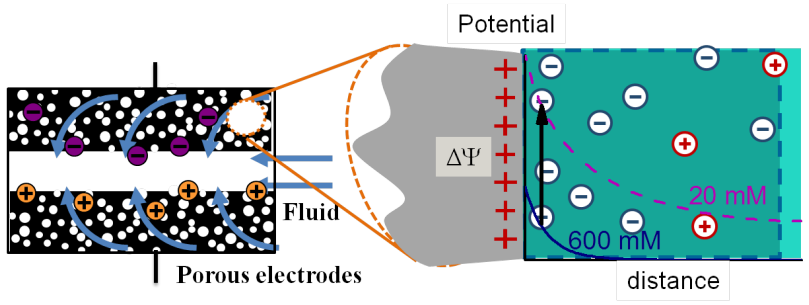

FIGURE 2.4: Left: schematic representation of capmix cell. Right: electric potential profile for EDL at 20 mM and 500 mM of sodium chloride concentration when the surface charge is maintained.

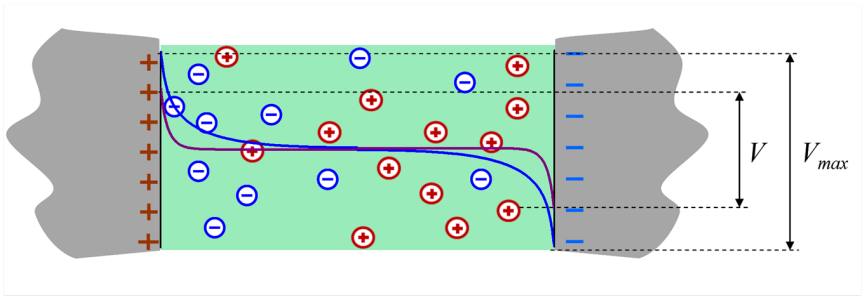

FIGURE 2.5: Electric potential profile between two oppositely charged electrodes. In the equilibrium, the voltage between electrodes decays inside the EDL.

If we place two counter electrodes inside the solution and we charged them till a V potential, the equilibrium electric potential profile is as shown

in Fig. 2.5. An electric double layer is also generated on the opposite electrode with the reversal situation. If the electrodes are not connected to a circuit, the potential between them increases upon ionic strength decrease. If the electrodes are identical, the voltage rise (that is, the difference between the voltage at low and high ionic strength, see Fig. 2.5) will be in this case twice the voltage jump in every electrode: $\Delta V = V_{max} - V = 2\Delta\Psi$. The analogy is not complete, since the charge in the EDL is volume distributed, and hence, the potential profile is not linear. Also, surface charge and potential are not linearly dependent. Furthermore, a complete analysis must take into account that there are other interactions between ions, as excluded volume effects, which are not part of this simple analysis (see section 2.4). However, the qualitative picture remains the same.

Fig. 2.6 is a schematic view of all the stages in the CDLE cycle. Both the circuit steps and the charge as a function of the potential for a single electrode of the cell are represented:

- **Step 1 or charging step**. Electrodes immersed in salty water are connected to a voltage source set at a certain potential V. This voltage will be referred to as the working potential. Ions redistribute in the solution until a certain electronic charge grows at the electrode surface and the potential of each electrode reaches half of the source potential value $\Psi = V/2$.
- **Step 2**. The circuit is opened and salty water is replaced by fresh water giving rise to double layer expansion. As shown in the graph, the electrode surface potential increases ($\Delta\Psi$) because the capacitance decreases at a constant surface charge.
- **Step 3 or discharging step**. The circuit is closed again. The cell, which is now at a higher potential, is discharged through a resistance, bringing about a decrease of both capmix cell voltage and charge.
- **Step 4**. The circuit is opened and the fresh water is replaced by salty water again, leading to a further decrease of the voltage below the source value.

Because the same amount of charge Q is given to the cell at some average

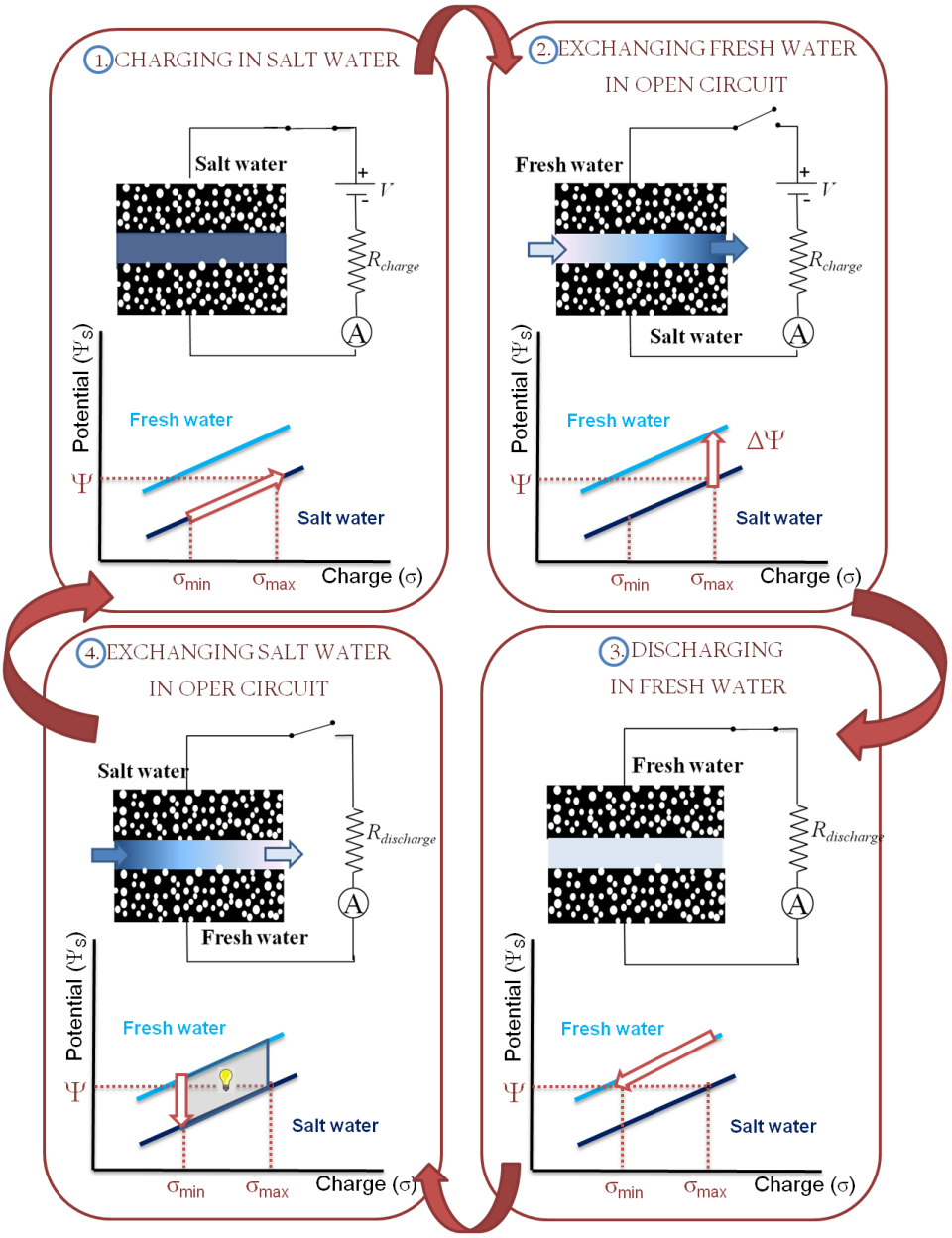

FIGURE 2.6: The four CDLE cycle steps. In each step is included the cell process, the circuit stage and the theoretical cell potential-charge relationship.

potential V, and returned from the cell at a larger average potential $V+\Delta V$, a net energy $Q\Delta V$ is gained in each cycle. This is the **origin of the positive energy balance**: electrical work is made available, without use of any kind of selective membranes or electromechanical converters, like dynamos or turbines.

The area of the cycle in Step 4 of Fig. 2.6 represents the net extracted work per unit area of electrode which is roughly proportional to the product of the voltage rise in step 2 and the charge exchanged in step 3. The net energy that can be obtained per unit interface area is given by:

$$W = \int_{\sigma_{min}}^{\sigma_{max}} \left[\Psi_S(\text{fresh}) - \Psi_S(\text{salty})\right] \mathrm{d}\sigma \tag{2.13}$$

2.3. Thermodynamic analysis

The mixing of solutions is a spontaneous process in which there is a certain decrease of free energy. If we consider the solutions ideal and homogeneous, that is, ions do not interact between each other, the internal energy is only a function of temperature, and the mixing does not imply any change of either internal energy or temperature, and hence there will be no exchange of heat or mechanical work needed. Making this process in a system with adiabatic and rigid or diathermal and mobile walls does make no difference. Since water can be considered incompressible, then Gibbs free energy variation is given by:

$$\Delta G = -T\Delta S. \tag{2.14}$$

On the other hand, in the presence of a charged surface, the solution is not homogeneous, and hence, during the mixing process as that in Step 2 in Fig. 2.6 there is an increase of the internal energy due to the increase of the electric potential in the EDL. If this process is performed in a cell with adiabatic walls, then the increase of electric potential involves a decrease of temperature. If, however, there is thermal equilibrium with the surroundings, the increase of electric potential in the EDL produces an increase of the internal energy by heat absorption (Fig. 2.7a). With similar arguments,

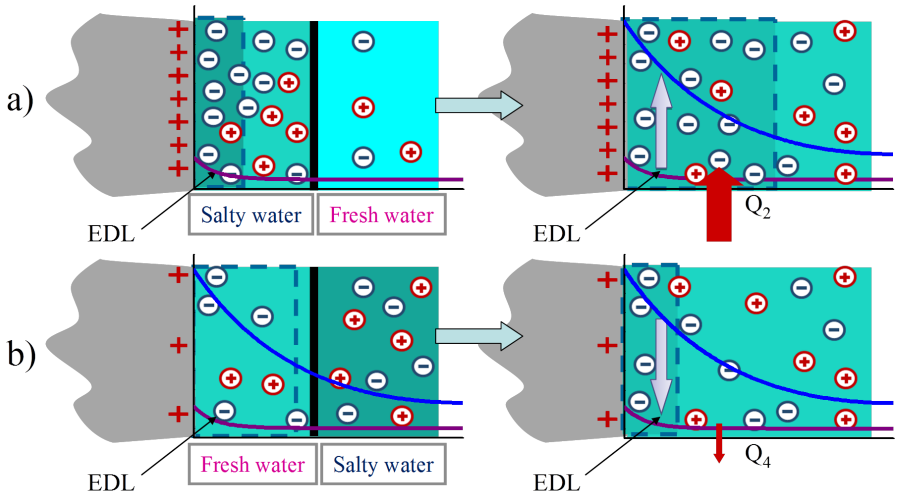

FIGURE 2.7: Electric potential in the ionic solution in presence of a charged surface during the different steps of a CDLE cycle. Steps 2 (a) and 4 (b) are schematically represented.

we can examine the mixing when it is the fresh water in contact with the charged surface (Step 4 of the CDLE cycle, Fig. 2.7b). In this case, during the mixing there is a decrease of the electric potential in the EDL, but in this case the surface charge is lower, and so the total number of ions that are mixed. Hence, in the cycle there will be a net absorption of heat in steps 2 and 4, that is transformed into work in steps 1 and 3.

On the other hand, in step 2, there is neither a mechanic nor electric work, but just an entropy increase. Being the mixing an irreversible process, $T\Delta S_2 \geq Q_2$ and hence

$$\begin{aligned} \Delta U_2 &= Q_2 > 0 \\ \Delta G_2 &= \Delta U_2 - T\Delta S_2 \leq 0 \end{aligned} \tag{2.15}$$

And we can conclude that this step of the cycle is spontaneous. In the case of step 4,

$$\begin{aligned} \Delta U_4 &= Q_4 < 0 \\ \Delta G_4 &= \Delta U_4 - T\Delta S_4 < 0 \end{aligned} \tag{2.16}$$

hence, the process is also spontaneous.

It can be concluded that this process is thermodynamically possible. However, a machine that works between salty and fresh water reservoirs has no equivalence in thermal machines, since in this case the process is made at a constant temperature. Hence, one cannot compare the CDLE with a Carnot cycle. However, an analogy with a thermal machine can be performed by considering that this process is developed at constant temperature, and hence, the free energy plays the role of the internal energy of a thermal machine. On the other hand, the high chemical potential and low chemical potential reservoirs of a CDLE machine play the role of the hot and cold reservoirs in a thermal machine. With this analogy, it is demonstrated in [69] that an equivalent Carnot cycle, that is, with maximum efficiency and made of reversible processes, can be designed for a system working with high and low chemical potential reservoirs. While in the CDLE cycle, the mixing steps 2 and 4 are performed at a constant EDL charge, the mixing steps should be performed with constant number of ions in the EDL if the maximum efficiency is sought. This can be achieved by continuously charging the surface while the solution is diluted in step 2, and hence, compensating the dilution by the increase of charge, and reversely, by continuously discharging the surface while the solution is concentrated in step 4. Of course, this cycle is not realizable, since it is not possible to experimentally control at every time the number of ions entering the EDL.

2.4. Theoretical model predictions: ion charge and size effects

The charging potential of the capmix cell electrodes can be relatively high (several hundred mV) and the pore diameter can be as low as 1 nm. In these conditions, simple models assuming low potentials and planar interfaces may not describe the phenomenon accurately. Furthermore, the

behavior of the ions close to the wall is another source of difficulty, as they can even lose their hydration shell (fully or in part) under the EDL field. This is the case of ionic liquids [70, 71], and is the basis of the supercapacitances that are found with activated carbons with pores of size below 1 nm, but can happen even for small, monovalent, well hydrated ions like Na^+, as has been shown by molecular dynamics simulation [72]. As a consequence, a Stern layer can be formed with ions, which are partially dehydrated due to strong chemical or electric interactions with the surface. However, there is no evidence of such strongly adsorbed ions at the carbon-sodium chloride interface. In the following theoretical model, only the traditional image of a charge-free Stern layer determined by the distance of minimum approach of hydrated Na^+ and Cl^- ions will be considered.

It is critical to properly calculate the relation between charge and potential at the EDL, in order to predict the experimental conditions leading to the maximum performance of the process.

We will focus on the modeling of the solution-pore wall interface inside the porous material, which is of course just part of the description of the complete electrode. This is far more complex than we can reach in this thesis. As in other analyses of the electrochemistry of porous electrodes, time effects will be ignored and only steady state situations will be considered; furthermore, no distinction will be made on the exact position in the electrode of the interface being described, an issue that is of utmost importance when modeling the whole electrode, as discussed by Newman and Tobias [73]. These authors stressed that the macroscopic description means in fact an average of the variables of interest over regions small in comparison with the whole electrode but large in relation to the typical pore size. Computational simulations, on the contrary, require some assumption regarding the pore geometry. For instance, Lim et al. [74] considered cylindrical pores with semicircular openings, whereas Yamada et al. [75] based their model on a swarm of spherical porous particles.

For our purposes, existing models on the description of the EDL potential profile at interfaces with different geometries [66, 76–83] cannot be applied

to porous electrodes because such models are usually restricted to dilute suspensions, so that the likely overlap between EDLs from opposite walls of the pores is not considered. Theoretical models including EDL overlap and ionic size effects have been applied to salt free suspensions [80], and are based on cell models, which are appropriate in the case of homogeneous distributions of non-contacting spherical particles [79].

Here we propose a perhaps more realistic approach in which **the porous electrodes are modelled as a network of cylindrical pores**. In addition to being very intuitive, this geometry has the additional advantage of an easy control of the quantities determining the phenomenon: pore radius, porosity, wall potential and ionic strength. Hence, we will include the following aspects in our simulations:

- **Non-Planar EDL**: inside the activated particles, the most abundant pores are typically less than 10 nm in diameter, and curvature effects on the electric potential profile can be significant.
- **EDL overlap**: it is likely in the smallest pores and with the less concentrated solutions.
- **Moderate charging potentials**: larger energies can be obtained if large amounts of charge are transferred back and forth at very different potentials. For fixed values of the salinity, it may be necessary to explore potentials as high as 500-600 mV. In such conditions, the interfacial region can be largely enriched in counterions, to the extent that the point charge hypothesis for ion structure leads to unrealistically high counterion concentrations in the vicinity of the pore wall. This fact, together with the high salinity of the sea water means a non negligible role of the size of the ions.

Such treatment will lead to a theoretical prediction of the maximum energy that can be physically extracted in a CDLE technique. In this model, design-dependent issues, such as ohmic losses, pumping energy requirements, ineffective wetting and others are not considered.

2.4.1. Point-like vs. finite-volume ions

Here we perform a mean field analysis of the structure of the EDL, and so, the electric potential distribution will be given by the Poisson equation (Eq. 2.1) solved together with the Boltzmann distribution (Eq. 2.2). Since the system can be envisaged as a network of cylindrical pores with charged walls, σ being its surface charge density, we need to solve the Poisson equation inside the cylindrical volume occupied by the solution. A diffuse layer will be formed, which will compensate for the wall charge. The radius of the cylinder, $r = R$, is representative of the pore size and the volume fraction ϕ of the cylinders is the porosity ε.

The boundary condition for Eq. 2.2 at the particle surface is:

$$\Psi(R) = \Psi_S \tag{2.17}$$

while the second boundary condition stems from symmetry considerations of the pore, so that at the cylinder axis:

$$\left.\frac{d\Psi}{dr}\right|_{r=0} = 0 \tag{2.18}$$

Note that this boundary condition is compatible with EDL overlap, since it does not restrict the potential at the axis to zero value. With these equations, the potential profile can be calculated as a function of the surface potential, the particle concentration, the pore size, and the ionic concentration.

The surface charge density σ, can be calculated following Eq. 2.6, where the beginning of the diffuse layer corresponds to the cylindrical pore wall. From electroneutrality arguments, we can also obtain such charge by integration of the charge density inside the pore (Eq. 2.4). Once the surface charge has been calculated, the differential capacitance per unit area C_d of the EDL is obtained from Eq. 2.12. Finally, the extracted work in every cycle, such as the shadowed area in step 4 (Fig. 2.6), can be calculated with Eq. 2.13.

In Fig. 2.8a we represent the expectations of the Boltzmann distribution for a point ions model (PIM) in the case of moderate surface potential (100

mV) and sea water concentration (600 mM). It can be observed that the largest part of the potential decay occurs in the first nanometer. Such behavior is not realistic since, using excluded volume arguments, the ionic concentration cannot exceed a certain value depending on ionic size, typically c_{MAX} ≈10 M in the best case. This modifies the predicted profiles of potential and concentrations, and limits the validity of the Poisson-Boltzmann approximation to, for example, 160 mV for a 20 mM solution or 70 mV for a 600 mM solution.

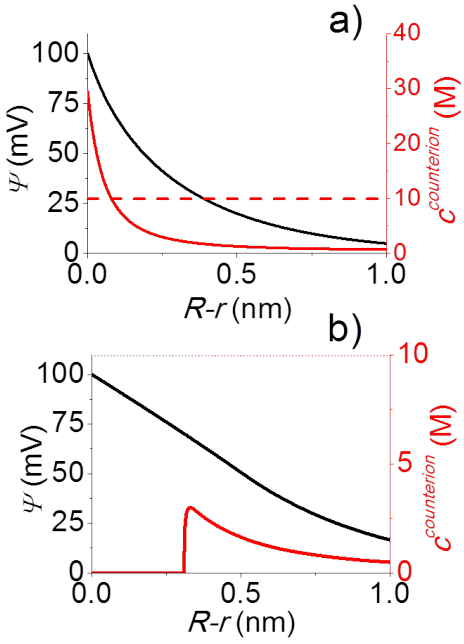

FIGURE 2.8: Potential (black line) and counterion (red line) profiles (r=0 in the axis) inside a cylindrical pore for Ψ_S=100 mV, R =5 nm and c =600 mM). a) Point ion model. b) Finite volume ions with c_{MAX} = 10M.

The interaction between ions can be taken into account by using sophisticated models as reported in [78, 84, 85]. These consider both coulombic and excluded volume interactions between every pair of ions, instead of using a mean field approximation. They provide a detailed profile of the electric potential and predict interesting effects like charge inversion [78].

However, we are not interested in the precise profile of the electric potential, but rather in the effect of the finite volume of ions on the total stored charge in the EDL. Hence, we use a mean field approximation in which excluded volume is taken into account in the excess electrochemical potential of every ionic species i:

$$\mu_i^{excess} = k_B T \ln f_i \tag{2.19}$$

by an activity coefficient f_i that accounts for the ion-ion interaction. This approach will be referred to as extended-volume model (EVM) hereafter. An extensive analysis of the different approximations is given in [76] and some of the consequences on the differential capacitance of the EDL are studied in [86]. We use the approximation provided in [87, 88], that, in the case of two ions solutions, leads to:

$$c_i = \frac{c_{i0} \exp\left[-\frac{z_i e \Psi}{k_B T}\right]}{1 + \sum_{i=1}^{2} \frac{c_{i0}}{c_{i,MAX}} \left[\exp\left(-\frac{z_i e \Psi}{k_B T}\right)\right]}, i = 1, 2 \tag{2.20}$$

If, in addition, the existence of an excluded volume between particle surface and hydrated ions is taken into account, then Eq. 2.1 must be solved separately in three regions. In the first one, between the particle surface and the radius of the smallest ion, say ion 1, $c_1(r) = c_2(r) = 0$. In the second region, where the biggest ion, say ion 2, cannot stay, we can write $c_2(r) = 0$. For larger distances to the surface, Eq. 2.1 must be solved considering both ionic species given by Eq. 2.20 [79]. Accordingly, new boundary conditions must be used, that is, the continuity of the potential and the normal component of the electric displacement at the boundary between every pair of regions:

$$\Psi(r = r_1^-) = \Psi(r = r_1^+) \tag{2.21}$$

$$\Psi(r = r_2^-) = \Psi(r = r_2^+) \tag{2.22}$$

$$\frac{\mathrm{d}\Psi}{\mathrm{d}r}\Big|_{r=r_1^-} = \frac{\mathrm{d}\Psi}{\mathrm{d}r}\Big|_{r=r_1^+} \tag{2.23}$$

$$\frac{\mathrm{d}\Psi}{\mathrm{d}r}\Big|_{r=r_2^-} = \frac{\mathrm{d}\Psi}{\mathrm{d}r}\Big|_{r=r_2^+} \tag{2.24}$$

Since we are dealing with high surface potentials, coions will be practically absent inside the EDL, and hence, the charge, electric potential profiles, the surface charge and differential capacitance will be mainly determined by the characteristics of the counterion. Here we have analysed the case of NaCl, with hydrated radii $r_{Na^+} = 0.6$ nm and $r_{Cl^-} = 0.45$ nm. The cases of negative and positive surface potentials are not symmetrical, since the counterion will be different in each situation. For the solution of the above equations and boundary conditions, we used the routine BVP4C in Matlab®software.

2.4.2. Results and Discussion

EDL overlap and surface curvature

Fig. 2.9 summarizes two fundamental aspects of this work: the effect of the EDL overlap and the surface curvature. This can be done through the comparison of the electric potential profiles inside the EDL in the case of cylindrical and planar interfaces for different salt concentrations. The potential decay for the planar interface is steeper at all concentrations. As a consequence, the surface charge is larger in this geometry.

It is also clear in this Fig. that even for electrolyte concentrations as high as 50 mM, the potential does not go to zero at the center of the channel, making apparent the phenomenon of EDL overlap. This is very significant for the technique, since the presence of overlap modifies to a large extent the surface charge and gives rise to a capacitance much lower than expected for non-overlapping double layers. Finally, consideration of surface curvature is relevant, as expected, for low ionic strength, when the potential is underestimated at all channel positions if planar interfaces are assumed. To sum up, the EDL capacitance would be overestimated if either EDL overlap or surface curvature are neglected. Thus, hereafter we will take into account both effects in our calculations.

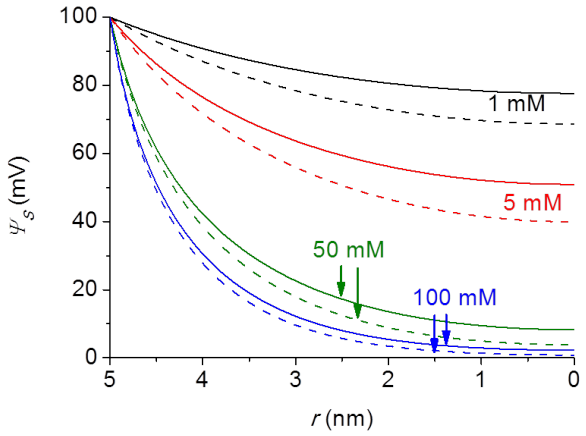

FIGURE 2.9: Electric potential profiles inside a cylindrical pore of radius R =5 nm, surface potential Ψ_S=100 mV, and with NaCl solutions of the concentrations indicated. Solid lines: cylindrical geometry, dashed lines: planar geometry.

Differential capacitance of the EDL

In Fig. 2.10 we summarize the profiles of electric potential (a) and charge density (b) inside the pore as predicted by EVM for the case of a 5 nm pore radius immersed in NaCl solutions, with negative potentials. Note that, contrary to PIM predictions, an unlimited counterion accumulation close to the surface is prevented by the finite ion size. The saturation in the counterion concentration extends over larger distances from the surface the larger $|\Psi_S|$, thus reducing the average electrostatic interaction between the ions and the latter. This leads to a less efficient screening of the surface charge and hence, to flatter potential profiles and lower surface charge increase with surface potential, as compared to that attainable with point ions. At a certain potential (for instance, $\Psi_S = -100$ mV and 600 mM, or about $\Psi_S = -250$ mV and 20 mM, (Fig. 2.10b) the counterion concentration reaches its maximum value at the distance of nearest approach. At that potential, $\sigma(\Psi_S)$ exhibits an inflection point (Fig. 2.10c), hence the capacitance reaches a maximum (Fig. 2.10d).

The significance of a finite ion volume consideration is made clear in

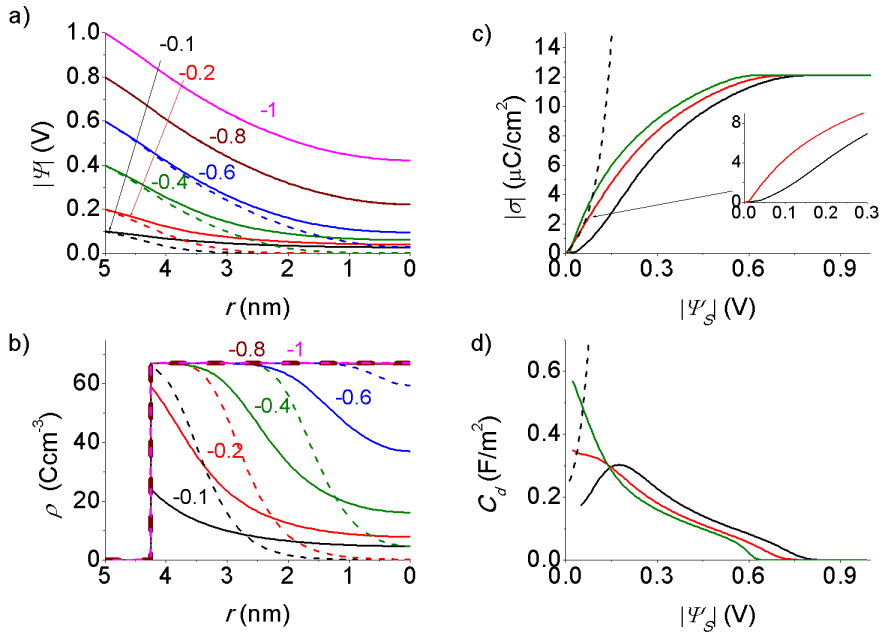

FIGURE 2.10: Potential (a) and charge density (b) profiles inside a cylindrical pore of R =5 nm, in 20 mM (solid line) and 600 mM (dashed line) NaCl solutions. The surface potentials in volt are indicated. c) Surface charge density as a function of the surface potential for the same pore radius and 20 mM (black line), 100 mM (red line) and 600 mM (green line). Dashed line: PIM predictions for 20 mM NaCl solution. d) Same as c) but for the differential capacitance.

Fig. 2.10c,d where the predictions of the PIM are included for the sake of comparison in the case of 20 mM NaCl. It can be seen that neglecting the actual ion dimensions may introduce orders of magnitude differences in our estimation of EDL quantities and mainly EDL capacitance, particularly in the case of moderate to high charging potentials. The maximum in the capacitance is observed at higher potentials when the ionic strength decreases, as confirmed in Fig. 2.11, corresponding to 20 nm pore radius.

In Figs. 2.10 and 2.11 we also observe that, after the maximum, the capacitance decreases and it can even go to zero for very narrow pores. Due to excluded volume effects, the surface potential determines the EDL thickness, and in fact the charge can be constant over the whole pore, as in Fig. 2.10b for the curves corresponding to NaCl 20 mM and Ψ_S =800 mV.

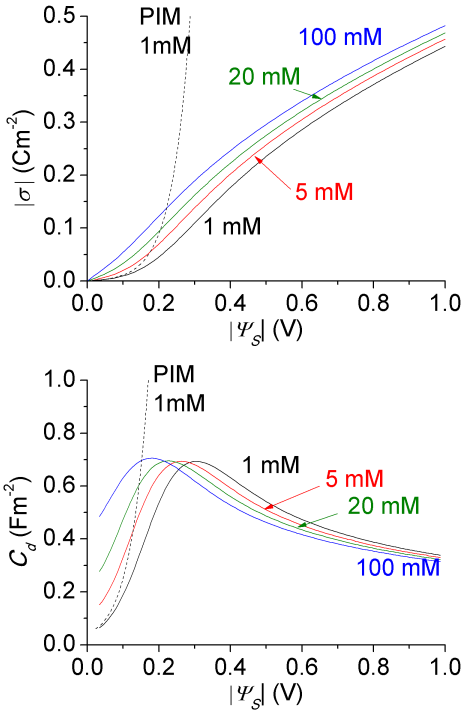

FIGURE 2.11: Surface charge density (upper panel) and differential capacitance (lower panel) as a function of the surface potential for a cylindrical pore of R =20 nm, immersed in NaCl solutions of the concentrations indicated. The point ion model (PIM) predictions for 1 mM are shown for comparison.

In this case, the pore can be saturated of counterions, and an increase in potential does not bring about a subsequent increase in charge (compare the initial slopes for the curves corresponding to Ψ_S =600, 800, and 1000 mV in Fig. 2.10a, and the constancy of the surface charge in Fig. 2.10c above 600 mV). This manifests in a zero differential capacitance, as seen in Fig. 2.10d. Note that this occurs at lower potentials as the ionic strength increases (around 800 mV for 20 mM and 600 mV for 600 mM): this is a manifestation of the fact that while the total accumulated charge is larger for larger ionic strengths, saturation takes place at lower potentials. Summarizing, the observed trend is a consequence of the combination of EDL overlap and EVM, since it only occurs when both aspects are taken into

account in Fig. 2.10a. Once this situation is reached, the potential and ionic concentration profiles do not depend on the bulk concentration, since the pore is saturated. That is the reason why the potential profile becomes independent of the ionic strength. Note finally that a zero value value of the differential capacitance is never reached in the case of larger pore radius (Fig. 2.11), where the large difference between the sizes of the channel and the counterions prevent the occurrence of saturation.

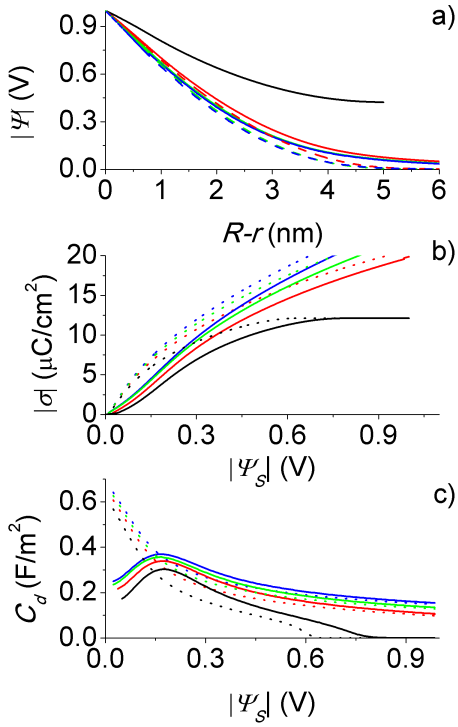

FIGURE 2.12: a) Profiles of the absolute value of the potential for $\Psi_S = -1V$, NaCl 20 mM (solid lines) and 600 mM (dashed lines). b) Surface charge density as a function of surface potential (in absolute values), for NaCl 20 mM (solid lines) and 600 mM (dashed lines). c) Differential capacitance of the EDL as a function of the absolute value of the surface potential. In all cases, pore radii: 5 nm (black line), 10 nm (red line), 20 nm (green line), and 100 nm (blue line).

It is also noticeable in Fig. 2.10d that, while the stored charge increases with the ionic strength (Fig. 2.10c), at certain potential the capacitance at 600 mM is lower than at 20 mM. This is a manifestation of the fact that

in the case of 600 mM, an increase in surface potential (for example, from 200 mV to 400 mV), is mostly balanced by the excluded volume repulsion near the surface. Hence, ions accumulate far from the surface, effectively increasing the EDL thickness as it would happen if the ionic strength were reduced. In summary, the presence of excluded volume effects sets a sort of equivalence between increasing the surface potential and reducing the ionic strength (that is, increasing the Debye length).

In Fig. 2.12 we compare the results obtained for different pore radii. In Fig. 2.12a we observe that the electric potential profile is less affected by EDL overlap for larger pore radius. As a consequence, the potential decay is steeper and the surface charge larger (Fig. 2.12b), and so is the capacitance (Fig. 2.12c). For pores larger than 5 nm, the counterion distribution suffices to efficiently screen the surface potential before reaching the saturation. Because of this, the surface charge does not reach a plateau and the differential capacitance does not enter the saturation regime (i.e. remains distinct from zero). We also observe that for pore radius larger than 10 nm, the size is not so discriminating.

Extracted work

As mentioned, this investigation is justified by the possibility of obtaining a net amount of energy by properly taking advantage of the capacitance changes above described. In Fig. 2.13b we represent the amount of work W that can be obtained if operating cycles as those drawn with arrows in Fig. 2.13a are performed. For the point ion model, W increases rapidly with the increase in potential, but, as we have shown, this leads to unrealistically large ionic concentrations near the surface. If the excluded-volume model is used instead, the capacitance cannot exceed a certain value, and as a consequence, neither can W.

Viewed from another point, one can say that the energy depends on the distance between the curves $\sigma(\Psi)$ corresponding to low and high salt concentrations, and such distance increases with the surface potential as long as the capacitance at 600 mM is larger than that at 20 mM. This occurs at low potentials (Fig. 2.12c), and hence W increases when the surface po-

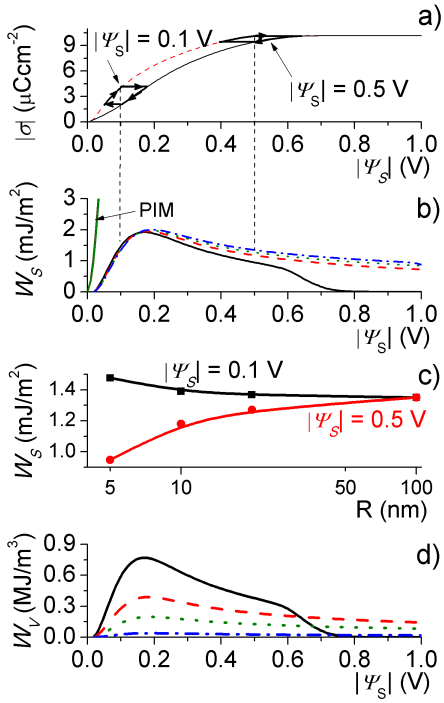

FIGURE 2.13: (a) Surface charge density vs. surface potential for 20 mM (solid black line) and 600 mM (dashed red line). Two operation cycles, corresponding to low and high charging potentials, are shown; (b) Extracted work per unit area for 20 mM-600 mM exchange, as a function of charging potential for different pore radii: 5 nm (black line), 10 nm (red line), 20 nm (green line), and 100 nm (blue line). The point ion model (PIM) predictions are shown for comparison. (c) Specific extracted work as a function of pore radius for low and high surface potentials; (d) Same as (b), but per unit volume of electrode.

tential raises from zero to some critical value. At this point, the relation between the capacitances is reversed, and the $\sigma(\Psi)$ dependences approach each other, leading to a decrease in extracted energy. For still larger potentials, charge saturation can occur for both ionic strengths in 5 nm pores, and this provokes that the stored charge does not vary with surface potential, hence the extracted work goes down to zero. As expected, this situation does not occur for larger pore radii, because the saturation regime is not reached.

A bizarre result is also observed in Fig. 2.13b: while the capacitance in-

creases with pore radius (Fig. 2.12c), the specific work at low potentials slightly decreases. This prediction can be understood if we take again into account that, as mentioned, the extracted work is not directly related to the capacitance, but to the differences between $\sigma(\Psi_S)$ corresponding to low and high salt concentrations at a given surface potential, that is, to the difference between the capacitances. In Fig. 2.12b we observe that, at low potentials, the pore radius has a larger effect on the $\sigma(\Psi_S)$ dependences corresponding to 20 mM than on those corresponding to 600 mM, because the EDL thickness is larger in the former case. This leads to a decrease of the area between both curves in Fig. 2.12b and, hence, to a lower extracted work with increasing the pore radius. On the other hand, at high potentials the saturation of the counterion concentration occurs at larger charge and potential the wider the pore. This provokes a shift of the maximum extracted work towards larger potentials (Fig. 2.13b).

Of course, the larger the surface area, the larger the extracted energy. This means that more energy can be harvested during operation by either increasing the porosity or decreasing the pore size. In the latter case, one must keep in mind the results in Fig. 2.13c, demonstrating that this can be self-defeating. Hence, it is not trivial to predict whether smaller pore size will lead to larger extracted energy. If the latter quantity is referred to the electrode volume, W_V, the negative effect on W_S of increasing R is compensated for by the increase in total surface area ε, as both specific quantities are related as $W_V = W_S \frac{2}{R}$ (see Fig. 2.13d). This important aspect will be experimentally discussed in section 4.4.

Finally, it may be convenient, for comparison with other techniques, to have an estimation of the theoretical efficiency of the CDLE method. There is no definite way to do this, but one possibility is to compare the work obtained in one CDLE cycle with that achievable as proposed by Pattle [17]. Thus, the free energy decrease produced by the mixing of one cubic meter of 20 mM solution with a large volume of 500 mM would be 2.3 MJ. Comparing this value with the maximum energy extracted shown per unit volume of electrode in Fig. 2.13c (charging voltage around 200 mV), the maximum efficiency would be 32%.

2.5. The capmix cell as as an EDL capacitor

The capmix cell behavior is basically similar to a typical electric double-layer capacitor (EDLC), a type of supercapacitors. But whereas capmix cell takes advantage of the large changes in capacitance attained when the solutions are exchanged for producing electrical energy, EDLC are made just for storing energy.

An electric double layer capacitor stores energy by accumulating ions in the pores of two electronic conductor electrodes, such as activated carbon, bathed by ionic conductor like as organic or aqueous electrolyte. Another difference is that the capmix cell is designed to permit solutions exchange while commercial EDLC are always sealed with its own solution inside. Apart from these two main differences, the understanding of capmix cell processes and kinetics is closely related to the well-developed EDLC fundamental theory and its knowledge is essential to optimize salinity difference energy extraction by a porous electrode cell.

An electric double layer capacitor stores energy by accumulating ions in the pores of two electronic conductor electrodes, such as activated carbon, bathed by ionic conductor.

In this section, we will first analyze the fundamental characteristics of double-layer capacitors and afterwards, we will study two EDLC phenomena that may affect CDLE processes. These are: the unavoidable self-discharge mechanisms, whose control is important for optimizing energy extraction cycles, and the time-dependent redistribution of charge in porous electrodes, which strongly affects the initial charging process of the capmix cell.

2.5.1. Fundamentals

The storing of electrical energy for practical purposes in electrical double-layer capacitor (EDLC) was first proposed and claimed as an original development by Becker in 1957. He used for this first experiment a couple of carbon electrodes in an electrolytic solution. A few years later, commer-

cial double layer capacitors were originated in the Standard Oil of Ohio Research Center (Cleveland, USA) in 1961 and 1962 [89]. Since then, many developments involving a plethora of nanostructured materials prepared by deliberate design for double-layer capacitors electrodes has been extremely advantageous for enhancing electronic, ionic and molecular transport [90].

Ordinary capacitors have a very small amount of charge storage, that is, they have a low energy density. On the contrary, the EDLs of electrode/solution interfaces can reach up to 100 F/g due to the sufficiently large accessible electrode areas that are realizable, for instance, by high-area carbon powder. In this case, only an excess and a deficiency of electron charges on the respective capacitor plates have to be established on charge and the reverse on discharge. It is for this reason that electrical double layer capacitors charging and discharging processes are highly reversible.

However, in some cases of double-layer charging, partial electron transfer does occur, giving rise to pseudocapacitance. Pseudocapacitance is similar to the energy storage of batteries. In this case, the charge is achieved by an electron transfer that produces chemical state changes in the electroactive material according to Faraday's law (hence the term of Faradaic reactions). Indeed, the carbon material which has been chosen for salinity difference energy extraction, is far from being electrochemically inert and its reactivity has been extensively studied. Oxidation or reduction of the redox functionalities that are initially present in various carbon formulations give rise to electrochemical reactivity. Due to such reactivity, a significant redox pseudocapacitance arises together with the desired predominant double layer capacitance. In fact, with some carbon materials, it appears that the pseudocapacitance can amount to 5-10% of the total realizable capacitance and scales approximately with this last one. In this context, the pseudocapacitance effect in double-layer capacitors will enhance charge leakage and may be an important cause of self-discharge mechanisms [91].

2.5.2. Details of self-discharge mechanisms

EDLCs usually exhibit greater rates of self-discharge than do most battery electrodes. The reason is due to the ease with which the potential on charged EDL can be disturbed by an impurity or surface redox couple. The driving force of self-discharge is thermodynamically the same as that which provides current and power when the capacitance is discharged through a load resistance, but then the resulting process is one of controlled discharge, which is different from that for spontaneous self-discharge. This phenomenon diminishes its performance characteristics and should be controlled to improve such devices. Thus, the self-discharge behavior is a matter of major practical significance in EDLC operation. However, to date, very little work has been done to elucidate these self-discharge mechanisms.

It must be emphasized that an ideal, nonleaky capacitance, corresponding to the **ideally polarizable** electrode, never suffers self-discharge. Self-discharge of a charged capacitor can occur only if some Faradaic electron transfer processes can take place. Most double-layer capacitors fall long way below this ideal.

Although the actual explanations of this self-discharge are not completely clear, the following self-discharge mechanisms were mainly proposed [91, 92]:

1. If the capacitor has been **overcharged beyond the respective decomposition potential limit of the electrolyte**. In this case, the leakage process corresponds to a Faradaic charge-transfer reaction [93]. In terms of equivalent circuit representation, the charge leakage process corresponds to a potential-dependent Faradaic resistance R_f operating in parallel across the double-layer capacitance, its value increasing with declining potential.
2. If the capacitor material and/or its electrolyte contain **impurities** that are oxidizable or reducible within the potential range corresponding to the potential difference across the capacitor on charge, then the capacitor becomes to some extent nonpolarizable, again with Faradaic charge leakage currents that are potential dependent. Trace quan-

tities of transition metal ions can commonly occur as impurities in some carbons. Also, oxygen which is usually adsorbed on carbon materials, can be reduced providing redox reactions.

3. Self-discharge can also occur by **internal redox reactions** involving some of the functional groups, for instance, those of the quinonoid kind, commonly residing on the edges of graphitic particles.

4. If the whole device has **internal ohmic leakage pathways**, for instance, due to incomplete sealing of bipolar electrodes or inter-electrode contacts. Then, self-discharge will take place as though the capacitor were discharged slowly trough a load resistor.

5. Capmix cell has the particularity of not having been sealed as all commercial EDLCs. This could produce, at least in part, **oxidative effects on the carbon cathode** due to the interaction of oxygen dissolved in the feed water. This is based on the known phenomenon of carbon interaction with oxygen/water leading to positive charge of carbon surface and formation of a double layer consisting (in pure water) of hydroxyl anions. The process could be generalized schematically as:

$$C_{surface} + O_2 + 2H_2O \rightarrow C^{4+}_{surface} + 4OH^-$$

All these mechanisms could be included by the representation of a self-discharge equivalent circuit model shown in Fig. 2.14. Note that self-discharge of a capmix device differs in a significant way from that which may occur in a regular capacitor or at a single electrode. Two oppositely charged electrodes with their own EDLs are represented to clarify the role of its component. The essential difference is that a EDLC consists of two interfacial double-layer capacitances separated by an electrode resistance (R_e) plus usually a resistance in series (R_s, the solution resistance). Moreover, self-discharge can go on in either or both of the double-layer interfaces due to the already mentioned faradaic mechanisms. The corresponding resistances may not be the same. The reason is that one of the electrodes will be charged positively and the other negatively. That means that different types of redox reactions due to impurities might be present.

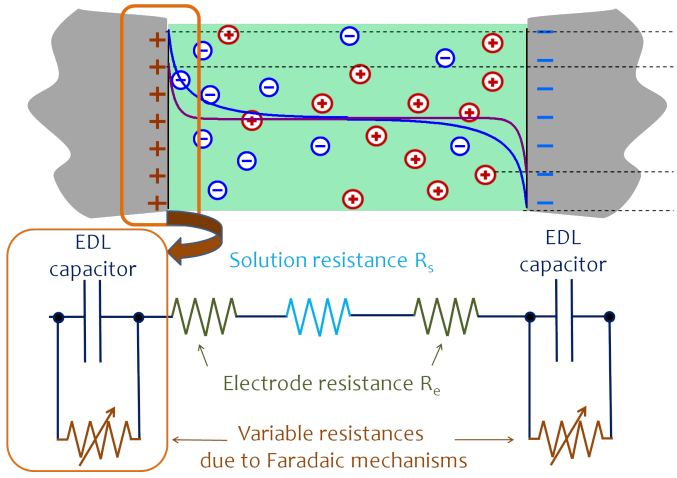

FIGURE 2.14: Up: Sketch of two oppositely charged electrodes. Down: Self-discharge equivalent circuit [91].

2.5.3. Charge redistribution at porous electrodes

As it is known, high surface area materials are chosen for EDLC (electrical double-layer capacitors) in general, and concretely for capacitive energy extraction methods, due to the large capacitance density and hence large energy density. In spite of these obvious advantages, important disadvantages arise with porous electrode material when a charging process is carried out. Two of the most important are: (1) the low values of the currents in the inner elements of the surface of the porous matrix and (2) the contact resistance of the particles constituting the porous matrix. Consequently, when a charging current goes through an electrolyte-containing porous electrode matrix, the available electrode area is not charged simultaneously at a uniform rate throughout the matrix. This can be understood by the schematic representation in Fig. 2.15 (left) of a single positively charged pore which could be part of a whole porous matrix. As it can be seen, it takes time for the negative ions to enter the inner part of the electrode. This means that although the measured current tends closely to zero, porous electrodes are far from being completely charged. This non-uniform current rate leads to the phenomenon called **charge redistri-**

bution. When the charging pulse is terminated, the electrical distribution of charge in the matrix will relax to achieve a uniform charge distribution across the distributed interfacial double layer. This will result in a decline of potential at the external region of the matrix at the expense of a progressively distributed increase of the voltage across double layers in inner regions.

The principle involved in this situation can be represented in an elementary way by a simple equivalent circuit with three or more capacitive and resistive elements as shown in Fig. 2.15 right. Upon charging by a voltage applied from an external source connected at AB, capacitor 1 will tend to be charged in a shorter time than capacitor 2,3...through R_1,R_2... This will appear phenomenologically as an aparent self-discharge of the capacitor network, as observed in relation to the potential measured at AB. This charge redistribution will continue throughout the CR network matrix until the open-circuit potential distribution becomes uniform within the matrix [91, 94].

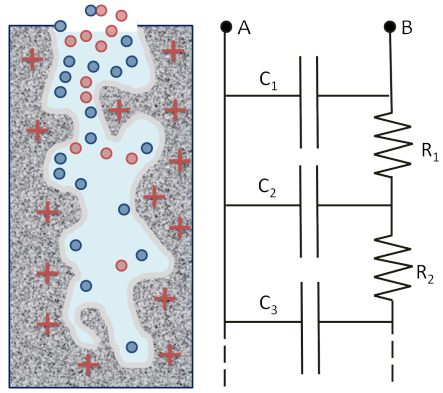

FIGURE 2.15: Left: schematic representation of the charge redistribution phenomenon on a single charge pore. Right: charge redistribution equivalent circuit.

This phenomenon is observed in the capmix cell mainly during the charging process. In this sense, it is very important to ensure uniform charging conditions throughout the whole porous matrix prior to setting up the CDLE cycle. However, in the experiments, this depends on the degree of wetting of the carbon particle. In fact, it has been found [95] that the frac-

tion of surface actually in contact with the solution is only around 10% of the total area, producing a unefficient exchange of salinity inside the pore. Hence, the pore distribution may play an important role and the apparent self-discharge might be just a redistribution of charge carriers [96, 97]. Therefore, strictly speaking, this is not only a self-discharge process in the sense of battery technology but it might be also affect capmix cycles in terms of extracted energy.

2.6. Summary and conclusions

In this chapter, we have presented the fundamentals of Capacitive double layer extraction (CDLE) method, which is part of the capmix techniques. With this aim, we firstly described in detail the electrical double layer at equilibrium and some models that throughout history has been used to properly describe it. Secondly, based on this theoretical basis, we expounded the principles of the CDLE technique and its associated energy production cycle. In CDLE, a pair of porous (typically activated carbon) electrodes are immersed in a high-salt (sea water, say) solution, and externally charged by connecting them to a power source. At constant charge (open circuit), low-salt solution (river water, for instance) substitutes the sea water, producing an electrical double layer (EDL) expansion, and subsequently an increase in potential. The energy produced comes from the recovering of part of the charge externally provided, but at that increased voltage. Thirdly, a thermodynamic analysis is needed in order to understand the basis that allows energy production by salinity exchange.

Afterwards, we have presented a model for the extracted energy in an ideal cycle of the Externally-Charged-Capacitive-Method. This model is based on the structure of the EDL for a cylindrical pore and takes into account the EDL overlap and the size of the ions (NaCl in this case). We have analysed the effect of the pore size and the ionic strength: as a rule, the stored charge is lower than that obtained without taking into account both the geometry and the possible overlap of neighbour EDLs. But the most significant effects are observed when the ionic size is considered. We find that there is a surface potential delimiting two regions with different be-

haviours: for low potentials the EDL qualitatively behaves as it does with point ion models but with important quantitative differences. At larger potentials important differences with respect to the point ion model are found, as follows:

- The EDL thickness increases with the surface potential, being larger than the Debye length.
- The capacitance C_d increases with the surface potential Ψ_S for low $|\Psi_S|$. At certain value of the latter, C_d reaches a maximum and displays a decreasing tendency with increasing potential. The position of the maximum depends on the ionic strength.
- For the smallest pore size considered, and potentials around 600 mV, the pore is saturated with counterions. As a consequence, both the capacitance and the extracted energy decrease to zero. This is not observed for larger pore size because saturation is expected for surface potentials larger than 1 V, the maximum value considered in this paper.
- The extracted energy per unit surface area increases (decreases) with pore size for low (high) potentials. Geometrical effects bring about an increase of the extracted energy per unit volume of electrode when the pore size is reduced and the surface potential remains moderate. which is the case of interest.

The model concludes that the ionic size limits the extracted energy that can be obtained with this method to far smaller values than those predicted for point ions. Also, in order to obtain the maximum energy, the electrode potential cannot exceed a value of around 200 mV.

Finally, electrical double layer capacitor theory offers an important view about how the CDLE cell behaves and some important aspects that should be taken into account in order to maximize the electrical energy production by mainly achieving a current leakage reduction.

3

Materials and Methods

We will now consider how the ideas described in our previous chapter can be implemented in practice. Recall that we need a conductor/solution interface in which the electrolyte solution contacting the solid can be exchanged in a controlled way. Additionally, we will develop a measurement procedure in order to obtain capmix energy cycles. In this chapter, we will first focus on the materials employed and afterwards, we will detail different methodologies that must be performed to extract energy by capmix techniques.

3.1. Materials

3.1.1. Capmix cell

The capmix cell consists of two parallel graphite collectors coated with carbon films and facing each other.

Capmix cell has been designed for this thesis [98]. Its design purpose is to serve as a compartment where water could be exchange among the two faced activated carbon electrodes which were already illustrated in Fig. 2.4. Fig. 3.1a shows a picture of this measuring capmix cell. As it can be seen, two electrodes must be situated facing each other. One part of the electrode is used as the electrical contact, and it is a graphite cylinder 2 cm in diameter and 0.5 cm thick (Fig. 3.1b). The other part built with an activated carbon film of the same area (Fig. 3.1c) placed on the top of graphite collector. The two electrodes are separated by a 600 μm plastic film spacer.

3.1.2. Porous electrode development

Carbon is an element almost uniquely suited for fabrication of electrical double layer capacitors. From an electrochemical point of view, this element is relatively, though not entirely, unreactive and thus has a potential voltage range of almost ideal polarizability, approaching 1.0 V in aqueous solution (detail in section 2.5.2). Moreover, activated carbon films are chosen in order to maximize charge exchange and the huge interfacial area

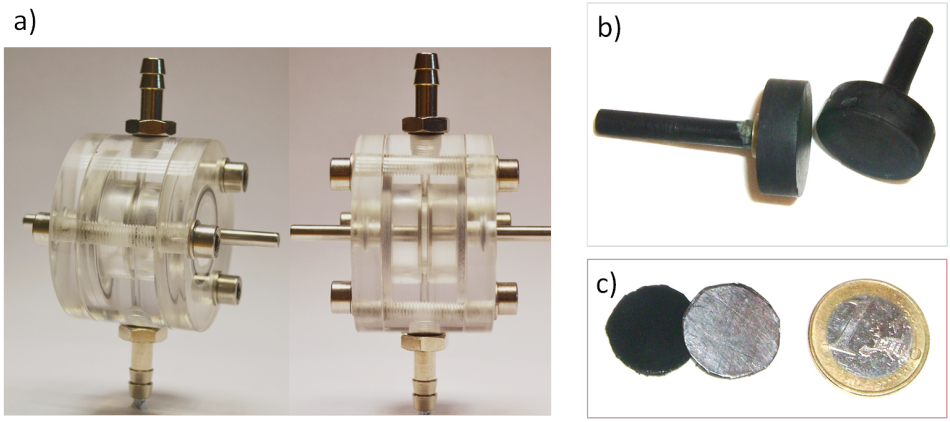

FIGURE 3.1: a) Picture of the capmix cell. Components of the capmix cell: b) Graphite collector and c) carbon films

of nanoporous carbon particles fulfill this condition. We can see an example of activated carbon particles in Fig. 3.2. It illustrates the geometry and internal structure of one of the samples, namely TE-11. Note that the particles are spherical in shape, with a rather wide size distribution. This in itself is not a problem, since a varied size distribution favours a better packing of the electrode. The internal porous structure is also visible in this high-resolution transmission electron micrograph.

The carbon films of Fig. 3.1c were made as described in [58], that is, by mixing activated carbon powder with a binder solution. The solvent used (1-methyl 2-pyrrolidone, NMP) was from Merck (Germany) and the binder, polyvinylidene fluoride (PVDF) was manufactured by Arkema (USA), under the tradename Kynar HSV 900. The method of preparation of the carbon films comprises first of all drying the carbon powder in an oven at 105°C for 24 h. Afterwards, the powder was mixed with a solution of PVDF and NMP at a concentration of 3% by weight. The dissolution was performed at 75 °C in a heated magnetic stirring plate. For the preparation of the carbon-binder slurry, 90 g PVDF solution was mixed with 26.93 g carbon and mixed in a ball mill grinder (Retsch, Haan,Germany), for 30 min at 450 rpm. Afterwards, the mixture was kept under moderate vacuum and finally cast on a graphite current collector assuring uniformity on the film

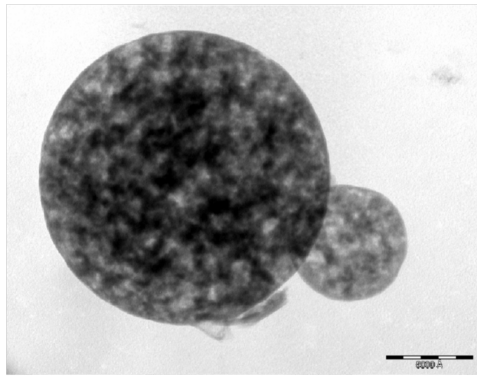

FIGURE 3.2: Transmission electron microscope of the TE-11 activated carbon particles used. The bar size is 500 nm. Sample provided by Mast Carbon Group.

(by, for instance, doctor blade, aerosol painting or simply painting).

Numerous activated carbon samples have been tested during this thesis. Most of them have been supplied by an UK company which is specialized in synthetic nanoporous carbons, Mast Carbon Ltd. In the following list, we sum up the description of the these mentioned carbon samples and Table 3.1 shows their specific surface area:

* **Samples SC-1 and SC-2:** SC-1 was prepared by activation (40% burn-off) of mesoporous carbon beads (250-500 μm in diameter) derived from mesoporous phenolic resin beads prepared by the patented method of Tennison et al. [99]. The carbon sample SC-2 was prepared by oxidation of SC-1 in air at 320 °C to give additional 15% burn-off and decorating the surface with oxygen containing functional groups [99].

* **Samples SR-03, SR-23 and SR-51:** SR-03 was prepared by straightforward activation at 900 °C (50% burn-off) of microporous granular carbonisate of phenolic resin [99]. Activation of the same carbonisate with carbon dioxide at 800 °C in the presence of catalytic quantities of calcium oxide resulted in preferential development of small mesopores to give samples SR-23 (35% burn-off) and SR-51 (44% burn-off).

* **Sample TE-11:** The synthesis of TE11 differed from the others in

the fact that the starting resin was intensively stirred to create very fine resin beads, and ethylene glycol was added as pore former. The samples were then vacuum-dried to remove this compound and activated to 35 % burn-off in CO_2.

* **Norit:** The powder was DLC Super 30, from Norit (The Netherlands), with a BET surface area of 1600 m^2/g.

TABLE 3.1: Specific surface area of Mast activated carbon samples.

Carbon Samples	Specific surface area (m^2/g)
SC-1	1423
SC-2	1489
SR-03	1870
SR-23	927
SR-51	959
TE-11	1170

In other cases, we have also used already manufactured activated carbon film. Concretely, we used Voltea carbon films by Voltea B.V., The Netherlands. These commercial available carbon films contain approximately 300 g per square meter of film.

3.1.3. Carbon particles characterization

The capmix concept relies on a physical concept for the EDL structure, in which only coulombic interactions are present. However, in real systems other water structure-mediated interactions can take place, like hydrogen bonding, hydrophilic-hydrophobic interaction, etc. In some cases, such forces are stronger than electrostatic ones and hence, a fixed charge in the inner part of the EDL appears. Due to the different kinds of ionic species that sea water has, it is more than probable that such fixed charge exists, this modifying the relation between charge and potential and affecting the capacitive mixing cell cycle. Hence, an exhaustive characterization of the charge at the Stern layer as well as a chemical analysis of the ionic species

and complexes present in the river and sea water is interesting. To reach this aim, we employed electrophoretic mobility measurements as a function of pH and the ionic concentration of a background electrolyte. The electrophoretic mobility was in all cases measured three times by triplicate in a Malver Nano ZS (Malver Instrument, UK), which work on the basis of the autocorrelation of the light dispersed by the partickes when they are moving under the action of the electric field.

When requiered, dynamic (or AC) electrophoresis was additionally used, for instance, in the characterization of the polyelectrolyte coating of the particles. In fact, it has been shown [77] that this quantity is much more sensitive than standard electrophoresis to the structure of the charged interface. For these experiments, we used an Acoustosizer II from Colloidal Dynamics (USA), based on the electrokinetic sonic amplitude (ESA) method. In this, an AC electric field with frequency between 1 and 18 MHz is applied to the suspension, and from the amplitude and phase of the induced ultrasound, the dynamic mobility (u_d) can be obtained as a function of the field frequency.

The wettability of the carbon samples was characterized via contact angle determinations at room temperature (20 $\pm$ 1 °C) using a Ramé-Hart 100-00 230 goniometer (USA) provided with a Pixelink PL-A662 CCD camera (Canada).

3.1.4. SE and CDP electrodes

In the CDLE technique the electrodes are used without treatment while in the SE technique the activated carbon films are coated with anionic and cationic polyelectrolytes. The coating was produced by keeping the commercial Voltea carbon films in contact with 50 mL solutions of the respective anionic and cationic polymer solutions under magnetic stirring during 24 h. After that time, the films were thoroughly rinsed with deionized water and the electrodes were placed on the cell as shown in Fig. 1.5. Two anionic polyelectrolytes were tested: poly (sodium 4-styrenesulfonate) or PSS, and poly(acrylic acid) or PAA. The cationic polymers investigated were PDADMAC (poly (diallyldimethyl ammonium chloride)) and PEI

(poly (ethyleneimine)). All of them were purchased from Sigma Aldrich (USA) and the typical molecular weights (M_w) selected were: 70 000 and 200 000 g mol^{-1} for PSS; 100 000-200 000 and 200 000-350 000 g mol^{-1} for PDADMAC; 15 000 g mol^{-1} for PAA and 2 000 g mol^{-1} for PEI. Fig. 3.3 shows the structure of the two main polymers used. Additionally, an alternative SE procedure was also tested which started by contacting the carbon particles (not the Voltea preformed films) with the standard PSS and PDADMAC solutions. We used Norit DLC Super 30 activated carbon particles. Afterwards, we dried out the particles and made the carbon slurry as described above [58]. This resulting slurry was cast on a graphite film.

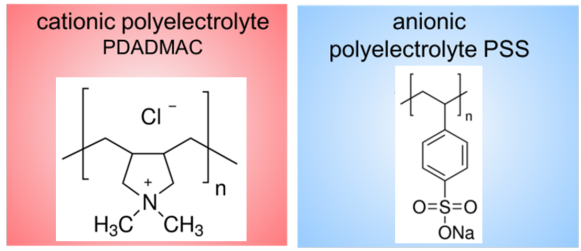

FIGURE 3.3: Structure of the two main polymers used: the anionic poly (sodium 4-styrenesulfonate) or PSS illustrated on the right, and the PDADMAC (poly(diallyldimethyl ammonium chloride)) on the left.

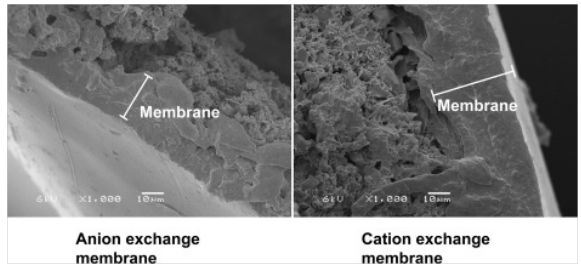

FIGURE 3.4: Scanning electron microscopy images showing the morphologies of the ion exchange membrane coating layers [60].

For CDP experiments, two ion exchange membranes from Fumatech (Bietigheim-Bissingen, Germany) were used covering commercial Voltea carbon films: an anionic membrane ionomer (FAS solution, 24 wt% in NMP) and a cationic membrane ionomer (FKS solution, 17 wt% in NMP). Scanning electron mi-

croscopy (SEM) images of cross-sections of the ion exchange membranes, each at a magnification of 1000, are shown in Fig. 3.4. A dense membrane structure 20-40 μm thick, with no pores, can clearly be seen in the SEM image of each type of membrane [60].

3.1.5. Capmix stacking

Capmix stacking is needed to explore methods for adding individual cells in order to increase the amount of energy that can be extracted from blue energy by capmix methods. To reach this aim, we focus on finding optimum configuration of the multi-electrode setup. Fig. 3.5 shows two different stack designs that have been tested. Fig. 3.5a shows a scheme of the individual cell association designed in stack#1, based on our optimal device, already described in section 3.1.1. As shown in Fig. 3.5a, the cell consists of several units. In the case of two and three units, the central films were obtained by coating both sides of the graphite substrate with the activated carbon layer.

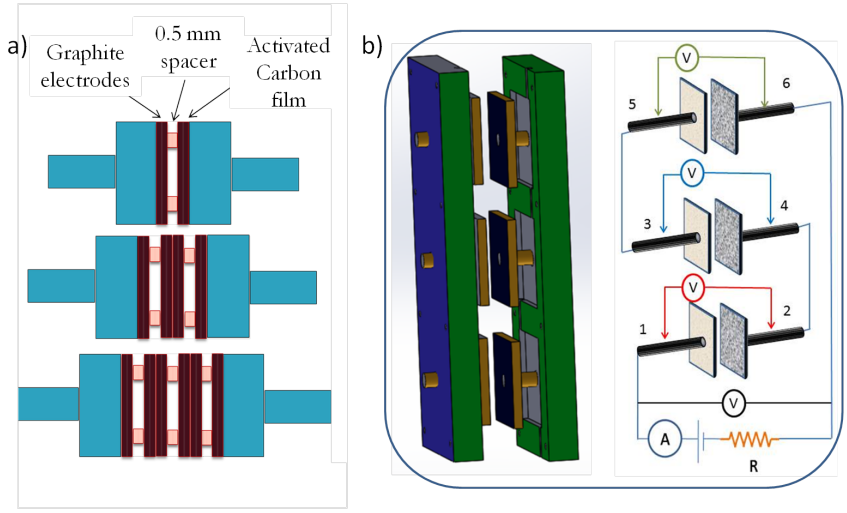

FIGURE 3.5: a) Sketch of the association of individual cells used in stack#1. b) (Left) Sketch of stack#2 configuration. (Right) Electrical connection in series of the sealed stack.

With the aim of analyzing the behavior of every unit in the stack, we

designed the stack#2 (Fig. 3.5b). In this case, the carbon films were cut into 30×30 mm^2 pieces and placed in contact with square graphite collectors. This stack is basically the same configuration as stack#1, but individual determinations of voltage are possible for each cell. All the electrodes are in contact with the same solution bath, but now adjacent cells are externally connected.

3.1.6. River and sea water solutions

Salty and river water solutions reservoirs are placed some 50 cm above the capmix cell level, and two electrovalves were employed for filling the capmix cell (Fig. 3.1a) with the corresponding solution through the bottom tube. Synthetic solutions of seawater and rivers were made at the laboratory with respective concentrations 30 g/L and 1 g/L of sodium chloride (Sigma Adrich, USA), which is equivalent to approximately 500 mM and 20 mM. The water used in the preparation of the solutions was deionized and filtered in a Milli-Q Academic system from Millipore (USA).

For some experiments, both real and simulated sea waters were also used. According to literature [100], simulated sea water (SSW) must contain the amounts of salts detailed in Table 3.2.

TABLE 3.2: Salt concentrations used for simulated sea water [100].

Salt	Concentration (mmol/L)
NaCl	400
$MgSO_4$	20
$CaCl_2$ $2H_2O$	10
$MgCl_2$	20
KCl	10
Br	1.7

Real samples for capmix experiments were taken from two different sources: in the Mediterranean sea, near the southern coast of Spain (Mediterranean real sea water, MRSW hereafter) and in the Gulf of Fonseca, a protected area of the Pacific Ocean, located in the middle west Central America,

among Nicaragua, Honduras and El Salvador. In order to check for the possible negative effects of either organic or inorganic particulate material in real sea water from the Mediterranean sea, some experiments were also conducted after previously filtering the water through 16, 11 and 5 μm pore size. These water samples will be denominated 16MRSW, 11MRSW, and 5MRSW, respectively. The alternatives for river water simulation were 1/30 dilution of MRSW.

For the oceanic real water samples case, three samples of river water were used: El Rebalse, Amatillo river and Pavana river. Seawater was taken in Puerto de la Union. The Gulf of Fonseca was chosen because of its hydrographic richness. Sea water at the entrance of the Gulf is characterized by a high salinity, about 35 psu (psu: practical salinity unit, it is equivalent to 1 g/L). Upstream, on the contrary, it is found a huge salinity decrease down to 1 or 2 psu [101]. This fact makes the Gulf of Fonseca an ideal place for blue energy studies.

3.2. Methodology

Two kinds of different capmix experiments can be carried out in order to perform energy extraction cycles. The difference depends on which remains constant during the charging and the discharging process, either the voltage or the current. In the first case, a power source is employed to fix the potential and in the second one, a current source guarantees that the closed circuit processes are performed at constant current. Fig. 3.6 shows an example of a CDLE experimental cycles where the two mentioned modes are carried out: constant voltage and constant current method. On both cases, it can be seen how the Capmix cell of Fig. 3.1a is connected to an external circuit where the voltage between both electrodes and the current going in or out of the cell is measured as a function of time. A Keithley 2700 (USA) bench multimeter and A PIC microcontroller (PIC16F684, Microchip Technology Inc., USA) were used for measuring and performing the different stages of the process at specified intervals while recording the data with a 7700 data acquisition card.

- **Constant Voltage Mode (CV)** It is basically what it has been already explained in section 2.2. Fig. 3.6a shows CV mode external circuit and at the same time, a representation of the potential and current as a function of time.
- **Constant Current Mode (CC)** This mode is represented in Fig. 3.6b. A constant current is firstly applied to the capmix driving the potential to a certain value (black line). The circuit is opened and fresh water provokes a potential rise in the cell (red line). Finally, the circuit is closed again and the current is forced in the opposite direction until the potential is again close to the same initial value (green line). The end step involves the entrance of salt water in the cell and the subsequent decrease of the potential is recorded (blue line).

It is worthy noting that in the discharging step (green lines in Fig. 3.6) there is a sudden decrease of the potential difference, followed by a slower decay. The first corresponds to the voltage drop inside the solution which depends on the value of the solution resistance (as shown in the equivalent circuit of Fig. 2.14) and the discharge resistor (or equivalently, discharge current value). This ohmic losses can be minimized to a certain limit by choosing an appropriate discharge resistance or current and by decreasing the distance between electrodes. Hence, part of the energy is not extracted but dissipated in the solution.

At every time the charge can be calculated by integration of the current vs. time representations in Fig. 3.6. Indeed, the black shadowed area corresponds to the delivered charged by the voltage or current source during the initial charging step, and the green shadowed one indicates the extracted charge during the discharging process after the voltage rise in fresh water.

The energy as a function of time can be calculated as:

$$E(t) = -\int_0^t V(t')I(t')dt' \tag{3.1}$$

where V and I are the measured voltage and current and hence, E(t) is the actual energy that exits the cell. Finally, the power is obtained as the average slope in the curve E(t) in successive cycles.

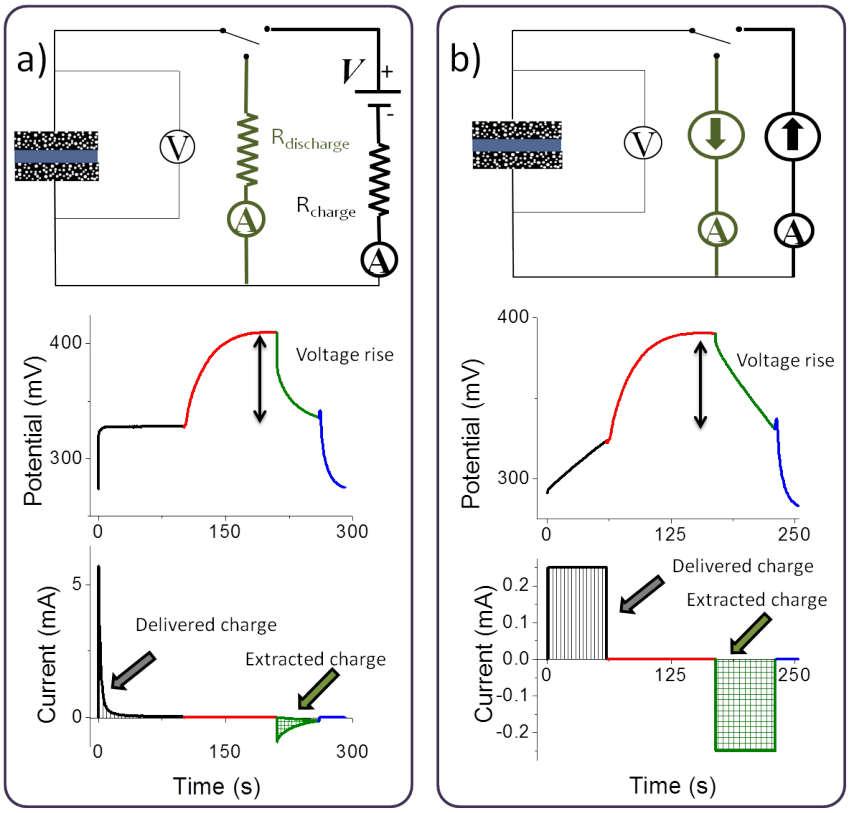

FIGURE 3.6: External capmix circuit and experimental measurements during a CDLE cycle: Current intensity vs. time and potential difference between the cell electrodes vs. time. for constant voltage (a) and constant current (b) mode. Sample: SR51 film.

4

Considerations for CDLE optimization

4.1. Introduction

Theories of EDL capacitance for CDLE (more details in section 2.4) predict that the voltage rise when salty and fresh water solutions are exchanged is about 80 mV on each electrode, while the surface charge density typically changes by 0.05 C/m^2. This means that in a complete cycle the energy obtained should be around 4 mJ per square meter of EDL. Furthermore, taking into account that the experiments are carried out with activated carbon or similar material with a specific surface area of $\approx$1000 m^2/g or more, the energy that might be made available could amount to 4 J/cycle with just 1 g of carbon per electrode. A power density estimation can be given: assuming that the mass of carbon is distributed on an area of 20 cm^2 (this would be the apparent electrode area), and that the cycle duration is 100 s, the power available would be 2 W/m^2, if the efficiency is 10 %. In contrast to RED and PRO, the predicted amounts of energy for CDLE are way larger than those experimentally achievable. In this situation, it is clear that further research is needed in order to increase the amount of energy and power available. Therefore, the main topic of the present chapter is the analysis of several experimental parameters that may reduce the existence of charge leakage by progressive discharge of the EDL, the incomplete wetting of the available pore area, hydrophobicity, oxidation of the activated carbon, etc. to improve the present situation towards the optimization of the CDLE cycle performance.

Firstly, it will be necessary to investigate some **operational issues** of the different cycle stages, going from the effect of the potential difference applied during the charging step to the optimum initial charging time. Moreover, a deep analysis of the cycle leakage is required in order to understand its effect and maintain acceptable energy extraction cycles.

On the other hand, we will consider the change in capacitance associated to another parameter apart from salinity variations, **temperature variations**: the capacitance decreases when temperature is raised, and hence, a cycle is possible in which some charge is put on the electrode at a certain temperature and returned at a higher one. We demonstrate experimentally that it is viable to obtain energy from electric double layers if these are suc-

cessively contacted with solutions at different temperatures. In addition, we theoretically and experimentally show that temperature and salinity variations can be conveniently combined to maximize the electrode potential increase and energy production.

Finally, it can be expected that the **carbon characteristics**, in particular, hydrophilicity of the pore walls, and pore structure, will be determinant. In fact, it is well known that the electrochemical response of EDL supercapacitors is strongly dependent on the degree of matching of the pore and solvated ion sizes. Additionally, **other salinity difference sources** have been analyzed giving way to brine and brackish water solutions which could be used to maximize the extracted power and reduce its environmental impact at the same time.

4.2. Operational issues on cycling efficiency

In this section, we present the work that has been done to increase the whole efficiency of the process. Firstly, we analyze the impact of current leakage on the overall cycle shape and subsequently, we carefully examine two experimental parameters: source voltage value and initial charging time.

4.2.1. Preliminary aspects of current leakage

Current leakage consists in the tendency of the charged electrodes to move towards a given "spontaneous" potential. Fig. 4.1 shows this effect on three consecutive cycles at constant voltage (a) and constant current (b) mode, both representing the cell potential versus the measured charge. Although caused by the same effect, opposite behaviors can be found on both representations: in constant voltage mode, cycles move towards the right, to higher charge values while at constant current, they shift towards lower potentials as it is indicated by the respective arrows.

As said, it should be noted that these behaviors are caused by the same unavoidable current leakage effect. When the voltage is fixed (Fig. 4.1a), the charge that is stored in the cell (delivered charge) is not completely re-

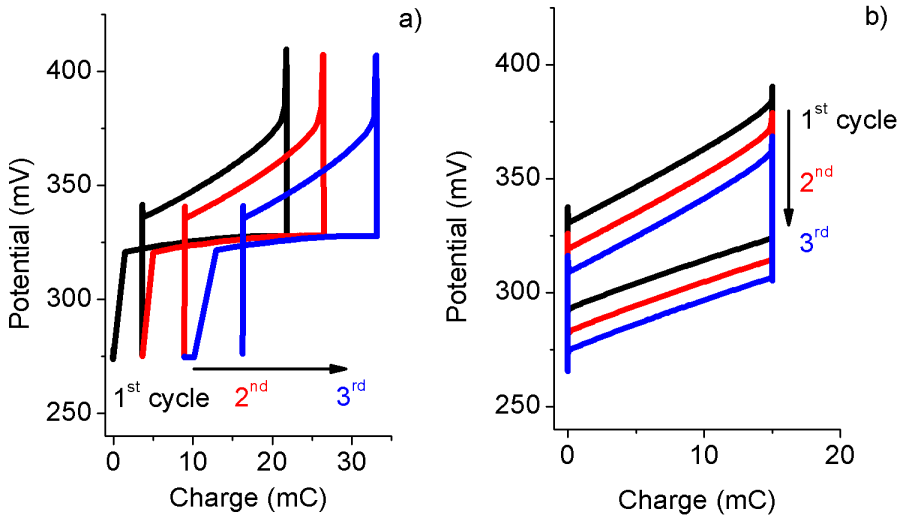

FIGURE 4.1: CDLE cyles represented by cell potential versus charge at constant voltage (a) and at constant current (b) mode. Sample: SR51 film.

covered in the discharging step (extracted charge) and these unbalanced values produces a cycle shift of approximately 0.01 mC/s. On the other hand, when the charge is fixed through constant current cycles (Fig. 4.1b), leakage current results in a decrease of the cell potential of about 0.05 mV/s. This effect manifestly points out the current leakage effect, which causes an important reduction in terms of the total extracted energy per cycle and may lead to an overall negative power.

In fact, dissipated energy caused by current leakage, although always present, becomes more apparent at constant voltage mode where the absence of current source does not force delivered and extracted charge to agree completely. Fig. 4.2 clarifies the significance of this effect by representing the cell voltage as a function of charge for the cycle of Fig. 4.1a. The green colored area in Fig. 4.2a represents the energy delivered by the power source during the charging step, and the purple one the recovered energy during the discharging step. It is easy to realize the width difference of both areas due to the mentioned charge imbalance. Fig. 4.2b shows the extracted energy and the lost energy. As it is known, the actual extracted

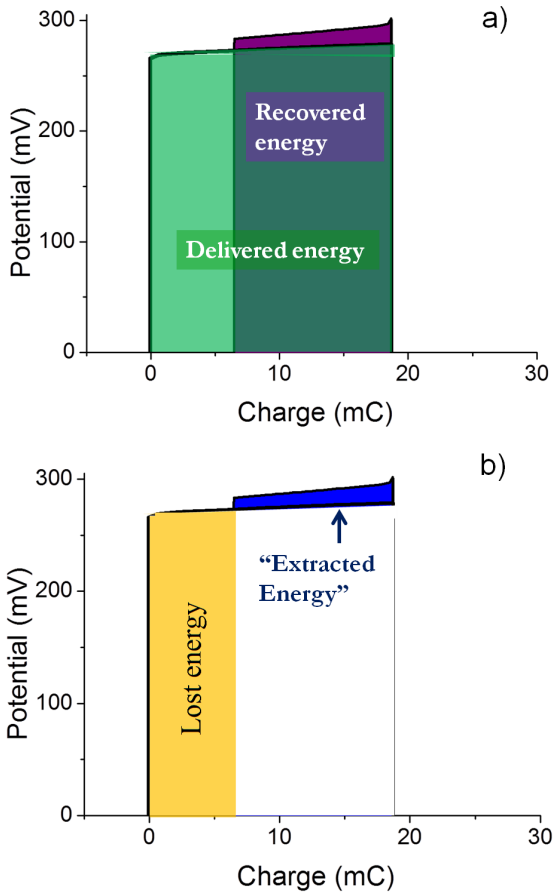

FIGURE 4.2: CDLE cyles represented by the potential difference between the electrodes vs. measured charge. Sample: SR51 film.

energy would be the difference between the delivered and the recovered energy. In an ideal condition, the blue colored area in Fig. 4.2b would be the extracted energy. However, in many cases, due to the leakage current, the presence of the lost energy represented by a yellow area in the same Fig. is unfortunately representative. This causes that the extracted energy should overcome these losses and even though this may happen, the actual extracted energy is clearly diminished.

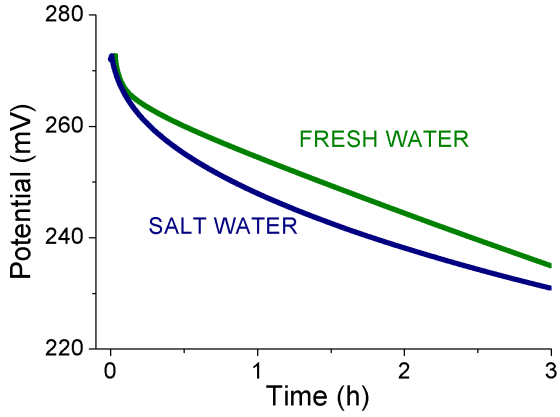

FIGURE 4.3: Potential as a function of self-discharge in salt and fresh water. Sample: SR51 film.

Once the impact of charge leakage is recognized on the overall cycle shape, it is key to explore if it is due to the self-discharging that has been largely studied in the EDL supercacitor literature (more details in section 2.5.2). To check for this, self-discharge measurements have been carried out. Self-dicharge can be measured by simply recording the potential difference between the two terminals of the supercapacitor at open circuit as a function of time after charging. Fig. 4.3 shows the CDLE cell voltage decrease by the self-discharge process for salt water and fresh water solutions. In this case, the voltage decay ratio is about 0.03 mV/s and 0.04 mV/s for salt and fresh water respectively for the first 100 seconds. Likewise, in Fig. 4.1b, we determined that the voltage decay ratio is approx. 0.05 mV/s. This could lead to conclude that both voltage decay ratios are quite similar in terms of order of magnitude and are likely to be explained by the same phenomenon. That is to say, the current leakage observed in all CDLE cyles is not more than the proper self-discharge of a typical supercapacitor and hence, the knowledge of the mechanisms that explain self-discharge in supercapacitors are likely to explain CDLE leakage processes too.

4.2.2. Working potential value

Although one could think that the potential rise is an intrinsic property of the EDL, the effect of the potential difference applied during the charging step might also affect the whole process even if the voltage is kept below the minimum value for faradaic reactions. In fact, such an effect was observed in the earliest implementations of the methods [49]. To avoid such faradaic reactions, the potential applied to the electrodes should never be higher than approximately 1 V [91], but below that value we have a whole range of working potentials, and their effect on the CDLE performance must be considered. This is illustrated in Fig. 4.4, where CDLE cycles are plotted for SR51 carbon film in the form of cell voltage vs. charge (a), together with the voltage rise, transferred and delivered charge (b), for different working potentials. This Figure demonstrates that:

- The voltage rise always increases for the studied working potentials, that is, less than 550 mV.
- Delivered and extracted charge also increase from around 2 mC to approximately 15 mC for the highest potential. This fact produces wider cycles as can be seen in Fig. 4.4a.
- The difference between the extracted and delivered charge undergoes a similar dependence on working potential, but even increases with it. This situation far from being favorable is the main cause of the CDLE cycle leakage. The reason is that we are far from the ideal situation of recovering the whole delivered charged.

These results offer a clue as to the optimum working conditions in the CDLE technique, but their justification is by no means straightforward. When the potential used for charging is raised, an effect not considered in equilibrium models is evidenced [51], and that is the self-discharge of the electrodes, because of current leakage [49] which is higher the larger the applied voltage. Overall, this goes against the extracted power as it can be seen in Table 4.1 where at the highest potential (512 mV) there is not a positive extracted power. On the contrary, the optimum working potential is found at an intermediate potential (340 mV) where the potential rise

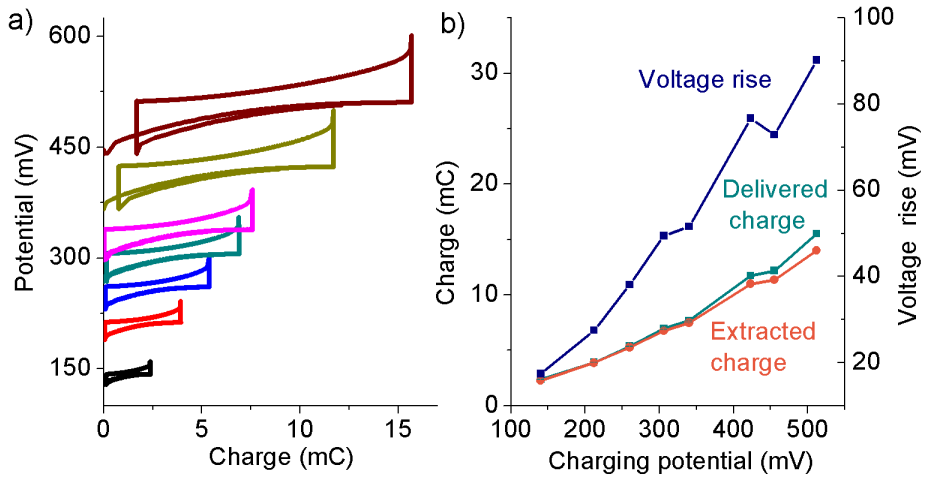

FIGURE 4.4: a) Measured charge as a function of cell voltage of the CDLE cycle for different working voltages in cells built with SR51 carbon films (a). CDLE cycles represented by cell voltage as a function of measured charge b) Voltage rise, extracted and delivered charge obtained for different charging source potential. Sample: SR51 film

TABLE 4.1: Extracted power for different working potentials.

Working potential (mV)	Extracted power (mW/m^2)
140	0.04
212	0.32
260	0.42
306	0.74
340	1.04
423	0.57
455	0.18
512	–

as well as the extracted and delivered charge are not as high as they could be but are able to compensate for the mentioned leakage.

4.2.3. Initial charging conditions

Initial charging conditions strongly determine CDLE cycle performance and should be considered carefully. The charge resdistribution effect (details in section 2.5.3) takes place at the porous electrodes during the inital charging process: short after disconnecting for solution exchange, the cell potential undergoes a rapid decrease, prior to a more monotonous trend. This is the charge redistribution inside the pores, as in fact demonstrated by the absence of such rapid decline if the charging times are enlarged [91]. Note that the discharge process takes a few hours if charging time has been long enough as to avoid charge redistribution (see Fig. 4.3). Therefore a protocol was followed to charge the capmix cell. This is resumed in the following stages:

- Charging cycles should be compounded of several cycles of flowing salt water at open circuit during 30 seconds and charging at constant voltage for 500 seconds.
- The whole charging process should last not less than two hours. However, it has been found that charging overnight improves the results by principally decreasing current leakage.
- An appropriate charging process has been carried out when after opening the circuit, the voltage decay between electrodes is not more that approx. 0.5 mV/s.

4.3. Temperature influence on CDLE

There are many industrial processes where water is used as coolant, and returned to the cold water reservoir, so that a mixture is produced of hot and cold fluids. The temperature gradient between them can be quite high in the case of thermal power plants, where heat transfer from hot to cold reservoirs is the most widely exploited route for producing electrical energy, but whatever the process where refrigeration is required, exergy is wasted by simply mixing the two kinds of water. Although temperature differences between the water input and output are hardly above 20°C, af-

ter being refrigerated in the power plant, waters near geysers or thermal waters in volcanic areas can reach 85°C or more.

In this section we propose taking advantage of solution temperature differences in the direct production of electrical energy. This can be done by properly using the capacitance changes induced in microporous electrodes by both a temperature and salinity difference. In fact, from Eq. 2.12, a change in the capacitance of the EDL is produced not only by changing the salinity of the solution in contact with the interface but, additionally, by changing the permittivity of the solution, by, for instance, increasing or reducing its temperature. Specifically, an increase in temperature produces a decrease of the electric permittivity of water, and, thus a decrease of the differential capacitance. As a consequence, a larger electrode potential for given charge is produced.

Double Layer Permittivity Exchange method aimd to obtain electrical energy from just temperature difference among two water solutions.

In the case there are no salinity differences between the solutions used, but just temperature variations, we propose to denominate it DLPE (or **Double Layer Permittivity Exchange**) to this technique. In Figures 4.5, we present a cycle designed for obtaining electric energy from just temperature differences. At the first stage the electrodes are externally connected to a battery with potential difference V in the presence of cold water. At equilibrium, the same potential difference will be established between both electrodes. Each of them will acquire a surface charge equal to σ_{min} in absolute value, and a potential difference $|\Psi_S| = |V|/2$ with respect to the solution in the space between them. Then, in open circuit, cold and hot waters are interchanged (step 2 in Figure 4.5). As a consequence of the temperature increase, the permittivity decreases and so does the EDL capacitance. Since the circuit is open, this provokes an increase of the electric potential to $|\Psi_S| + |\Delta\Psi_S|$ at the electrode-solution interface. In order to take advantage of this increase in potential, we next discharge the electrodes (step 3) over the external source. Since the potential of the electrodes is larger, some charge will spontaneously migrate to the battery at a larger potential, resulting in a positive energy balance. A new equilibrium is at-

tained, and the potential returns to the initial value but with a difference surface charge σ_{max}. For closing the cycle, we exchange hot by cold water in open circuit (step 4). Finally, we connect again the battery to the cell filled with cold water (step 1) and return to the initial potential and charge density values.

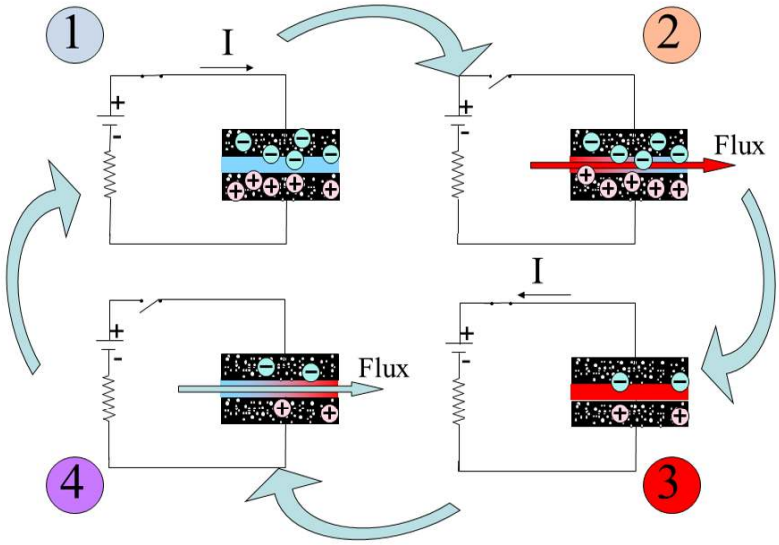

FIGURE 4.5: Cell processes during every step of the DLPE cycle (1: cell charged in cold water; 2: hot water in 3: electrode discharge. 4: cold water in.)

Thus it is possible to use the temperature gradients that are generated in rivers when their water is used in industrial processes, even if such water is only used for refrigeration and no contamination other than thermal one takes place. Additionally, the mixture of hot river water and cold sea water (as in the mouth of a river coming into a much colder ocean, mostly if the river water has been previously employed in the refrigeration of power plants) may be advantageous as well, by adding the effect of temperature changes to that of ionic contents differences.

Exploiting the temperature effect on energy production systems is an idea present in other techniques. For instance, Sales [102] has recently proposed to use the so-called **thermal membrane potential**: an electric potential is

generated when hot and cold waters are contacted with anion and cation exchange membranes, respectively. That potential can be used in energy production by charging carbon electrodes in contact with the membranes, and discharging them through the external circuit. This is a modification of the capacitive mixing procedure known as CDP.

In this section, we show some results concerning the implementation of CDLE with temperature differences between the two solutions used in the exchange process. A theoretical model based on cylindrical geometry for the electrode micropores is described and its predictions discussed. Experimental results are also offered, and their agreement (at least qualitative) with the theoretical description is analyzed [95].

4.3.1. Theoretical predictions

The model used for the description of temperature influence for obtaining electric energy from salinity differences is basically the one already presented in section 2.4. Hence, we perform a mean field analysis of the structure of the EDL, and so, the electric potential distribution will be given by Poisson's equation (Eq. 2.1) where the temperature dependence of the electric permittivity of the solvent is implicitly indicated. For this work, the permittivity values of Table 4.2 were used at every temperature.

TABLE 4.2: Relative permittivity of water for different temperatures.

T(°C)	ε_m	T(°C)	ε_m
15	82.2	50	69.9
20	80.4	55	68.3
25	78.5	65	65.2
35	75.0	80	60.8
45	71.6		

This equation will be solved subject to the boundary conditions given by Eq. 2.17 and Eq. 2.18, and the relation between the ionic concentration and the electric potential at any point will be taken from the approximation of Eq. 2.20 which takes into account the excluded volume of ions. Since the

most abundant ions in natural waters are Na^+ and Cl^- we will restrict the analysis to this salt, although a more general solution composition can also be considered (as largely studied in section 6.2). Note that, as it has been explained, we also take into account the excluded volume between the particle surface and hydrated ions. Hence, Eq. 2.1 must be solved separately in different regions using the boundary conditions between every pair of regions from Equations 2.21. With the previous equations, the potential profile can be calculated as a function of surface potential, pore size, ionic concentration, and, in our case, temperature. The surface charge density, σ, can be obtained from Eq. 2.5. Finally, the extracted work in every cycle is calculated using Eq. 2.13 but it can be particularized for DLPE method where simply hot and cold waters may be exchanged:

$$W_S = \int_{\sigma_{min}}^{\sigma_{max}} \left[\Psi_S(\text{hot}) - \Psi_S(\text{cold})\right] \mathrm{d}\sigma \tag{4.1}$$

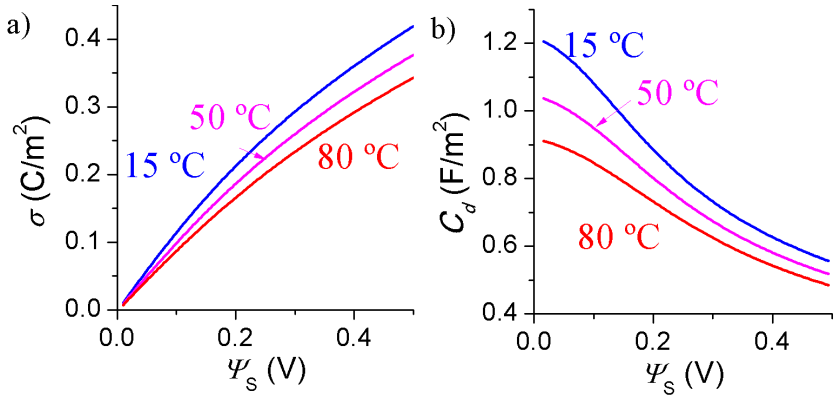

FIGURE 4.6: Surface charge density (a) and differential capacitance of the EDL (b) as a function of the surface potential for the temperatures indicated. Ionic concentration 2 M NaCl. Pore size: 5 nm. Ionic radii: Na^+ 0.36 nm and Cl^- 0.33 nm.

The predictions of this model are presented in Figure 4.6. Note how, as expected, both the surface charge density and the differential capacitance per unit area, C_d, decrease with temperature. It is also noticeable that the capacitance decreases with the surface potential instead of increasing with it as expected, due to the fact that a larger surface potential cannot be com-

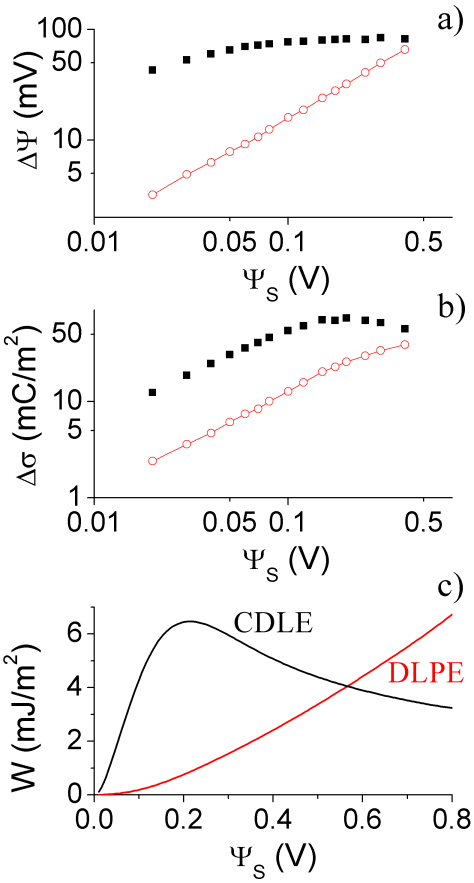

FIGURE 4.7: Theoretical results of a) potential jump in step 2, that is, when the cell capacitance changes from high to low by means of either salinity (CDLE, full squares) or temperature (DLPE, open circles) variations. b) Surface charge density exchanged between the external battery and the electrodes in the discharging step (Figure 4.5). c) Extracted work as a function of the potential difference between the electrode and the solution. Pore size: 5 nm. In DLPE: NaCl concentration: 0.5 M, temperatures 15 °C and 50 °C; in CDLE: temperature 15 °C, NaCl concentrations: 0.02 mM and 0.5 M.

pensated for by a larger accumulation of finite-size ions near the surface.

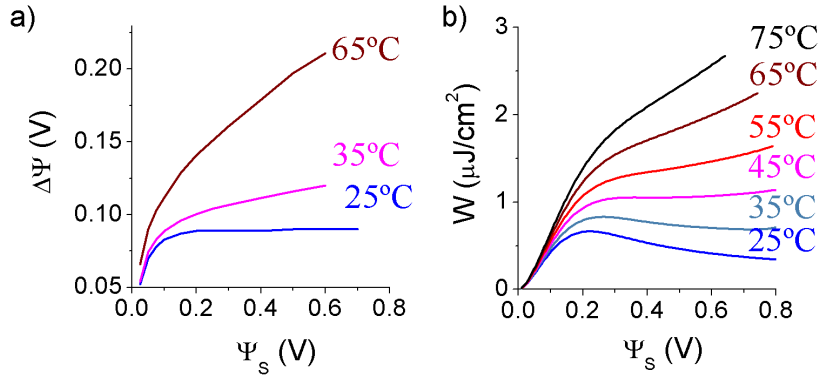

FIGURE 4.8: Theoretical results of the potential rise $\Delta\Psi$ (a) and extracted energy per unit interfacial area in CDLE+DLPE cycles (b) as a function of the electrode potential Ψ_S. Sea water in all cases: 25 °C. The temperature of the river water is indicated. Pore size: 5 nm. Sea water 0.5 M NaCl; River water: 0.02 M NaCl.

In Figure 4.7 we show the theoretical predictions of DLPE cycles as compared to CDLE ones. One important characteristic of the CDLE cycle is that the dependence of the potential rise $\Delta\Psi$ on the external charging potential reaches a plateau value for moderate electrode potentials (Figure 4.7a). In the case of the charge exchanged, $\Delta\sigma$, a maximum value is predicted (Figure 4.7b), so that beyond a given external voltage the exchanged charge and hence the extracted energy decrease, reducing the efficiency of the process [54], as shown in Figure 4.7c. In [54] it was shown that the maximum extracted energy comes out as a consequence of the predicted decrease of the differential capacitance of the salty water below that of the river water, beyond a given wall potential. Such effect has the consequence of a lower exchanged charge between the electrodes. Interestingly, this is not the case with DLPE: we can increase both the potential drop and the exchanged charge by increasing the electrode potential Ψ_S. We expect, hence, that at a certain potential the extracted energy in a DLPE cycle turns out to be larger than that achievable by means of the standard CDLE method (Figure 4.7c). From the comparison between CDLE and DLPE we can conclude that in general the salinity difference is a better technology, and that the potential

advantage of the new proposal is the large availability of water with thermal gradients. In addition, it is, in principle, possible to find a working voltage above which it would be feasible to use DLPE with advantage as long as a temperature difference of about 35 °C is available.

Considering that they stem from similar principles, it will be clear that DLPE and CDLE are not incompatible. We can perform a cycle in which cold salty water is exchanged with warm river water in a sort of **CDLE+ DLPE** technique. Theoretical predictions in Figure 4.8 confirm the advantage of this approach: we can expect to have a monotonous increase of the voltage jump, and thus, of the extracted energy with the working potential. Furthermore, the energy extracted can be up to five times larger if river water is 50 °C above sea water. Even for more realistic temperature differences (45 °C to 25 °C, say), a factor of two in the energy gain is achievable.

4.3.2. Experimental Results

DLPE demonstration

In Fig. 4.9a we show an example of the voltage between electrodes in a DLPE cycle. For this example, we have used 20 mM, which is a reasonable value for the salt concentration of a typical river. The stages of Fig. 2.6 are clearly distinguishable for the case where hot and cold waters are exchanged. In particular, the above figure demonstrates that upon exchanging cold by hot water, the voltage increases. A note must be added concerning the possibility of generation of thermoelectric effects in the hot-water stage. If it is assumed that the cables connecting the cell to the voltmeter are 0.5 m long, and taking into account that the thermoelectric power of Cu is 4 μV/K, it can be estimated that at most 0.2 mV could be added to the voltmeter reading, but this value is about 20 times smaller than the maximum voltage measured in DLPE.

CDLE and DLPE compared

In Fig. 4.9b succesive cycles like that in Fig. 4.9a are shown in comparison with CDLE cycles. We can observe that the values of V_{cell} are lower in DLPE than in CDLE cycles, for otherwise identical charging conditions. Note that because the extracted work depends on both the charge exchanged with the external voltage source and the potential jump under solution exchange, and both are lower in DLPE, we can predict a reduced extracted work with the latter technique. However, we can improve on these results, as described below.

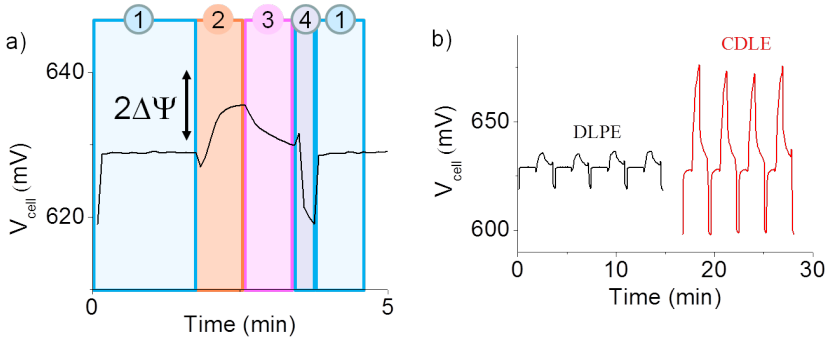

FIGURE 4.9: Experimental results of the cell potential, V_{cell}, as a function of time. a) A single DLPE cycle. $|\Delta\Psi|$ is the voltage jump in each electrode. b) Succesive cycles of DLPE (black) and CDLE (red). Charging voltage $V = 630$ mV; solution used in DLPE: 20 mM NaCl at 25 °C and 50 °C; exchanged solutions in CDLE: 20 and 600 mM NaCl at 25 °C.

Both techniques together

A clear way of improving on both DLPE and CDLE used separately is the use of both techniques together. Data in Fig. 4.10 proves that optimum conditions can be found in which properly combining temperature and salinity differences makes it possible to maximize the voltage rise in the mixed CDLE+DLPE technique. If 600 mM is the concentration of the sea water and 25°C its temperature, $\Delta V = 2\Delta\Psi$ can be as high as 80 mV if the river water (20 mM NaCl) is at 75°C. Note however that upon increasing the salty water concentration up to 1 M the improvement is reduced and

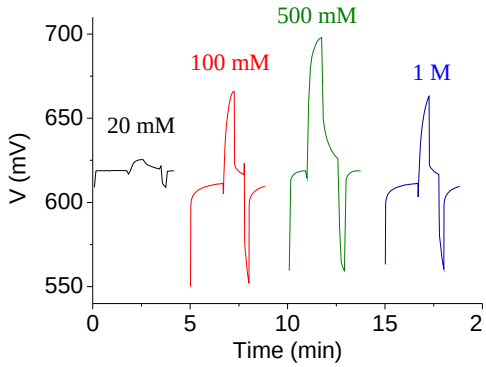

FIGURE 4.10: Experimental voltage between electrodes as function of time for CDLE+DLPE cycles in which a 20 mM NaCl solution at 75 °C is inside the cell during the discharging step while the charging steps are performed with a solution of the concentration indicated and at at 25 °C.

the advantage of using higher salinity is compensated for by a likely larger loss associated to the high conductivity of the solution.

In fact, the presence of charge leakage can be made clear when considering the experimental charge-potential cycles, similar to that shown in Fig. 2.6. From the measurement of both the current through the external load and of the cell voltage, together with the cycle duration (Figures 4.11) it is possible to evaluate the charge-potential cycle, and the results are plotted in Fig. 4.12. Note that the area of the cycle increases with the river water temperature (and so does the energy extracted, in consequence), and furthermore the cycles do not close properly, indicating charge losses, mentioned in detail in this thesis (section 2.5.2).

The increase of energy density obtained with river water temperature is explicitly shown in Fig. 4.13a. Even if the temperature difference available is moderate (35-55°C) the power can be increased by a factor of 2-4. This is a clear confirmation of the feasibility of the mixed technique in easily achieved conditions in practice. As an additional advantage, we have evaluated the energy production for increasing charging voltages. As predicted by the data in Fig. 4.7, the energy associated to the DLPE process always increases with the charging voltage, contrary to CDLE alone, where

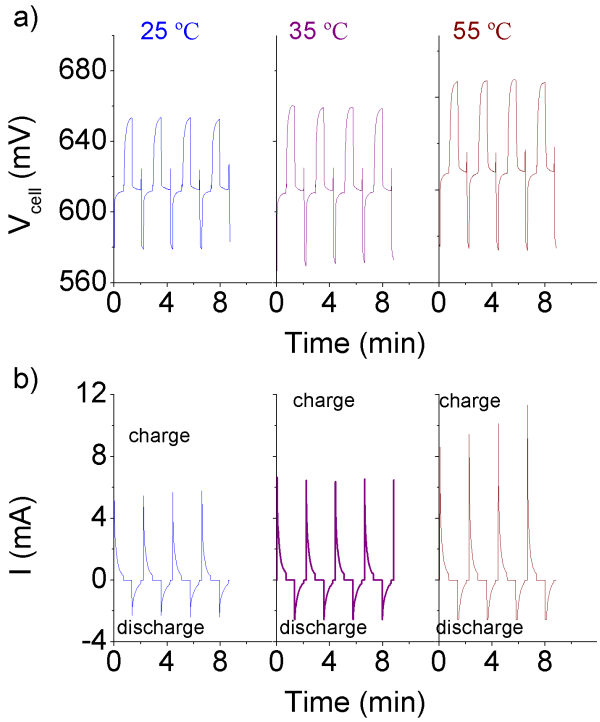

FIGURE 4.11: Experimental cell voltage (a) and electric current through the cell (b) as a function of time for CDLE+DLPE cycles in which a 20 mM NaCl solution is inside the cell during the discharging step and at the temperatures indicated. In all cases, the charging step is performed with a 600 mM solution at 25°C.

a maximum is theoretically and experimentally found [51, 54]. In contrast, the results in Fig. 4.13b demonstrate that we can always gain energy by increasing the source voltage as far as the limit imposed by faradaic reactions is not surpassed.

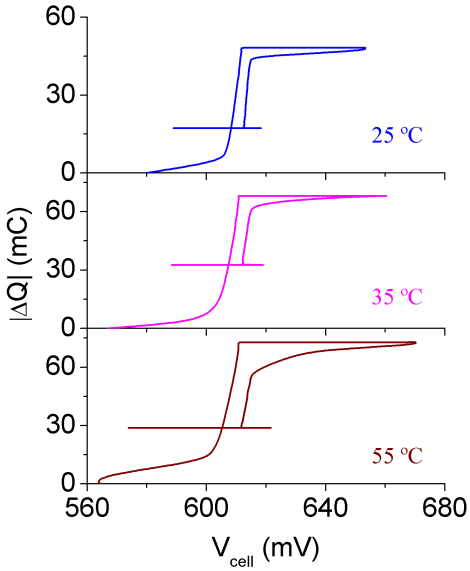

FIGURE 4.12: Experimental ΔQ -V_{cell} cycles for CDLE (25 °C-25 °C) and CDLE+DLPE (25 °C-55 °C and 25 °C-75 °C).

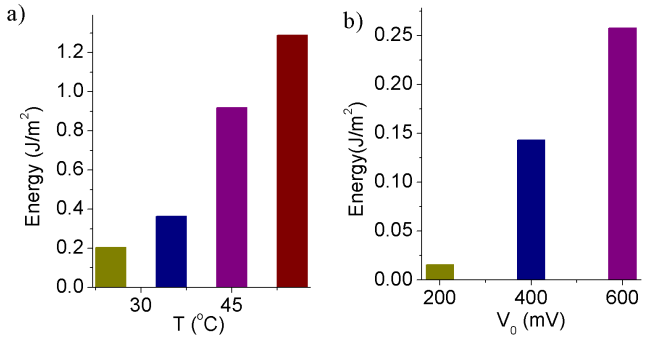

FIGURE 4.13: Experimental values of the extracted energy per unit apparent surface area of elctrode for CDLE+DLPE cycles. a) Charging solution: NaCl 600 mM at 25°C; discharging solutions: NaCl 20 mM at the indicated temperatures and 620 mV charging voltage. b) Charging solution as in a) and discharging solution: NaCl 20 mM at 75°C, for the indicated charging voltages.

4.4. Carbon materials requirements

4.4.1. The role of carbon wettability

Carbon wettability is obviously a determinant property of the electrodes. In the Capmix techniques, the need for exchange brings about the requirement that ions in the EDLs should be able to go in and out of them and they will most probably be hydrated, at least partially. The hydrophilicity of the carbon used for the electrode preparation is hence an important issue. In order to check for this, we prepared two kinds of carbon particles, named SC-1 and SC-2 hereafter, with almost identical pore size distribution, but quite different in their hydrophobic/hydrophilic balance. Fig. 4.14a shows the great similarity between both samples, concerning their pore sizes. With this, we can be sure that the differences in CDLE performance, if any, must come from their different surface characteristics.

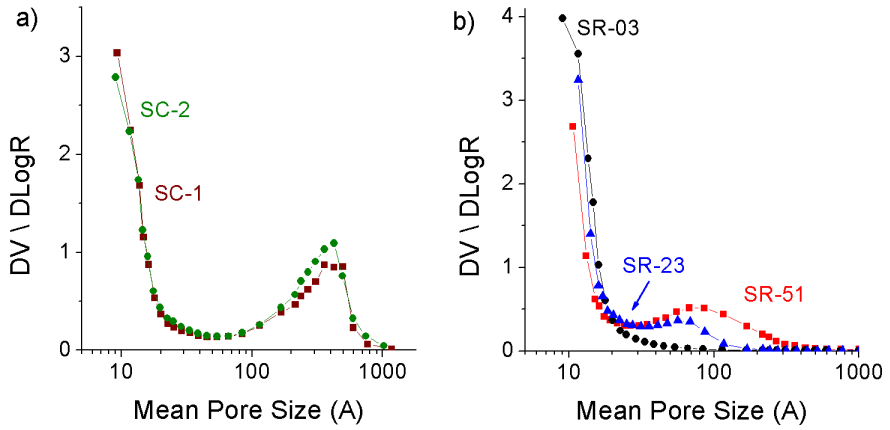

FIGURE 4.14: Specific pore size distribution for samples SC-1 and SC-2 (a) and samples SR-03, SR-23 and SR-51 (b).

With the aim of evaluating the wettability of these samples, we carried out contact angle measurements. The advancing contact angle (θ_a) is measured when a liquid droplet of known volume is carefully deposited on the solid surface. Once this angle is determined, the drop volume is reduced, thus retreating the contact line, and the receding contact angle (θ_r) can be

measured. It is commonly assumed that during this process, a film of the liquid is left on the solid and thus the latter angle will be smaller than the former, because it is measured on an already wetted surface. The difference between the two angles is called contact angle hysteresis [103] and an approach has been proposed relating both angles to the surface free energy of the solid, γ_s, which is crucially important for our study [103, 104]. This can be done as follows:

$$\gamma_s = \frac{\gamma_L(1+\cos\theta_a)^2}{2+\cos\theta_a+\cos\theta_r} \tag{4.2}$$

where γ_L is the liquid surface tension, water in our case ($\gamma_L = 72.8$ mN/m). The advancing contact angle was measured after depositing 6±2 μL droplets on the surface, and for the receding contact angle this volume was reduced to 4±2 μL. One example is shown in Fig. 4.15.

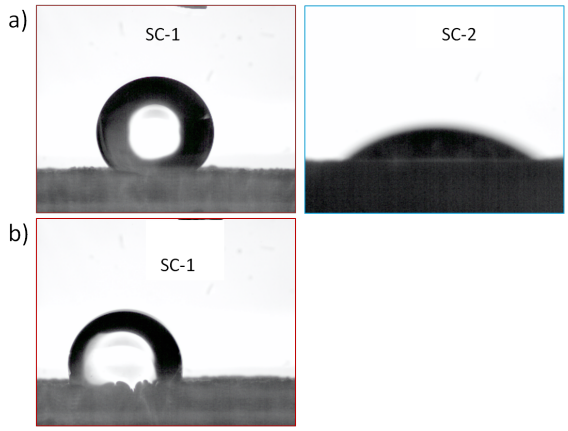

FIGURE 4.15: Droplets formed for advancing (a) and receding (b) contact angle measurements for carbons SC-1 and SC-2. The receding contact angle could only be measured for the former, and it was taken as zero for SC-2.

The results are presented in Table 4.3, together with the surface free energy calculated by means of Eq. 4.2. The Table also contains the data pertaining to the samples SR which will be used for our analysis of the effect of pore size distribution (see below). It is easy to conclude that sample SC-1 is very hydrophobic whereas carbon SC-2 is, on the contrary, characterized

TABLE 4.3: Advancing and receding contact angles of water on samples SC-1, SC-2, SR03, SR-23 and SR-51. The receding angle in SC-2 was not significantly distinct from zero. The surface free energy γ_s was calculated from Eq. 4.2.

Sample	θ_a (°)	θ_r (°)	γ_s (mJ/m^2)
SC-1	125 ± 3	84± 7	8.5± 1.6
SC-2	29 ± 5	–	66.0± 2.1
SR-03	86 ± 5	49± 2	31 ± 4
SR-23	110 ± 2	74± 8	16± 1
SR-51	107 ± 3	61± 4	17± 2

by hydrophilic behavior.

An independent characterization of the hydrophobicity can be done by electrophoretic mobility determinations, u_e, of the samples as a function of pH. The dependence of u_e on pH is an indirect proof of increased hydrophilicity, considering that the presence of more dissociable groups per unit surface area will manifest in both an increased hydrophilic character and an increased surface electric charge. Fig. 4.16a shows that the electrophoretic mobility of both samples is negative in most of the pH range, but only SC-1 presents an isoelectric point $pH_{iep} \approx 4$, while SC-2 remains negative through the whole pH variation. This is a manifestation of a larger density of OH^- ions, in the latter sample, after an oxidation treatment.

We can now explain the results obtained when the two carbons are used in CDLE cycles, as shown in Table 4.4 the fact that hydrophobicity hinders the required ion exchange is evident. The voltage rise in SC-1 is almost half that is for SC-2 for otherwise identical conditions. In addition, the results in Table 4.4 show that extracting power is only possible for SC-2 sample. These important differences between the carbon samples demonstrate its completely opposite CDLE performance.

4.4.2. Samples with different pore size distributions

In this part of the thesis, attention will be specifically paid to the balance between micropores, mesopores and macropores. It can be foreseen

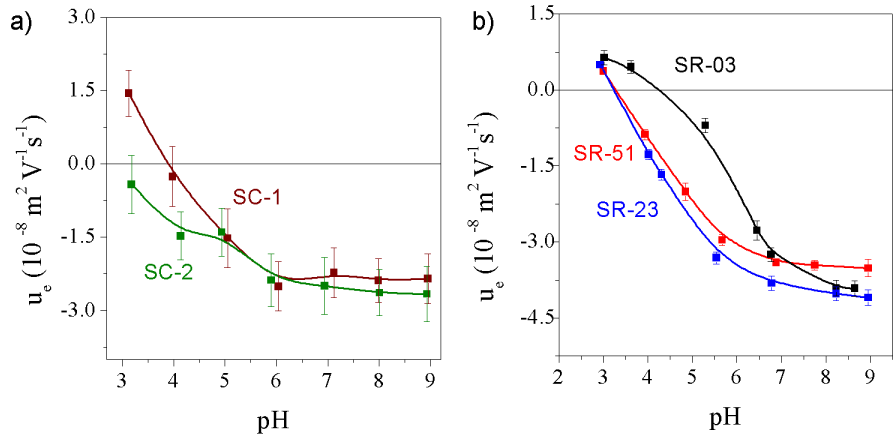

FIGURE 4.16: Electrophoretic mobility of the carbon particles SC-1 and SC-2 (a) and of particles of samples SR-03, SR-23 and SR-51 (b) as a function of pH in a constant ionic strength of 1 mM NaCl.

TABLE 4.4: Voltage rise and extracted power in samples SC-1 and SC-2.

Sample	Voltage rise (mV)	Extracted power (mW/m^2)
SC-1	24	–
SC-2	50	0.4

that this pore size distribution must also be an essential property of the carbon used in the CDLE process, for some reasons. One is the possibility of EDL overlap in the pores (and eventually constant potential inside them), which is clearly dependent on the channel dimensions. Secondly, the ratio between the ion and pore sizes determines the ease with which the ions can diffuse inside, and even if they are hydrated or (at least, partially) dehydrated [105]. In addition, the amount of charge transferred is limited by the possibility of EDL saturation (even pore saturation in the case of small pore radius) due to the finite volume of counterions. All these aspects may be determinant in the resulting kinetics (associated to the rate of ion adsorption-desorption in the EDL) and energy production (as the voltage rise and charge transferred will be reduced if ion exchange is incomplete). Even if exchange is not required, as in the supercapacitor

technology [89, 105], the pore size distribution is considered as the most important design parameter, taking into account the relationship between microstructure and ion accessibility to the pores.

Carbon samples with pores in the 5-10 nm range favour water exchange and reduce charge leakage.

In order to analyze the implications of the pore size distribution on CDLE, we used the samples SR-03, SR-23 and SR-51, with different pore structures, as shown in Fig. 4.14b. The three samples can be however considered as equivalent from the point of view of their surface free energy. The data displayed in Table 4.3 indicate that they are moderately hydrophobic (with surface free energies closer to that of SC-1 than to SC-2). Fig. 4.16b gives us further indication of the similarities of the surfaces from the electrochemical point of view: the electrophoretic mobility u_e of the three kinds of carbon particles is plotted as a function of pH in 1 mM NaCl. Note that the mobilities measured are intermediate between those of SC-1 and SC-2 (Fig. 4.16a), confirming that the treatment applied for the pore size variation does not affect the electrical surface functionalities sufficiently as to alter the wettability of the carbons.

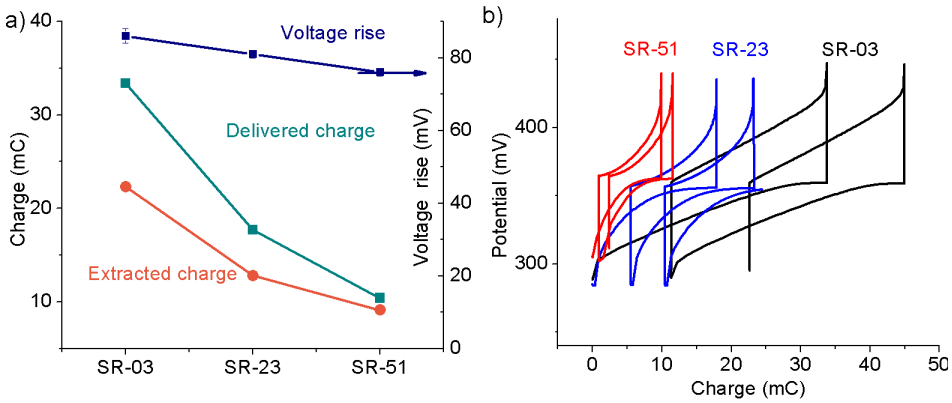

FIGURE 4.17: a) Voltage rise, extracted and delivered charge for samples SR-03, SR-23 and SR-51. b) Voltage vs. charge CDLE cycles representation for the same samples.

The important point here is the consideration of the effects of the pore size distribution on the CDLE response. Fig. 4.17 shows some representative re-

sults, obtained with layers of the indicated carbon particles. As the theoretical predictions [54] indicate, the effect of the average pore size on the voltage rise is almost negligible, in all cases approx. 80 mV as Fig. 4.17a shows. On the contrary, as it was expected, increasing the amount of pores in the 1 nm range produces an increase of both the delivered and the extracted charge (22 mC in SR-03, to be compared to 9 mC in SR-51, for instance, in the extracted charge). However, in Fig. 4.17a, it is also observed an increasing difference between delivered and extracted charge for smaller pore size. This fact dominates the eventual extracted power and is caused by charge leakage. This can be easily seen in Fig. 4.17b where cell voltage versus measured charge is represented. The shifts between successive cycles are clearly larger for sample SR-03 and SR-23. Considering that SR-51 contains a significant amount of pores in the 5-10 nm range, charge leakage reduction can be explained by assuming that the larger pore fraction behaves as a sort of solution reservoir, in which salt and fresh solutions are easily exchanged, leading to a favorable diffusion of counterions in and out of the small pores. Indeed, in SR51 was the only sample where power extraction was possible, achieving 1 mW/m^2.

4.5. Salinity difference effect

The research to date tends to focus on the natural process of mixing river water with seawater in river mouths, as the main source of blue energy [19]. In recent past, other salinity difference sources have also grown in importance, specially in water-scarce regions where river water is primarily used as the tap water source. For instance, concentrated brine water from desalination plants can be paired with waste water from a treatment facility, reducing desalination energy cost [30] and avoiding its severe impact on the ecological environment in oceans. In this section, we continue our study of section 4.3, where we analyzed the advantage of using higher salinity on DLPE+CDLE cycles. Here we propose the study of the effect of exchanging solutions on CDLE cycles with concentrations different from the commonly used river (20 mM) and sea (500 mM) water.

Theoretical predictions [54] demonstrate the advantages of using larger

salinity difference. Fig. 4.18a represents surface charge density as a function of surface potential for four ionic concentrations: 1 M, 500 mM, 300 mM and 20 mM of sodium chloride. As it is observed, when concentration increases over 300 mM, the distance among the curves seems to be closer. This is an important prediction of our model and it is due to the finite ion size. Although concentration increases, an unlimited counterion accumulation close to the surface is prevented. This leads to a less efficient screening of the surface charge and hence, to flatter potential profiles and lower surface charge increase with surface potential. This produces that voltage rise and cycle charge do not increase linearly with the salinity difference. Fig. 4.18b represents this tendency of the voltage rise and cycle charge for different solution combinations in CDLE. Note that the largest cycle charge and voltage rise corresponds to the highest concentration difference (20 mV vs. 1M). And, as we know, both parameters are key for maximizing the extracted energy.

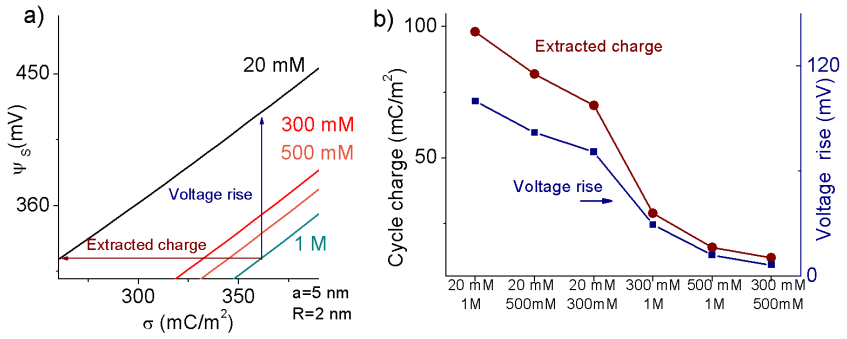

FIGURE 4.18: a)Surface charge density vs. surface potential for four ionic concentrations: 1 M, 500mM, 300mM and 20 mM b) Voltage rise and cycle charge for six different pairs of exchanged solutions.

Experimental results shown in Fig. 4.19 confirm the predictions of our model. Fig. 4.19a shows the same tendency of the voltage rise and the extracted charge as Fig. 4.18b. However, we are not able to predict the same values and this is due to the already mentioned current leakage. In Fig. 4.19b, the extracted power is shown. Note that positive extracted power is only found for the three first cases (20 mV vs. 1 M, 500 mM and

300 mM) reaching its maximum at 1.4 mW/m^2 for the largest salinity difference.

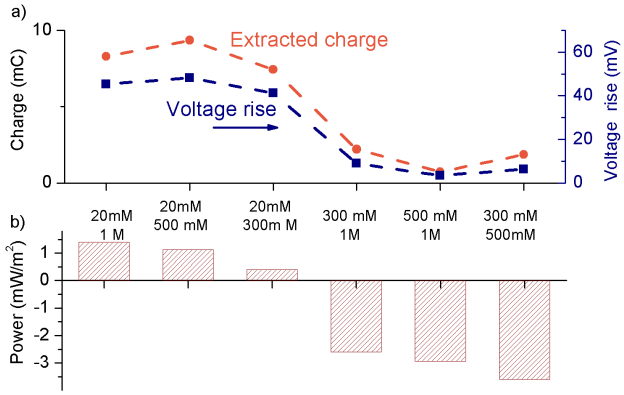

FIGURE 4.19: a) Voltage rise and extracted charge for six different pairs of exchanged solutions. b) Extracted power for these same cases.

These results examine the promising feasibility of CDLE for different salinity sources. CDLE performance can be maximized by enlarging the salinity difference among the solutions exchanged. This fact gives the opportunity to other water solutions, in particular, highly contaminating brine solutions, which might be a low cost feed.

4.6. Summary and conclusions

In this chapter, we have experimentally shown that the CDLE method can be significantly improved if some parameters are properly selected. We have demonstrated that improvements are expected to come from: minimization of the charge leakage, optimum selection of the working potential and adequate charging process to maintain stable and reproducible energy production cycles.

Extracted energy by the CDLE technique can also be improved if the temperature of the solutions is suitably chosen. The results discussed show that the technique based on the dependence of the electric double layer

capacitance on temperature can be used as a new approach to the extraction of electrical energy from thermal gradients without the need of electromechanical converters. However, considering that the CDLE+DLPE technique is just starting to be implemented, it is reasonable to expect significant improvements in efficiency and power density when the technology is further developed. In addition, it can be used in combination with other well known sources of renewable energy, such as solar thermal plants, geothermal extraction, or even home solar collectors as a source of heat during the long periods of inactivity.

Subsequently, we have shown that the average pore size of activated carbon particles, in relation with the EDL thickness and the ion diameter is, as expected, a determinant quantity. Optimum CDLE results will be obtained if the carbon used in the electrodes has a significant fraction of mesopore population which behaves as a sort of solution reservoir allowing easy water exchange. Additionally, results would be improved if hydrophilized activated carbon materials are employed: this might look counter-intuitive, since carbon oxidation can be favored in such case. However, the fact that hydrated ions must be cyclically exchanged with the contacting solutions compensate for this possible drawback. Finally, this chapter would not be complete without the inclusion on this research of other less common salinity sources that could improve extracted power as well as its positive environmental impact, as it is the case for saturated water solutions which mean an important potential risk to aquatic resources.

5

The Soft Electrode Method

5.1. Introduction

In this chapter we propose a new capmix method: we call it **soft electrode (SE) technique**, and it takes advantage of the two main capmix procedures described in section 1.2.4: CDLE (based on EDL expansion) and CDP (Donnan potential method). We call *soft* electrodes to conductive electrodes made of an activated carbon core and a polyelectrolyte layer, either cationic or anionic. The SE method allows the generation of electrical energy due to changes in both the EDL capacitance of the carbon electrodes and the Donnan potential of the polyelectrolyte layer when solutions are exchanged. It has been shown that such modification leads to an important reduction of the leakage current [57, 106]. Similarly to an auto-generated cycle, characteristic of the CDP method, there is no need for an external power supply, and electricity generation is directly produced by the mixing process. Like in the CDLE method, the potential difference in the cell is associated to the processes occurring on the pores of the particles themselves, no matter the presence of membranes. Hence a relatively thin polyelectrolyte layer suffices and likely results in a decrease of the overall cost of the method.

Soft electrode method allows the generation of electrical energy due to changes in both the EDL capacitance and the Donnan potential.

In the first place, the purpose of this chapter is to elaborate a model of the operation of the soft electrode method, based on the electrokinetic theory of soft particles. We will analyze how all the features of the model are experimentally reproduced [53]. We will perform a deep study of the energy and power achievable by the SE method in comparison to CDP. The objective is to find out whether the advantages of not needing membranes can be a chance to take the best of both capmix techniques while approaching CDP extracted power [63].

5.2. Principles of Soft Electrode Method

In Fig. 5.1 we represent the principles of soft electrode technique. We begin by considering two soft conductive particles immersed in a salty water solution that intends to simulate sea water. In panel (b) it is represented the potential profile Ψ with respect to that in the bulk solution. The voltage difference between particles is $V = \Psi_S(+) - \Psi_S(-)$, where the subscript S indicates the surface properties, and the sign + (-) indicates the particle with the cationic (anionic) polyelectrolyte shell.

At the initial stage (stage 0), the cores are uncharged and contacted with a salty solution. We restrict ourselves to the case that the polyelectrolyte layers are thick enough for the Donnan potential $\Delta\Psi_D^{\pm}$(salty) to be established (positive in one layer , negative in the other) and the potential profile of Fig. 5.1b-stage 0 is generated. For the sake of clarity, we are considering an antisymmetric situation of the polymer charge density, and this leads to $\Delta\Psi_D^{+} = -\Delta\Psi_D^{-}$. Since the particles are not charged, no electric double layer (EDL) is formed on the particle surface and the potential profile is flat. As a consequence, the surface potential Ψ_S with respect to the bulk solution is $\Psi_S^{\pm} = \Delta\Psi_D^{\pm}$ (salty), and the potential difference between both particles is $V = \Delta\Psi_D^{+}$(salty) $- \Delta\Psi_D^{-}$(salty) $= 2\Delta\Psi_D^{+}$(salty).

If we externally connect both particles, some charge will be transferred from left to right. Particles become charged and EDLs are formed close to their respective surfaces, leading to a potential jump $\Delta\Psi_{EDL}$ (salty) opposite to the Donnan potential. The process stops when particles become equipotential, that is $\Delta\Psi_D^{+}$(salty) $= -\Delta\Psi_{EDL}$(salty). The potential profile is represented in Fig. 5.1b-stage 1. Note that the potential profile in this case differs from the previous stage in the vicinity of the core surface, where an EDL is created.

Next we disconnect the external circuit and change the solution to a dilute one (fresh water). Both Donnan potentials increase in absolute value and on the other hand, since the charge on the particle surfaces is fixed, also the potential jump at the particle/solution interface $\Delta\Psi_{EDL}$ increases in absolute value, as a consequence of the double layer expansion [48]. Being the latter increase of smaller significance, the change to a fresh solu-

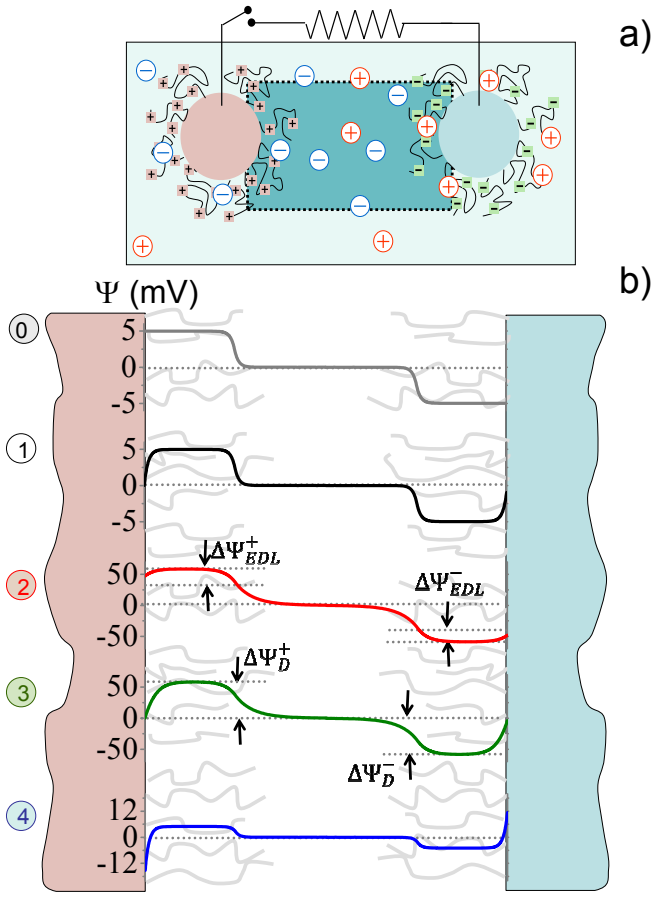

FIGURE 5.1: a) Schematic representation of two carbon particles coated by a cationic polyelectrolyte (left particle) and an anionic one (right particle) immersed in an electrolyte solution and externally connected through an electric circuit. b) Equilibrium electric potential profiles (see text) with respect to the bulk solution between the surfaces of both particles after the different steps of the cycle. 0: particles in salty solution, open circuit; 1: particles connected; 2: open circuit, fresh water; 3: particles connected; 4: open circuit, salty water. Note the different scales of the ordinate axes in stages (0,1), (2,3) and 4.

tion results in a net increase of the surface potential, as shown in Fig. 5.1b-stage 2. The surface potential becomes $\Psi^{\pm}_{S} = \Delta\Psi^{\pm}_{D}(\text{fresh}) + \Delta\Psi^{\pm}_{EDL}(\text{fresh})$, and the potential difference is now $V = \left(\Delta\Psi^{+}_{D}(\text{fresh}) + \Delta\Psi^{+}_{EDL}(\text{fresh})\right) -$

$\left(\Delta\Psi_D^-(\text{fresh}) + \Delta\Psi_{EDL}^-(\text{fresh})\right)$. This results in a gain of stored energy. In the next step we reconnect again both particles. Since there is a potential gradient directed to the right, charge is transferred in this direction, leading to a current flow in the external circuit. The potential profile is again modified only close to the core surface, in accordance to the change of surface charge. The process stops when particles become equipotential, and this occurs when $\Delta\Psi_D^+(\text{fresh}) = -\Delta\Psi_{EDL}(\text{fresh})$, as shown in Fig. 5.1b-stage 3.

Finally, in open circuit configuration, we exchange fresh for salty water, and both potential rises $\Delta\Psi_D^{\pm}$ and $\Delta\Psi_{EDL}$ decrease, reaching the situation in Fig. 5.1b-stage 4. In this case, the potential profile in the vicinity of the electrode does not change with respect to the previous stage, but it is shifted following the change of the Donnan potential at the polyelectrolyte shell. Once the circuit is closed again, the potential difference drives a charge back to the left electrode until stage 1 is reached.

This process is similar to that of CDP, but the potential difference that can be generated between electrodes made of these particles has a different origin. In CDP, membranes are in contact with solutions of different salinities at each side, and hence, with different Donnan potentials. Hence, a membrane potential is generated and this is the surface potential on the electrode [26, 52, 58]. In the process of Fig. 5.1, polyelectrolyte layers are attached to the particles, and hence, the surface potentials are directly the Donnan potentials.

The energy that can be extracted per unit area of interface in the cycle of Fig. 5.1 is :

$$W = \int_{\sigma_2}^{\sigma_3} \left(\Psi^+(\text{fresh}) - \Psi^-(\text{fresh})\right) \mathrm{d}\sigma + \int_{\sigma_4}^{\sigma_1} \left(\Psi^+(\text{salty}) - \Psi^-(\text{salty})\right) \mathrm{d}\sigma \tag{5.1}$$

where σ_i is the surface charge density at step i of Fig. 5.1.

The electric potential Ψ follows Poisson equation (Eq. 2.1):

$$\nabla^2\Psi(\mathbf{r}) = -\frac{\rho_{elec}(mathbfr)}{\varepsilon_0\varepsilon_m} \tag{5.2}$$

where ρ_{elec} is the volume charge density at position $\mathbf{r}$ in the solution.

The charge density in the conducting core is set to zero at the beginning. We assume that the polyelectrolyte shell is uniformly charged and that it is permeable to the solution. Hence, in this region the charge density is the sum of the charge density of the polyelectrolyte (ρ_{pol}) and that of the solution. Finally, outside the polyelectrolyte layer, the charge comes from free ions in the solution. As it was explained, typical electrodes are made of a swarm of porous microparticles such that two kinds of pores are present: macropores (space between microparticles) and micropores (inside the microparticles themselves). The surface area associated to the latter is far larger than that of the former. In this case, the whole electrode will be modeled as a concentrated suspension of **spherical nanoparticles** instead of a network of cylindrical pores (section 2.4). The potential profile inside the pores will be hence represented by the potential around a given nanoparticle. We assume that at least the outermost layers of carbon particles are coated with the polyelectrolyte, and the problem of potential distribution in the pore is solved for a single particle taking into consideration the possible double layer overlap between neighbor particles. Eq. 2.1 must be solved separately in three regions:

$$\begin{cases} \nabla^2\Psi(\mathbf{r}) = 0 & \rightarrow \text{core} \\ \nabla^2\Psi(\mathbf{r}) = -\dfrac{1}{\varepsilon_0\varepsilon}\sum_{i=1}^{N} z_i e c_i - \dfrac{\rho_{pol}}{\varepsilon_0\varepsilon_m} & \rightarrow \text{soft layer} \\ \nabla^2\Psi(\mathbf{r}) = -\dfrac{1}{\varepsilon_0\varepsilon_m}\sum_{i=1}^{N} z_i e c_i & \rightarrow \text{solution} \end{cases} \tag{5.3}$$

The ionic charge density, c_i, similarly follows the Boltzmann distribution from Eq. 2.2. Spherical symmetry is assumed for solving the problem, so the quantities of interest will depend only on the radial coordinate r.

The problem is totally defined by the boundary conditions at the interfaces:

$$\begin{aligned} \left.\frac{\mathrm{d}\Psi}{\mathrm{d}r}\right|_{\text{core surface}} &= -\frac{\sigma}{\varepsilon\varepsilon_0} \\ \left.\frac{\mathrm{d}\Psi}{\mathrm{d}r}\right|_{\text{bulk}} &= 0 \end{aligned} \tag{5.4}$$

In the boundary between the polyelectrolyte layer and the solution, the continuity of electric potential and its derivative must be satisfied:

$$\begin{aligned} \Psi|_{SC^+} &= \Psi|_{SC^-} \\ \left.\frac{\mathrm{d}\Psi}{\mathrm{d}r}\right|_{SC^+} &= \left.\frac{\mathrm{d}\Psi}{\mathrm{d}r}\right|_{SC^-} \end{aligned} \tag{5.5}$$

where SC^- (SC^+) indicates the inner (outer) sides of the boundary between the polyelectrolyte coating and the solution.

By solving these equations, the potential profiles in Fig. 5.1 can be obtained, whereas the surface charge on the core for a given potential follows from Eq. 5.4. Furthermore, if the polyelectrolyte layer is thick enough, the potential reaches a uniform value different from that at the bulk solution, namely the Donnan potential. This decays to zero outside the polyelectrolyte layer in a distance of the order of the EDL thickness. An example of a whole theoretical cycle is shown in Fig. 5.2. Note that the area of the shadowed region (3.1 $\mathrm{J/m^2}$ in this case) is the energy density that can be extracted in this process.

5.3. Implementation

Obtaining energy from the soft carbon electrodes requires, in the simplest way, connection to the external load resistor as Fig. 5.1a shows. The cycle we implemented included the following steps (Fig. 5.3): short-circuit of the electrodes in sea water; open circuit and fresh water in (25 s); connection of the cell with the external resistor (measured current 0.75 mA at most) (55 s); open-circuit and sea water in (25 s); connection with the external load (55 s), current (0.5 mA maximum) flows in opposite direction. The voltage and current were continuously recorded; alternatively, in order to make it easier to compare with the theoretical cycles like that in 5.2, the instantaneous charge can be computed by integration of the intensity vs. time data, and the energy at each time calculated as the product of the measured voltage and the calculated charge.

From the linear fitting of the energy vs. time data, a value of average

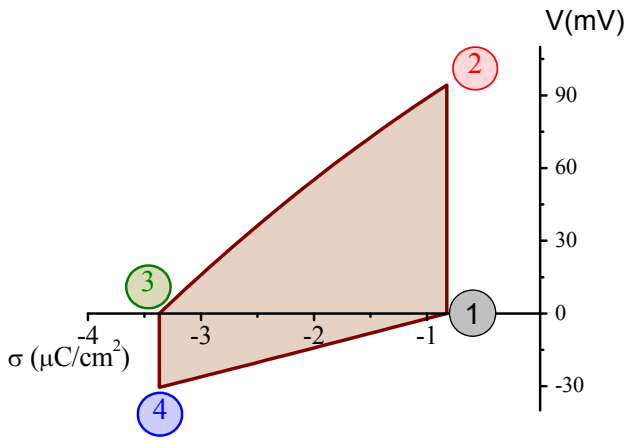

FIGURE 5.2: Voltage between electrodes built with particles as in Fig. 5.1a as a function of the surface charge density for 20 and 500 mM NaCl solutions. The polyelectrolyte charge densities used were: $\rho_{pol} = 6 \times 10^6$ and -3.8×10^6 C/m^3 for the PDADMAC- and PSS-coated electrodes, respectively. The stages of the process are numbered as in Fig. 5.1b.

power can hence be obtained,as illustrated in Fig. 5.3d. We did not perform a systematic study of the timing optimization, but with the conditions described the power was (12.1±0.1) mW/m^2 (referred to electrode apparent area). Note that this power corresponds to an energy per cycle of 0.58 mJ, taking 160 s as the cycle duration. In order to compare this figure with the theoretical prediction given in Fig. 5.2, it is necessary to carry out an estimation of the effective interfacial area of the electrode for a given geometrical area. In our case, superimposing the experimental voltage drop in steps 2 and 3 with theoretical predictions would yield a surface charge density variation of 0.3 μC/cm^2. Since the charge transferred in that step is 18 mC (integration of the current-time data in Fig. 5.3b), we can conclude that the active area would be 6 m^2. Then the two cycles (measured and calculated) can be superimposed at the same scale, as shown in Fig. 5.3c. The shaded area would correspond to the portion of the cycle actually swept experimentally, and its value is 0.73 mJ. From this, we conclude that there is a reasonable agreement between theoretical and experimental energy evalu-

ations per cycle.

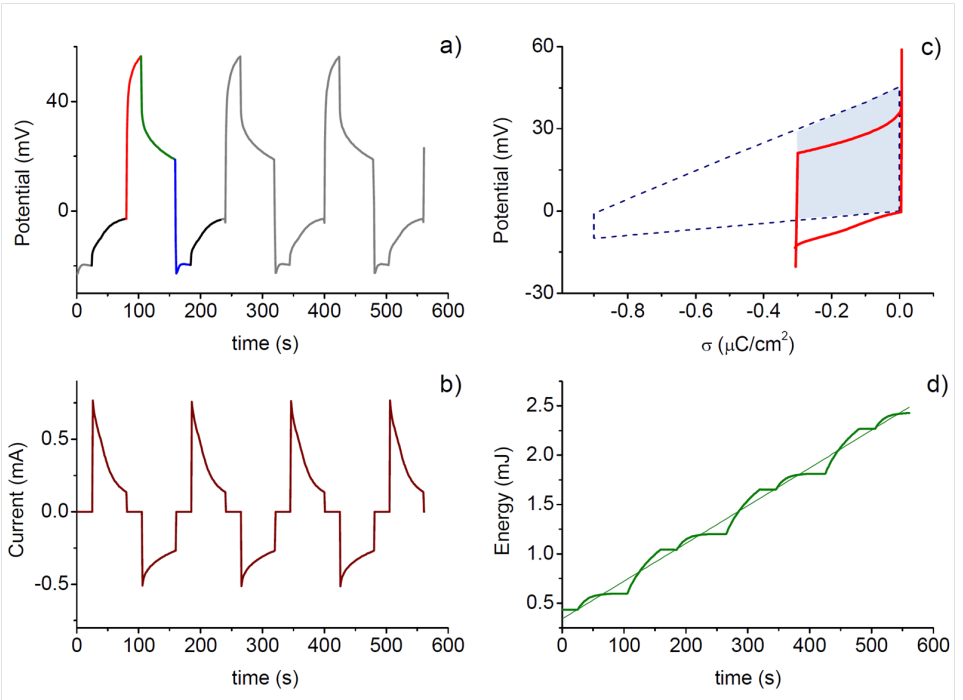

FIGURE 5.3: Voltage (a) and current (b) measurements in the cell as a function of time. (c) Experimental (solid red line) and theoretical (blue dashed line) cell voltage vs. charge density cycles; the shaded area corresponds to the portion of the calculated cycle swept by the experiment. The polyelectrolyte charge densities used for the simulation were: $\rho_{pol} = 6 \times 10^6$ and -3.8×10^6 C/m^3 for the PDADMAC- and PSS-coated electrodes, respectively [77, 107].(d) Accumulated energy as a function of time. The slope of the fitted straight line is the power. In this case, 12.1 mW/m^2 of electrode.

The calculation of the soft electrode efficiency η can first of all be carried out by the practical approach of comparing the area of the experimental cycle and the ideal one without leakage and internal resistance (denominated cycle efficiency): in such case, we obtain 36% (see Fig. 5.3c). Additionally, the fuel efficiency, η_{fuel} (Eq. 1.2), is around 0.8% for this experimental case whereas the values reported for CDP techniques reach approximately 20 % [58]. In this situation, further research is needed in order to understand such difference which might be probably related with an incomplete coat-

ing of the carbon films. This will be the principal objective of the following section: the understanding of how the two types of polyelectrolytes adsorb on the carbon surface and its implication on power extraction.

5.4. Polylectrolyte- versus membrane-coated electrodes

In this section, we will first analyze the differences between CDP and SE methods related to potential rise in open circuit voltage (OCV), and extracted power, that is, the essential information of the capmix cycles. We will also analyze the working principles of soft electrodes for parameter optimization. Thus, this research will be a first insight into polyelectrolyte layer behavior and is key for the improvement of the SE method.

Unless otherwise stated, the typical conditions of SE preparation (more details in section 3.1.4) were: 100 mM of 200 000 molecular weight PSS polymer and 100 mM of 100 000 molecular weight PDADMAC polymer. Other polyelectrolytes, concentrations and molecular weights will be specified when used.

5.4.1. Open Circuit Voltage

The voltage rise is a key factor in capmix cycles. Hence, in this section we first discuss the OCV results. In Fig. 5.4 we show the time evolution of the cell voltage when we introduce salt water and subsequently, fresh water for both methods: soft electrodes (Fig. 5.4a) and membranes (Fig. 5.4b).

SE and CDP voltage rise are quite similar. On the contrary, a significant difference on time response is found.

It is apparent from Fig. 5.4 that the voltage rise in similar for both cases: around 120 mV for SE and 140 mV for CDP. This is a promising result concerning the SE performance in terms of extracted energy. However, we found a very significant difference in time response that will affect the extracted power. As Fig. 5.4 shows, during fresh water flow, soft electrodes need approximately 200

seconds to reach the steady voltage rise, while membrane-based electrodes reach steady state in less that 10 seconds. Although the polymer shell is probably well-formed, as indicated by the voltage rise, the slow time response is an important drawback that should be addressed for improving the extracted power. Despite the different time responses of CDP and SE, a steady tendency towards constant voltage values is observed in both cases after the first solution exchange. This suggests that leakage can be considered negligible in the two kinds of measurements.

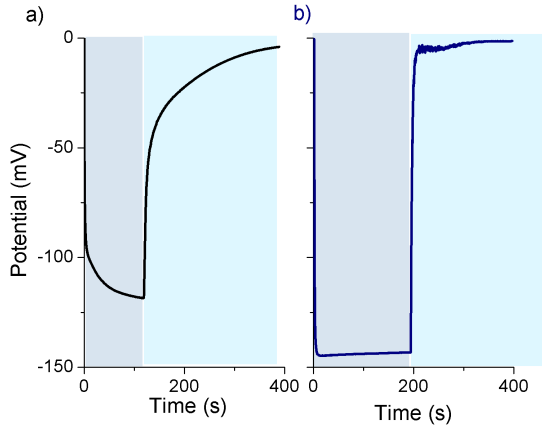

FIGURE 5.4: Open circuit measurements for soft (a) and membrane-coated (b) electrodes when we alternatively introduce salt and fresh water in the working cell. Dark-shaded areas: 30 g L^{-1} NaCl; light-shaded: 1 g L^{-1} .

5.4.2. Capmix cycles

In this section, we describe the results obtained for SE and CDP methods in constant current capmix cycles. As our goal is comparing SE with an optimized CDP cycle in terms of energy and power, we will perform two kinds of SE cycles differing in cycling periods. Thus, Fig. 5.5a shows the SE cycle obtained with the same timing as the optimum CDP cycle represented for comparison in Fig. 5.5b. With the aim of maximizing the energy obtained from SE method, even at reduced power, we also performed SE cycles extending the open circuit stages. This longer cycle is represented in

Fig. 5.5c and it lasts as long as needed to reach the SE maximum voltage rise, i.e. approximately 4 times longer than the the short cycle.

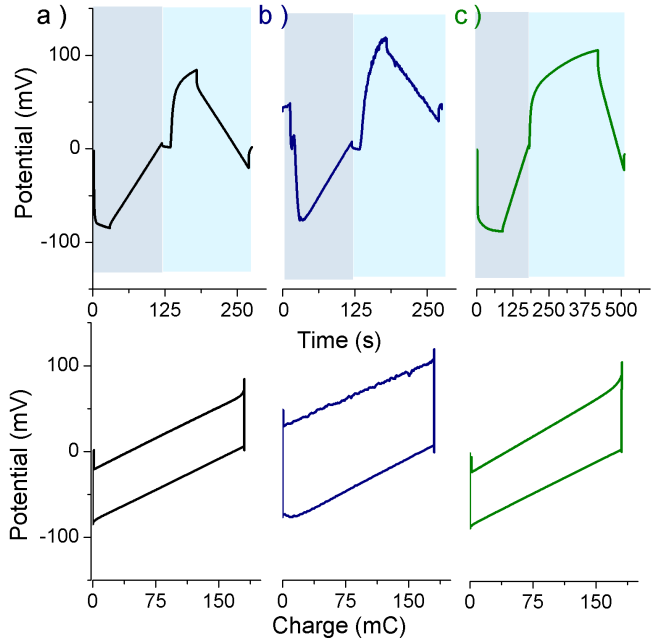

FIGURE 5.5: Constant current cycles for SE (a and c) and membrane-coated electrodes (b). In a) and b) the periods are equal, while in c) the period of the SE cycle is approximately 4 times longer. The corresponding potential-charge cycles are represented in the bottom figures.

Fig. 5.6 shows the extracted energy and power of the cycles in Fig. 5.5 for different charging/discharging currents. It can be seen that the energy obtained by SE as compared to CDP is about 30% lower in the most favorable conditions. However, the main difference between the two approaches appears when the extracted power is considered. In this case the maximum extracted power for SE (50 mW m$/^2$) is about half that obtained from CDP (105 mW $/\mathrm{m}^2$). Although this is a promising result, it is necessary to explore the SE process further to improve it.

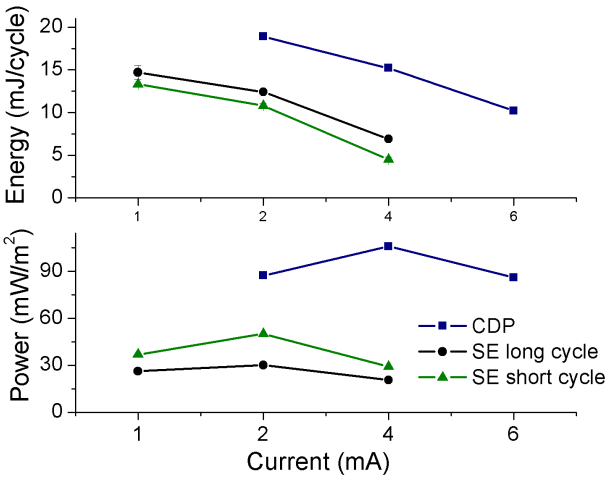

FIGURE 5.6: Energy per cycle (top) and power (bottom) extracted as a function of the current applied for the three kinds of cycles shown in Fig. 5.5.

5.4.3. Individual behavior of soft electrodes

To tackle this time response issue that apparently prevents the SE method from becoming a competitive alternative to CDP, we analyze each side separately in OCV measurements. That is, we assembled the cell with non-treated carbon film on one side, and the coated (either anionic or cationic) electrode on the other side of the cell. Fig. 5.7 compares both measurements. Note how PSS generates a comparatively large voltage rise (AB) with slow time response, while the cationic polymer PDADMAC generates a smaller voltage rise (AC) with a quick time response. These unexpectedly different electrode performances explain the above mentioned energy and power results (Fig. 5.6), and provides an interesting insight into the SE technique. In the following sections, we analyze which parameters can affect the described behaviors.

Polymer characteristics

The effect of polymer characteristics such as molecular weight, concentration or structure on the SE performance will be analyzed in this part. Let

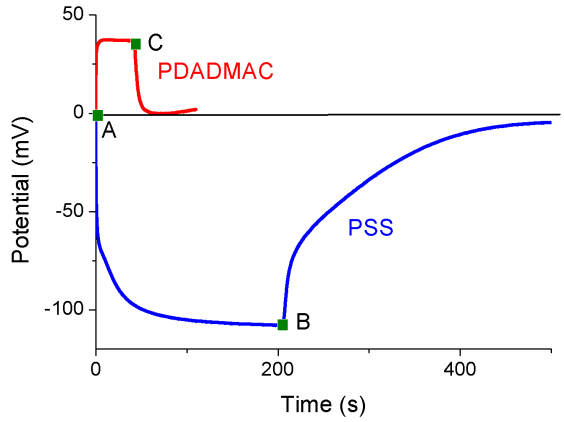

FIGURE 5.7: OCV measurements for carbon electrodes coated with cationic (PDADMAC) and anionic (PSS) polymers. AC and AB represent the respective voltage rise.

us first consider the OCV measurements when the coating is PSS as compared to a different anionic polymer, PAA. The OCV results are plotted in Fig. 5.8a,b for different anionic polyelectrolye concentrations. As observed, an increase in concentration leads to a larger voltage rise in both cases. However, the concentration needed and the overall voltage rise is different for each polymer: higher potential elevation with lower concentration is found for PSS. Fig. 5.8a also demonstrates that changing the molecular weight from 200 000 to 70 000 has a negligible effect on OCV measurements. Focusing now on time response differences, we can conclude that the polyelectrolyte characteristics have no influence on the kinetics of the SE cycle for anionic polymers. For instance, for the highest concentration in each case, the time needed to reach 90% of maximum OCV is quite similar: 200 s for PSS and 240 s for PAA.

Similarly, Fig. 5.8c shows the results for the cationic polymer PDADMAC (attemps to use PEI were unsuccessful probably because this is a low conductivity polymer producing a high internal resistance of the electrode). Note that, as in the case of PSS, although the voltage rise increases when increasing the concentration of PDADMAC, neither of the analyzed polymer characteristics has effect on the time response.

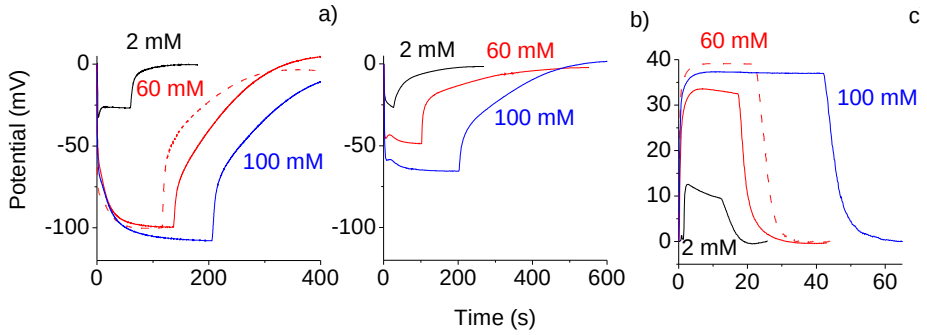

FIGURE 5.8: OCV measurements for single electrodes coated with: two different anionic polymers, PSS (a) and PAA (b), and the cationic polymer PDADMAC (c). The dashed line in a) shows the response of 60 mM PSS with lower molecular weight ($M_w \approx 70\,000$). The dashed line in c) corresponds to 60 mM $M_w \approx$ 200 000-350 000 PDADMAC.

Alternative SE fabrication procedure

In an attempt to get an insight into how polyelectrolytes coat the electrodes, we tried an alternative SE fabrication procedure that consists of treating the carbon particles and afterwards forming the film, instead of coating already formed carbon films. This method allows us to separate the role of the individual particles from the effect of the graphite support. The characterization of the coated particles was carried out by means of electrophoretic mobility (both DC and AC). As a reference, we also measured non-treated particles.

Fig. 5.9a represents the electrophoretic mobility of non-treated and polyelectrolyte -coated activated carbon particles as a function of NaCl concentration. As we can see, the particles were indeed coated by the cationic polyelectrolyte PDADMAC, as expressed by the positive mobility, while the same kind of measurements did not reveal any effect of anionic PSS on the mobility. Recall that the capmix experiments demonstrate that PSS is functional in producing voltage changes associated to ionic strength variations. Hence the results of Fig. 5.9a can be explained by hypothesizing that PDADMAC effectively coats the carbon particles, whereas electrostatic repulsion provokes that the negative polyelectrolyte is unable to form such a

homogeneous layer.

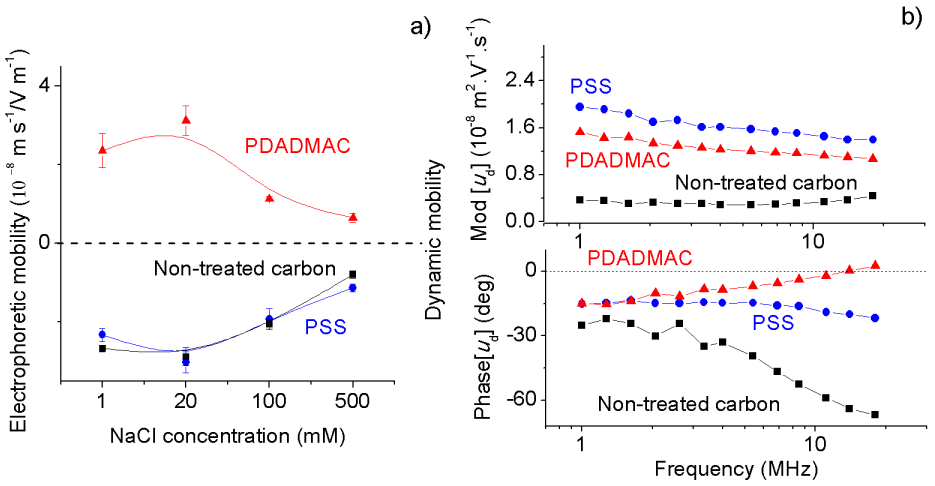

FIGURE 5.9: a) Electrophoretic mobility as a function of NaCl concentration. b) Modulus (top) and phase (bottom) of the dynamic electrophoretic mobility versus frequency. Both measurements for non-treated carbon particles (Norit) and for same particles coated with PSS and PDADMAC.

These arguments agree with dynamic mobility (u_d) data, typically more sensitive to the nature of the polyelectrolyte coating. Fig. 5.9b shows the effect of the field frequency on the modulus and phase of the mobility. The increase of the modulus of polyelectrolyte-coated particles compared to bare carbons is clear in this figure, indicating that both kinds of coated particles are more charged (either positively or negatively, depending on the coating) than bare ones. The phase of the mobility is particularly illustrative of the differences between the particles: both bare and PSS-coated carbons show increasingly negative values (approaching the theoretical limit of - 90° when the inertia would stop completely the motion). This tendency is slower for PSS-coated particles, precisely due to the larger charge provoking a larger surface conductivity. This is even more evident in the case of PDADMAC, whereby the decrease of the phase with frequency is in fact not observed (it can be expected at higher frequencies). This is a manifestation of a larger surface conductivity than in the case of either bare or

PSS-coated particles [77]. Summarizing, the electrokinetic data of Fig. 5.9 suggests that the two polyelectrolytes are linked differently to the particles.

One possible way to ascertain these widely differing adsorption mechanisms is to analyze the behavior of a simpler surface, such as pure graphite films (not covered with carbon shells and hence with very low surface area). To that aim, we simply immersed graphite collectors in PSS and PDADMAC solutions. Fig. 5.10 shows the OCV of a cell formed with each treated graphite films versus an untreated carbon electrode, compared to the results obtained with the whole carbon film (Fig. 5.7). Somewhat surprisingly, the results show that the activated carbon-free graphite film coated with PDADMAC behaves very similarly to the PDADMAC carbon coated electrode. On the contrary, the potential rise of the PSS-graphite film is much lower than in the case of the PSS-carbon electrodes.

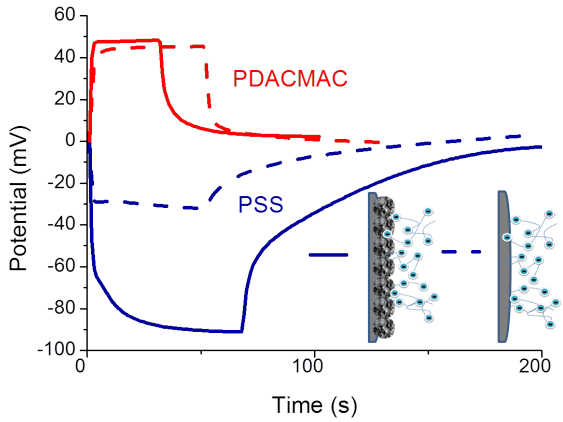

FIGURE 5.10: OCV kinetics for polymer-treated graphite films (dashed lines) and carbon films (solid lines).

In order to elucidate the origin of the differences observed, we performed HRTEM + EDX analysis of the three kinds of carbon particles: although the electron microscope observations can hardly allow to distinguish the location of the two polyelectrolytes, it might be expected that EDX can offer some clues. Fig. 5.11a shows the carbon and chlorine distribution on the PDADMAC-treated particle: note the homogeneity of the Cl distribution,

and its coincidence with that of carbon. We can conclude that the particles are uniformly coated with PDADMAC, as indicated by the presence of Cl, the counterion of the charged groups. On the contrary, Fig. 5.11b demonstrates that PSS is adsorbed differently: the presence of Na and S is mainly limited to the pores of the outermost (thinnest) layers of the particle, and the adsorption is not as uniform.

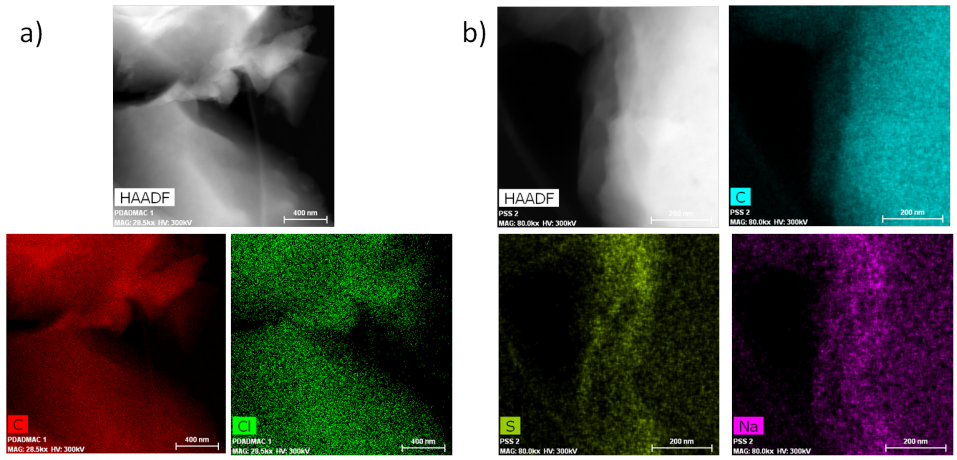

FIGURE 5.11: a) Top: HRTEM picture of PDADMAC-treated carbon particles. Bottom: EDX visualization of carbon and chlorine. b) Top: HRTEM picture of PSS-treated carbon particles (left) and EDX detection of carbon distribution (right). Bottom: EDX visualization of sulfur and sodium. In all cases the same area of the particle is observed.

This set of results jointly indicates that PSS coats the carbon film in a non-uniform way, probably reaching some depth in patches in the electrode. On the contrary, PDADMAC appears to produce a uniform layer, a configuration closer to a selective membrane, which reaches its Donnan potential in a very short time. In the case of PSS, ions encounter the polyelectrolyte as they diffuse in the activated carbon plug, and the potential rises as the concentration front reaches the adsorbed molecules. This explains the finding (not shown for brevity) that the time response (typically 200 s for steady OCV) of an electrode built with PSS-pretreated carbon particles is similar to that of carbon treated with the same polyelectrolyte (Fig. 5.7). For the same

reason, the response of PDADMAC-coated electrodes to salinity changes can be observed even without the need of the activated carbon particles (Fig. 5.10). This also explains why the OCV of electrodes built with particles pretreated with PDADMAC is similar to that of untreated particles (data not shown).

5.5. Summary and conclusions

In summary, the principle of extracting capacitive energy is used, taking advantage of the dependence of the Donnan potential with the salinity of the solution, in a similar way to CDP. The technique proposed is based on the simple deposit of a polyelectrolyte layer on the carbon films, called Soft Electrode (SE) method. The main difference is that the membranes are replaced by shells of polyelectrolytes, and that there is no space between the shell and the electrode surface, meaning that the potential difference between the electrodes is not related to the membrane potential but to the Donnan one. The subsequent research shed light on the different behaviours of both methods. We have compared the performances of two methods aimed at obtaining electrical energy from salinity gradients. CDP has reached so far the highest extracted power among capmix methods. However, some limitations still need to be considered, specially those concerning cost, fouling and the assembly difficulties.

On the other hand, our preliminary results suggest that the SE technique might become an efficient salinity gradient energy method in terms of voltage rise. However, the main difference between the two approaches is the comparatively slow SE time response. In an attempt to clarify the reason for this drawback, we evaluated separately the two polyelectrolytes (anionic: PSS; cationic: PDADMAC) coated electrodes. We found that PSS-based coating leads to high open circuit voltage and slow response, whereas PDADMAC electrodes behave the opposite way (lower OCV and faster response). A possible explanation for this might be found in the following: PSS seems to adsorb inhomogeneously on the pores of the outermost carbon layers. Therefore both the voltage rise and time response depend on how the exchanging solutions reach the polyelectrolyte patches.

On the contrary, in the case of PDADMAC, we probably have a homogeneous thin layer staying on the surface of the film, which reacts very quickly to salinity changes.

Soft electrodes appear to be a promising alternative or complement to existing capmix techniques. Further investigation on polymer selection, methods for film treatment and stability of the coating are needed to improve the power output. When time response issues have been solved, the SE technique can outperform other capmix techniques.

6

Towards capmix implementation in real world

6.1. Introduction

Up to this point, the vast majority of the research of this thesis has focused on the optimization of energy production within the limits of laboratory possibilities. This means that most of the work has been carried out with a single lab-scale capmix cell and with synthetic sodium chloride solutions as river and sea water sources. We now emphasize the need of moving on and considering real aspects that might play a crucial role on the whole capmix process. We will principally analyze the effect on energy extraction of solutions of a more realistic composition and moreover, we will explore some methods for stacking individual cells in order to increase energy and power production. Both steps are considered key to achieve a fruitful implementation of capmix methods.

Firstly, the effect of real water will be considered both theoretically and experimentally [108]. In this sense, we will focus on the presence of ions other than sodium and chloride and on the possible effects of other materials usually dispersed in natural water (mineral particles, microbes, shells, pollutants) by checking their accumulation in the carbon films used, after being exposed for a long period to natural sea water during CDLE cycles. Subsequently, we will move a step forward and we will perform an on site application in order to analyze the potential of blue energy by the soft electrode method. For this study, we describe experimental results using both real sea and river waters from the pacific coast of Central America, concretely, the Gulf of Fonseca. This area, situated among Honduras, El Salvador and Nicaragua, has been considered of special interest due to its hydrographic richness. The soft electrode method was chosen in this case due to its ease of assembly and transportation because neither power supply nor membranes are needed [109].

Finally, as it has been mentioned, we will also tackle a different but fundamental aspect towards capmix real implementation: the stacking possibilities of the capmix cells. The aim of this work is to find the optimum configuration of the multi-electrode setup for maximizing the energy and power outputs. Side-to-side (serial) configurations will be considered, and the results will be compared to theoretical predictions based on models for EDL

expansion and Donnan potential generation in carbon electrodes [110].

6.2. Real water effect on energy production

Both theoretical models and experimental implementations of CDLE [51, 54, 56, 111, 112] are based on the simplest kind of exchanging solutions, namely NaCl. All these efforts have led to the optimization of the characteristic parameters of the performance of the CDLE technique (see chapter 4), but the description reached needs to be completed, as neither sea nor river waters are just NaCl solutions. Therefore, and in order to succeed in future implementations, the following two effects should be taken into account. Firstly, the use of natural ocean waters may have the drawback that materials (shells, sand particles, microbial) dispersed in water will affect the process by their deposition on the electrodes.

On the other hand, there is a wide variety of ions present in natural water. The effect of electrolyte mixtures with more than two ionic species have been investigated in many practical situations such as supercapacitor technology, water desalination, biological processes and electrokinetics [55, 79, 113–116]. In the case of CDLE, since this cycle directly depends on the electric double layer (EDL) structure, the electrolyte mixture can affect the extracted energy.

In this chapter, we analyse the significance of realistic solution composition for the CDLE technique. We first model and simulate it theoretically, taking into account both ionic size and valency, and possible EDL overlap. We apply such model to solutions of more than two ions, since the presence of finite concentrations of Mg^{2+}, Ca^{2+}, SO_4^{-2} alters the charge-potential profiles, and, eventually, the energy production. We additionally perform experiments in which both natural and simulated water samples are used, paying special attention to the possible deposition of materials on the electrodes [108].

6.2.1. Theoretical predictions

We extend the model presented in section 2.4 to multi-ionic solutions. Similarly, we perform a mean field analysis of the structure of the EDL, and so, the electric potential distribution will be given by the Poisson equation (Eq. 2.1) subject to the boundary conditions of Eq. 2.17 and Eq. 2.18. Also, the relation between the ionic concentration and the electric potential at any point has been already presented in Eq. 2.20 which takes into account the excluded volume of ions. This means that close to the surface there is a region inaccessible for ions, which is a zero-charge Stern layer. Hence, Eq. 2.1 must be solved separately in different regions.

However, in order to solve the equations for the multi-ionic case, more regions than three should be considered. In the first one, between the particle surface and the radius of the smallest ion, say ion 1, $c^i(\mathbf{r}) = 0$. In the second region, where only the smallest ion can stay, we can write $c^{i\neq 1}(\mathbf{r}) = 0$. For the third region, where only ions 1 and 2 can stay, we can write $c^{i\neq 1,2}(\mathbf{r}) = 0$, and so on. Accordingly, new boundary conditions, but comparable to the original Eq. 2.21, must be used, namely, the continuity of the potential and of the normal component of the electric displacement at the boundary between every pair of regions:

$$\forall i = 1...N \begin{cases} \Psi(r = R - r_i^-) = \Psi(r = R - r_i^+) \\ \dfrac{\mathrm{d}\Psi}{\mathrm{d}r}\Big|_{r=R-r_i^-} = \dfrac{\mathrm{d}\Psi}{\mathrm{d}r}\Big|_{r=R-r_i^+} \end{cases} \tag{6.1}$$

With these equations, the potential profile can be calculated as a function of the surface potential, the particle concentration, the pore size, and the ionic concentration. Finally, the surface charge density, σ, can be obtained from Eq. 2.5 and the extracted work in every cycle from Eq. 2.13. It should be recalled that, roughly speaking, the area representing the extracted energy is $\Delta\sigma\Delta\Psi$. This is important to be stated, because from this it is clear that the extracted work can be increased by increasing either the charge exchanged $\Delta\sigma$, the potential rise $\Delta\Psi$, or both.

The examination of the extracted work in the CDLE device with real solutions is complicated by the fact that the predominant ions apart from Na^+

and Cl^- differ from these in both size and valency. These two parameters will be examined separately before addressing the mixed solution.

Valency

In terms of a classical description of the EDL [67] it is easily demonstrated that increasing the valency implies a larger counterion concentration in the EDL for a given surface potential, and hence, a steeper reduction of the electric potential in it. As a consequence, the surface charge density for a given surface potential will be larger for multivalent counterions. This picture is modified if we take into account excluded volume effects between ions and also between ions and the surface. To clarify the effect of the valency in this case, we will consider in this section that all counterions have the same size (0.428 nm). In Fig. 6.1a,b we represent the electric potential and the volume charge density profiles inside the EDL for different counterion valencies and two coion concentrations (c(Cl^-) = 0.02 M and 0.6 M). For the pore radius examined (R = 2 nm), EDL overlap (non zero potential at the pore axis) is apparent, particularly for the less charged counterion. On the other hand, excluded volume effects produce a maximum charge density (Fig. 6.1b) at the vicinity of the wall (this is magnified for the moderately high surface potential chosen, $\Psi_s = -500$ mV).

Increasing the ion valency leads to a reduction of $\Delta\Psi$ upon exchanging salinity in the CDLE cycle.

Fig. 6.1d shows the extracted work for different valencies of the ions in the solution. The presence of a maximum value at surface potentials below 0.3 V was already observed and discussed in section 2.4. This is an indirect consequence of the maximum value of the EDL capacitance due to excluded volume effects between ions. Note that increasing the valency reduces the amount of extracted energy, and this can be explained by carefully examining Fig. 6.1c. There we can see that the expansion of the EDL due to dilution is less pronounced the larger the valency. As a consequence, while the stored charge is larger for higher valency as expected, the charge vs. surface potential curves corresponding to both salinities are closer in the latter

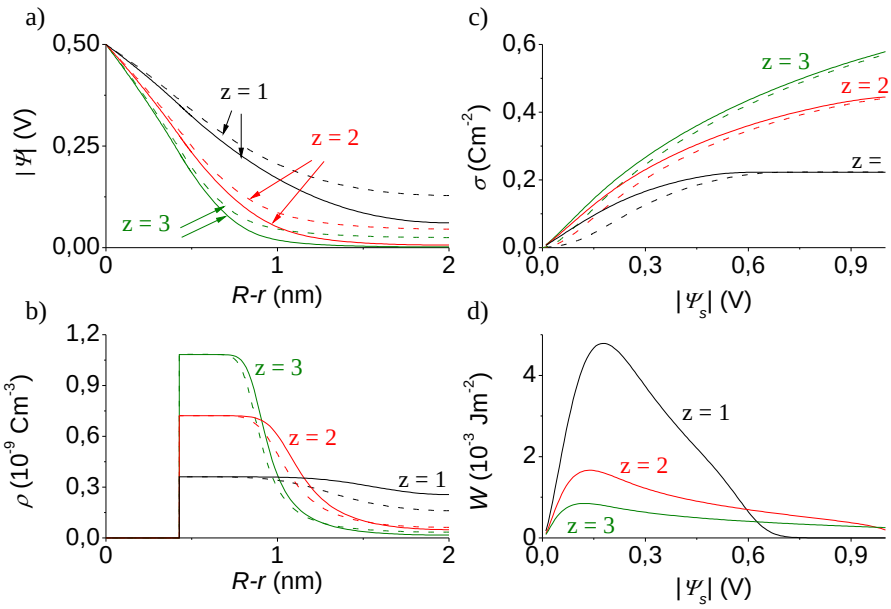

FIGURE 6.1: a) Electric potential and b) volume charge density profiles for a surface potential $\Psi_s = -500$ mV. Solid lines: c(Cl^-) = 0.6 M. Dashed lines: c(Cl^-) = 0.02 M. c) Surface charge density vs. surface potential for the same ionic strengths. d) Extracted work per unit area of pore when the solution considered in a-c are exchanged. In all cases, the valency of the cation is indicated. Ion size: 0.428 nm. Pore radius: 2 nm.

case (Fig. 6.1c). This means that the voltage rise at constant charge ($\Delta\Psi$, Fig. 2.6) decreases and, as a consequence, the extracted work is also reduced (Fig. 6.1d).

Effect of ionic size

The profiles of electric potential and volume charge density in the EDL are plotted in Fig. 6.2a and b for different ionic sizes and different surface potentials. The region of charge density saturation close to the pore wall extends over longer distances the larger the ionic size. The increased ionic volume in this case produces as well a lower value of the saturation charge density, a larger empty Stern layer, and a slower potential decay in the EDL. As a consequence, the surface charge density decreases by increasing

the size of the ions, as can be seen in Fig. 6.2c.

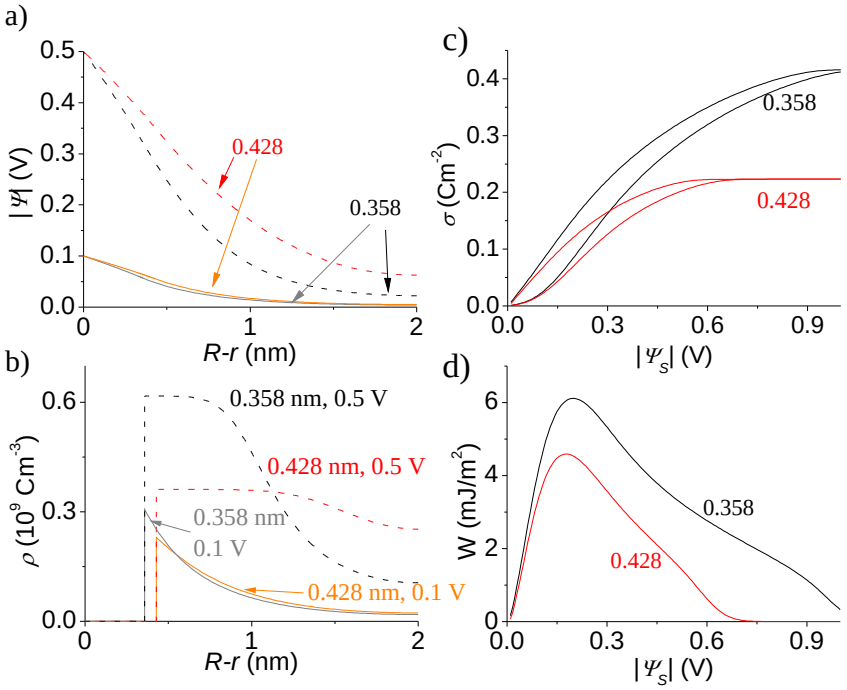

FIGURE 6.2: a) Electric potential and b) volume charge density profiles for surface potentials 0.5 V and 0.1 V, and salt concentration 600 mM. c) Surface charge density vs. surface potential for an ionic concentration 600 mM (solid lines) and 20 mM (dashed lines). d) Extracted work as a function of the surface potential upon exchanging the solutions in (c). In all cases the cation valency is $z = 1$. The cation radii in nm are indicated. Pore size: 2 nm.

Increasing the ionic size leads to a decrease of the maximum energy due to a decrease of the $\Delta\sigma$ of the cycle.

The consequences of this EDL structure on the amount of extracted work are illustrated in Fig. 6.2d. We can see that increasing the ionic size leads to a decrease of the maximum energy that can be extracted per unit area in every CDLE cycle, mostly because increasing the ionic size produces a lowering of $\Delta\sigma$ of the cycle. This can be compared to the valency effect (Fig. 6.1d), mainly associated to a reduction of $\Delta\Psi$ upon exchanging salin-

ity in the CDLE cycle.

Multi-ionic solutions

From the above results, we can expect a lower energy production when the counterion is Mg^{2+} (valency 2, ionic size 0.428 nm) as compared to Na^{+} (valency 1, ionic size 0.358 nm). However, we will find below that new aspects must be taken into account when several counterions with different valencies and sizes compete for the volume close to the surface. Furthermore, the concentration of Na^{+} and Cl^{-} in natural water is far larger than that of other bigger and more charged species. For simplicity we present the simplest case: two counterions and one coion. We choose Na^{+} and Mg^{2+} and the concentrations are given in order to preserve both their ratio in the sea and electroneutrality with respect to the coion (Cl^{-}) concentration. These values are listed in Table 6.1A.

TABLE 6.1: Ionic concentrations selected for simulations of sea and river waters [117]

A: Three ions		
Ion Ion	River Concentration (mol/L)	Sea Concentration (mol/L)
Cl^{-}	0.02	0.6
Na^{+}	0.0167	0.5
Mg^{2+}	0.00167	0.05
B: Four ions		
Cl^{-}	0.019	0.57
SO_4^{2-}	0.0005	0.015
Na^{+}	0.0167	0.5
Mg^{2+}	0.00167	0.05

The different volumes of Na^{+} and Mg^{2+} are accounted for in our model by considering that the maximum concentration attained by Mg^{2+} ions is smaller and the distance of closest approach to the surface is larger than in the case of Na^{+} ions. Information about the structure of the EDL in this

case is presented in Fig. 6.3. We observe that close to the particle there is an empty region followed by a region in which only Na^+ can be present. When we depart a distance enough as to allow the presence of Mg^{2+}, the concentration of Na^+ decreases, because the volume is occupied by the more charged Mg^{2+} ions. The effect is magnified for large surface potential (Fig. 6.3b). In this case, Na^+ concentration decays to zero as a consequence of the Mg^{2+} condensation close to the wall.

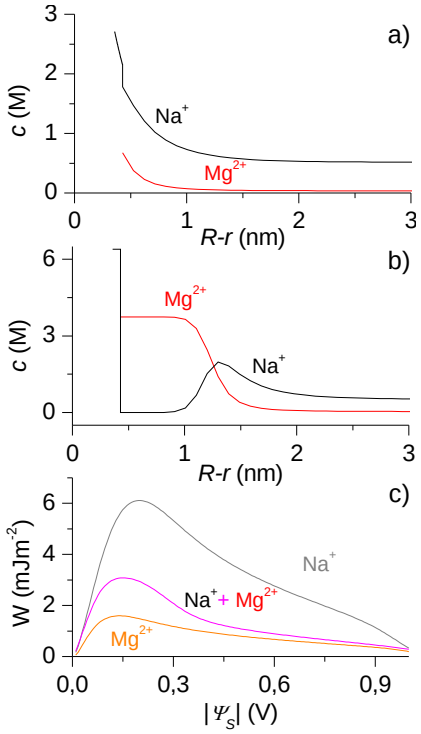

FIGURE 6.3: Counterion concentration profiles for the sea composition given in Table 6.1 and surface potentials 0.1 V (a) and 1 V (b). c) Extracted work per unit area vs. surface potential in the following cases: only Na^+ (sea concentration: 600 mM, river concentration: 20 mM); only Mg^{2+} (respective concentrations: 300 mM and 10 mM); both counterions present, with concentrations as in Table 6.1A. Pore radius 10 nm.

Hence, for moderate to large potentials, and despite the small concentration of Mg^{2+} as compared to that of Na^+, as soon as it saturates the interface, it determines the extracted work (Fig. 6.3c), since it is larger than Na^+

and gives rise to a lower stored charge. Because of its higher valency, the EDL expansion is also lower, and as a result, the extracted work is reduced.

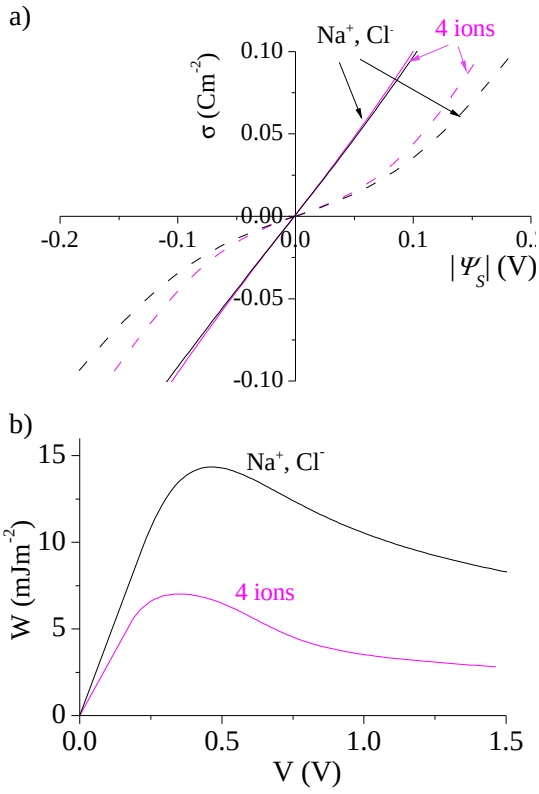

FIGURE 6.4: a) Surface charge vs. surface potential for 20 mM (dashed lines) and 600 mM (solid lines). b) Extracted work per unit area vs. the potential of the external battery. "4 ions" indicates that all ions in Table 6.1B are present with the concentrations there indicated. Pore radius 10 nm.

For the sake of clarity, in Fig. 6.3c we compare the results with those obtained when only one counterion is present, but in the concentration that it would actually have in the river or sea waters. These concentrations simulate the case of a hypothetical previous cleaning of the water from one of the cations. We can see that the extracted work in Fig. 6.3c is not the sum of the works extracted from *clean* waters containing only Mg^{2+} or Na^{+}, but an intermediate value, which is determined by the fact that Na steps aside

when Mg is present and hence, determines the expansion of the EDL. Note also that the effect is very large, in spite of the small amounts of the bigger ions.

Let us finally consider the whole picture with the most abundant ions in the sea: Cl^-, SO_4^{2-}, Na^+, Mg^{2+}, and take into account that the CDLE device consists of two oppositely charged electrodes, not symmetric because of the different sizes and concentrations of their counterions. In a real cycle, charge will be transferred from the positive electrode to the negative one, and hence, the measured potential rise would be the difference between those in each electrode: $V = \Psi_S^+ - \Psi_S^- = \Psi_S^+ + |\Psi_S^-|$. In Fig. 6.4a it is represented the surface charge density vs. surface potential between the electrodes for two cases: only Na^+ and Cl^- and the four ions mentioned. Again, although the mixture provides larger surface charge, the curves corresponding to 20 mM and 600 mM approach each other and hence, the CDLE cycle narrows. The effect on the extracted work is presented in Fig. 6.4b as a function of the potential difference between the electrodes. It is again confirmed that removing large multivalent ions from the solution will give out larger extracted work.

6.2.2. Experimental results

It should be noted that when natural water is used as fuel for a CDLE cycle, there are two aspects to take into account when results are eventually compared to laboratory-prepared NaCl solutions. On one hand, energy production can be altered by the mere change in composition, as we have shown above that both valency and size of counterions can substantially modify the EDL structure and hence the cycle area. On the other hand, natural waters contain suspended material which can additionally produce long-time effects such as electrode corrosion and fouling, which must be properly addressed. This will be dealt with in the following paragraphs.

In this part, we will use the water samples indicated in section 3.1.6. In one case, simulated sea water was prepared containing the amounts of salts detailed in Table 3.2. In the other case, real sea water was taken from the

south coast of Spain (Mediterranean real sea water, MRSW hereafter) and, in some cases, filtered through 16, 11 and 5 μm pore size filters, denominated 16MRSW, 11MRSW, and 5MRSW, respectively, in order to study the already mentioned effects of particulate material in energy production cycles.

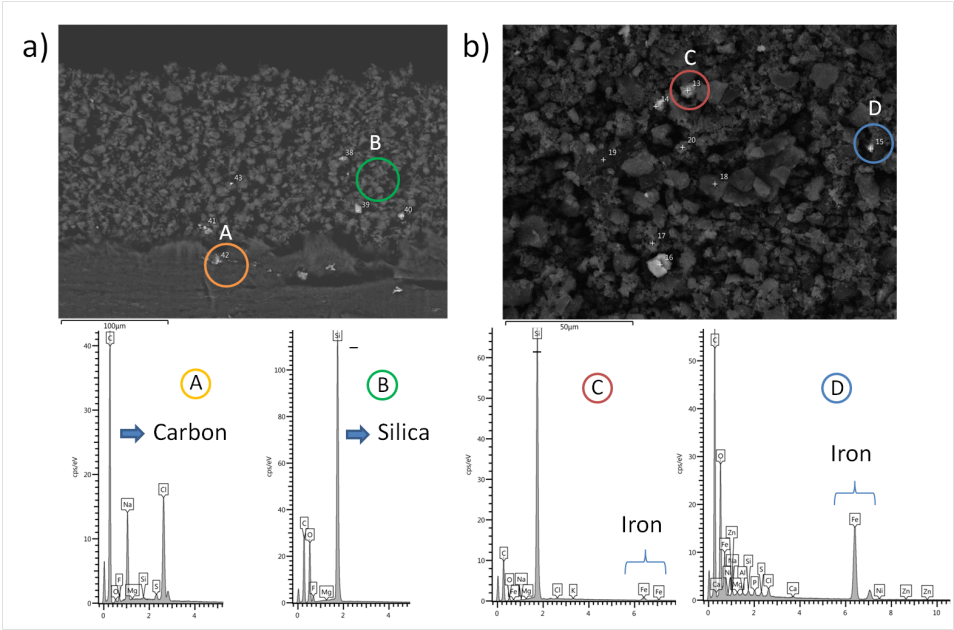

FIGURE 6.5: Top: SEM picture of the section (a) and of the top (b) of the carbon film after cycling natural sea and 20 mM NaCl solutions. Bottom: EDX spectra of the areas marked as A, B, C and D of pictures (a) and (b).

Study of electrode contamination

Prior to the comparison between NaCl and multi-ionic solutions, it appears interesting to analyse, from an experimental point of view, the effect of substances other than ionic species. For this purpose, we have used real sea water in a CDLE cycle, analyzing the effect of the deposits on the electrodes. In this case, the internal structure of the final carbon films was investigated by means of high-resolution scanning electron microscope observations, performed in a Gemini FESEM, from Carl Zeiss (Germany),

considering both transversal cuts of the carbon films, and also a top view of it. An EDX analysis was carried out on specific sites of the samples, in order to ascertain the possible presence of such impurities.

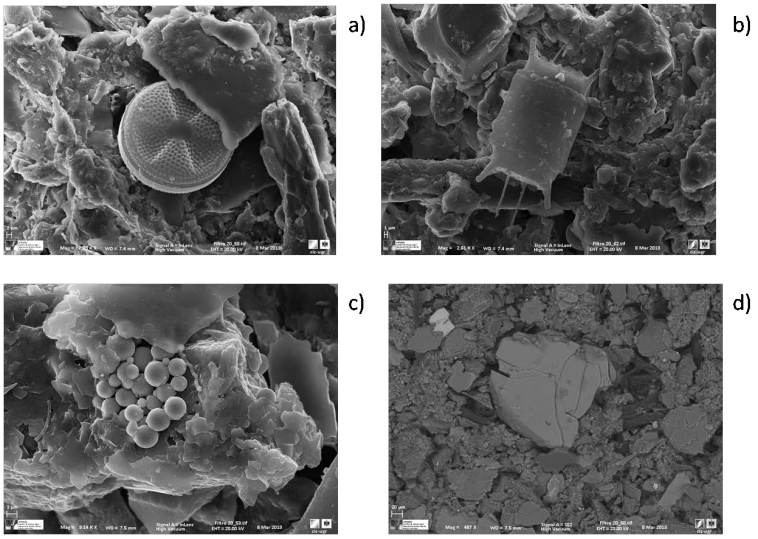

FIGURE 6.6: SEM pictures of the 16 μm filters after filtering natural sea water. (a,b) detail of deposited organic shells; (c,d): inorganic impurities.

Fig. 6.5a shows a transversal view of the carbon film. We can observe the graphite collector which is just below the carbon porous plug. The material composition is mainly carbon as it is shown by the EDX analysis in Fig. 6.5a. Note that a very small amount of materials from the sea water can go all the way through the carbon film. As expected, these are mainly silica or silicates and NaCl. The situation is, as expected, less pristine on the top of the film, that is, the area in immediate contact with the solutions. Fig. 6.5b shows the presence of considerable amounts of Si in some spots (deposited sand particles), and, interestingly, iron. This can come from oxides also in suspension or from corrosion from the valves used.

Although SEM pictures show that some impurities are however observable, both inside the carbon plug and, specially on top of it, it is surprising to find out that we rarely observe an important deposition on the carbon films after being exposed to natural sea water. Hence this drawback may

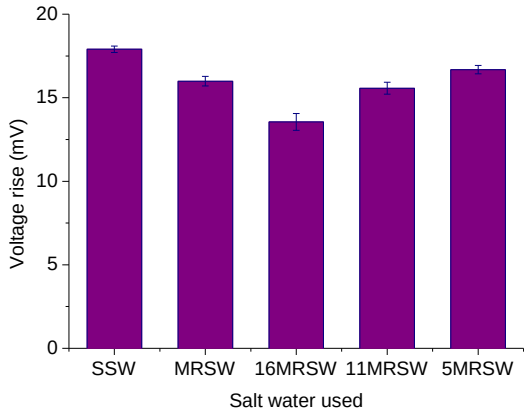

FIGURE 6.7: Voltage rise in the sea-to-river water step when diluted MRSW is used as river water against MRSW, with and without previous filtering through 5, 11 and 16 μm filter pore size.

not be crucial. This may be due to the large amount of river water that is used during the exchange process.

Some idea can be gained from the analysis of the materials deposited on the filters (Fig. 6.6) after natural sea water purification: EDX analysis (not shown) of areas of the pictures demonstrate the presence of spherical particles containing iron (probably iron oxide), as well as silica or silicates and calcium from shells of small animals.

These observations may explain that the negative effect of natural sea water deposits on the cycle performance, although certainly existent, is lower than expected at first sight: Fig. 6.7 shows that only when the filtration is brought to the low practical limit of 5 μm can we say that the value corresponding to artificial seawater is recovered, and water can be considered sufficiently free of impurities from the viewpoint of the CDLE technique. This could be expected from the SEM pictures in Fig. 6.5. There is no important deposition on the carbon film that would lead to a reduction of the extracted energy.

Influence of solution composition

In order to analyze the effect of the multi-ionic composition of natural water, we study separately its effect on the branches of the cycle where sea water is in contact with the electrodes and with river water. Hence, we firstly fixed river water at 20 mM NaCl concentration and studied the effect of using either NaCl 600 mM, SSW or MRSW. Fig. 6.8 shows the behavior of the CDLE cycles in the three cases. In Fig. 6.8a some examples are shown of the voltage variation when successive cycles are performed in the three cases. In this plot, the decrease of the voltage rise when either simulated or real sea waters are used is qualitatively demonstrated. A quantitative view is provided in Fig. 6.8b, where it can be observed that both the potential rise upon salinity exchange and the transferred charge after battery reconnection are reduced when simulated or real sea waters are used. As a consequence, the extracted energy is greatly reduced (Fig. 6.8c). This is in agreement with our theoretical predictions: despite the increase in the valency, the presence of multi-ionic solutions reduces the cycle performance, by reducing the charge transferred and the voltage rise. The effect is most important when MRSW is used.

Not only the overall result of a complete CDLE cycle is affected. The dynamics of the surface voltage upon exchanging salty and river waters may also be affected, since the diffusion coefficients are larger for Na^+ and Cl^- (respectively, 1.33×10^{-9} and 10^{-9} m^2/s) than for Mg^{2+} (0.70×10^{-9} m^2/s) and SO_4^{2-} (1.06×10^{-9} m^2/s). Indeed, this can be observed with a detailed analysis of the dynamics of the voltage after exchanging the solution, especially upon the river water exchange as it is presented in Fig. 6.9. There, it is confirmed that the rate of voltage variation is also dependent on the kind of salt, and in fact the rise appears slower for the sea waters (either simulated or natural) than for NaCl solutions.

Next, we maintain the same sea water (in this case we use a filtered sample, 16MRSW) and we measure the voltage rise for two different kinds of simulated river water. The results of using a simulated river water as 1/30 dilution of the sea water are shown in Table 6.2. The decrease in both the voltage rise and the transferred charge produces a reduction of the energy

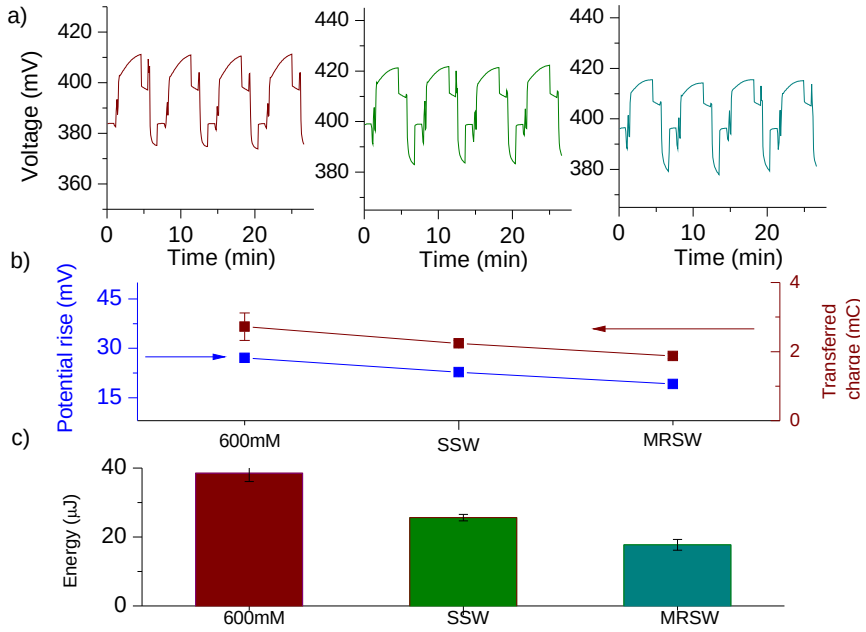

FIGURE 6.8: a) Examples of successive CDLE cycles when NaCl 600 mM (left), simulated sea water (center) and real sea water (right) are used. b) Potential rise (blue, left axis) and transferred charge (dark red, right axis) for the three salty waters examined. c) Extracted energy. In all cases, the river water is simulated with 20 mM NaCl solutions.

extracted in comparison to that obtained when pure NaCl solutions are used.

TABLE 6.2: Comparison of the voltage rise, extracted charge, and energy per cycle obtained with 20 mM NaCl and MRSW diluted 30 times as river water, in otherwise identical conditions: charging voltage $\approx$ 380 mV. 16 MRSW is used as salt water fuel

River Water	Potential rise (mV)	Extracted charge (mC)	Energy (μJ)
20mM	20.60 ± 0.17	1.64 ± 0.08	18 ± 1
1/30MRSW	13.6 ± 0.6	1.09 ± 0.04	7.8 ± 0.6

From the latter results, it is evident that the performance of the CDLE cycle will be also seriously compromised with the salt contents of the river

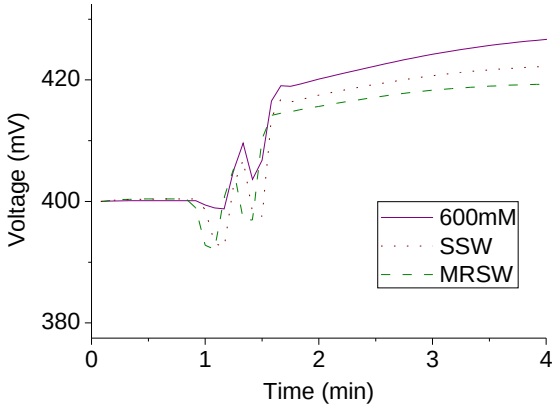

FIGURE 6.9: Detail of the sea-to-river water exchange part of the CDLE cycle, after shifting vertically the data in Fig. 6.8 for making the starting voltages coincident.

water. In fact, as shown, higher salt contents will produce a decrease on the energy extraction. A standard real river water is difficult to set, since the variability in river water composition is even larger than in sea water: it depends on the river basin, and even for the same river basin, it changes with the season, the rain regime, the human activities upstream, and so on. Thus, in this sense, we also find relevant to perform an on site analysis of river water solutions. This work will be presented in the next section and its aim is to shed some light onto these variables in order to advance towards the possibilities of this technique in a real context.

6.3. On site application: the Pacific coast of Central America

In this section, we present the results of an on site experimental study based on the soft electrode capmix technique with the aim of analyzing the potential of this method in the Central America regions. Concretely, we use real sea and river waters taken from the Gulf of Fonseca, an ideal place for blue energy studies [109]. This is a protected area of the Pacific Ocean,

located in midle-west Central America, among Nicaragua, Honduras and El Salvador, as it is illustrated in the map of Fig. 6.10 left. Sea water at the entrance of the Gulf is characterized by a high salinity, about 35 psu (psu: practical salinity unit, it is equivalent to 1 g/L). Upstream, on the contrary, it is found a huge salinity decrease down to 1 or 2 psu [101]. The map of Fig. 6.10 right indicates the location of the the salty and fresh solutions used in this work. Three samples of river water were taken in: El Rebalse, Amatillo river and Pavana river, as shown in the map in light blue. Seawater was taken in Puerto de la Union, as indicated in the same figure in dark blue. Solutions of seawater and river used as references were prepared at the laboratory with respective concentrations 30 g/L and 1 g/L sodium chloride. Sheets of activated carbon film were treated as detailed in section 3.1.4. In this case, we used 100 mM solutions of 200 000 molecular weight PSS polymer and 100 000 molecular weight PDADMAC polymer.

FIGURE 6.10: Right: Map of the Central America Left: map of the Gulf of Fonseca where fresh water samples (light blue) and sea water samples (dark blue) were taken.

Firstly, we studied the influence of real river waters from Gulf of Fonseca. Fig. 6.11a shows the open circuit potential evolution between the

electrodes of the capmix cell when real river water and reference fresh water solution are successively exchanged with reference salt water solution. It should be noted that this kind of measurements indicate the differences in Donnan potentials between both solutions for each case. Thus, open circuit voltage measurements reveal the potential application of this technique for different real concentrations. Surprisingly, it is found that that the potential difference between solutions is larger for the three real river waters as compared to the reference one, reaching a maximum of 250 mV for El Rebalse, which is indeed the one further from the coast. The reason for this result is probably that the samples were collected during the rainfall regime (October), and therefore, the salinity of the river water was less than the simulated one. This produces a voltage difference that almost doubles the reference potential measurement. Table 6.3 shows the electrical conductivities of each of the above mentioned river waters confirming the previous explanation.

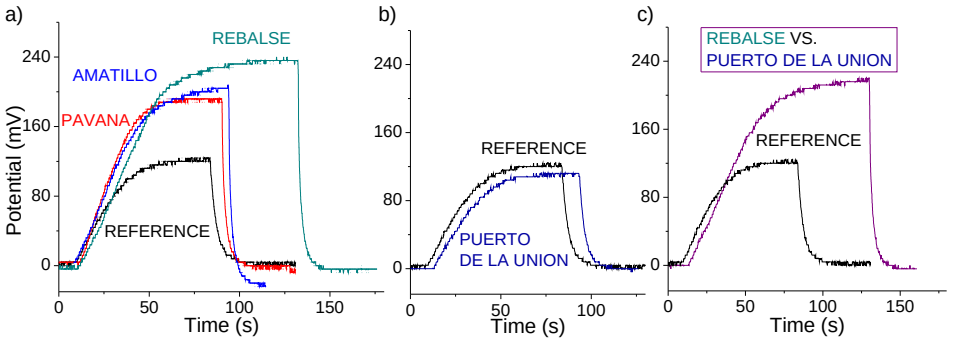

FIGURE 6.11: Evolution of the cell potential as a function of time: (a) when fresh water from rivers in the Gulf of Fonseca (El Rebalse, Amatillo, Pavana) are exchanged with salt water reference solution and (b) when salt water from Puerto de la Union is exchanged with reference fresh water and (c) more realistic case: salt water from Puerto de la Union exchanged with fresh water from El Rebalse. In all graphs is also represented the reference case: salt water vs. river water reference solutions (1 g/L and 30 g/L respectively).

Subsequently, the effect of real sea water in comparison with the reference sea water solution was studied. In these measurements, the reference fresh water solution was used for exchanging in both cases. Fig. 6.11b shows the evolution of the cell potential. As it can be seen, there is a small decrease

TABLE 6.3: Electrical conductivities of each of the measured river waters from the Gulf of Fonseca and fresh reference solution.

River Water	Conductivity
Rebalse	234 μS/cm
Amatillo	274 μS/cm
Pavana	570 μS/cm
Reference	5.19 mS/cm

in the potential difference from 120 mV to 110 mV when actual sea water is introduced. The reason for this measurable potential difference decrease is likely related to the effect of multivalent ions which are commonly present in real sea water (section 6.2). Ions such as magnesium or calcium produce a decrease of the double layer expansion and, also the larger size of theses ionic species is responsible for the decrease of the stored charge at the electrodes. These two factors working together bring about a reduction of the potential difference.

A final comparison will be presented of the evolution of the cell potential for realistic sea and river water solutions with the simulated concentrations of sodium chloride. Fig. 6.11c shows that, as expected from results above discussed, the potential difference is considerably improved by introducing river water from El Rebalse even when we use natural sea water from Puerto de la Union. Despite the presence of other ions, the use of unfiltered water and the possible presence of black water, we do not find a decrease of the potential difference. Indeed, an important increase is found associated to the lower salinity of the natural river samples during the experimental period. Thus, it can be concluded that soft electrode capmix techniques will be highly favoured during the rainy season, yielding results much better that those obtained with the laboratory reference.

An important increase of the energy extraction is found due to the lower salinity of the natural river samples collected in the rainy season of El Salvador.

6.4. Capmix cell stacking research

The predicted amounts of energy for CDLE are way larger than those experimentally achievable. In fact, theories of EDL capacitance (section 2.4) predict that the voltage rise when salty and fresh water solutions are exchanged is about 80 mV on each electrode, while the surface charge density typically changes by 0.02 C/m^2. This means that in a complete cycle the energy obtained should be around 2 mJ per square meter of EDL. Furthermore, taking into account that the experiments are carried out with activated carbon or similar material with a specific surface area of 1000 m^2/g or more, the energy that might be made available could amount to 4 J/cycle with just 1 g of carbon per electrode. A power density estimation can be given: assuming that the mass of carbon is distributed on an area of 20 cm^2 (this would be the apparent electrode area), and that the cycle duration is 100 s, the power available would be 2 W/m^2, if the efficiency is 10%. On contrast, experimentally, the power achieved is not higher that 10 mW/m^2. The reasons for this huge difference have already been explored: the existence of charge leakage by progressive discharge of the EDL (section 4.2), carbon hydrophobic characteristics (section 4.4), etc. Whatever the reason, it is clear that some method must envisaged in order to increase the amount of energy and power available, if the technique should become competitive at some time.

Furthermore, in order to implement this technique in an electronic circuit, higher voltages are required, more than 1 V being preferred. This goal can be achieved by either amplifying the output signal, which runs against the efficiency, or improving the cell design. In this section, we propose to increase the voltage output by associating several individual cells, as previously done with other capmix devices [60–62] and we show some possible ways to do this, both in CDLE and in polyelectrolyte-coated or soft electrodes [110].

The experiments to be described below were carried out using Norit DLC Super 30 activated carbon particles for the preparation of carbon electrodes following the indications of section 3.1.2. For the SE technique, the preparation conditions (section 3.1.4) were 60 mM of 200 000 molecular weight

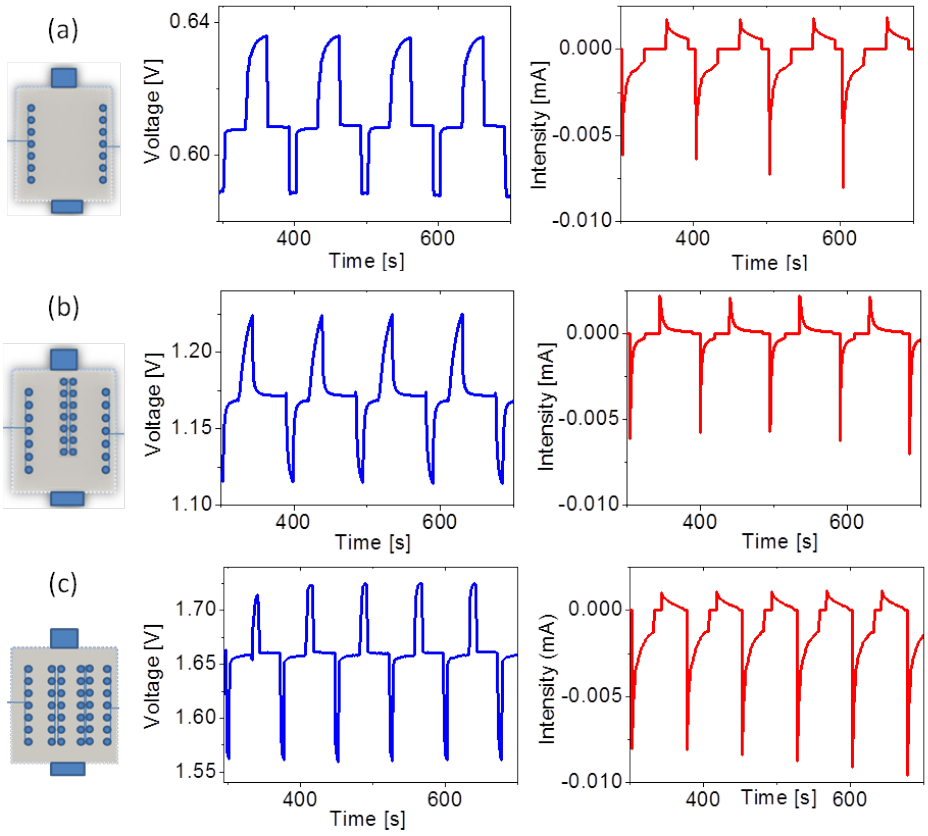

FIGURE 6.12: Voltage and current cycles in the CDLE experiments with one (a), two (b) and three (c) cells connected in series. The charging voltages were 0.605 V (a), 1.17 V (b) and 1.66 V (c)

PSS polymer and 60 mM of 100 000 molecular weight PDADMAC polymer. Finally, the designed cells association was detailed in section 3.1.5. In a first stacking approach, we simply connect the electrodes side-by-side and only the outermost ones can be connected to the external source (Fig. 3.5a). Alternatively, we will also design a stack where potential and current between cells can be measured (Fig. 3.5b).

6.4.1. Cell stacking in CDLE

We will consider the series association shown in Fig. 3.5a. It might be expected that by associating the electrodes back-to-back, the voltage rise linked to each pair would be multiplied by the number of cells. If the internal resistance per pair does not change substantially, then the current will be comparable to that of a single cell and as a result, the power would be increased by a factor equal to the number of individual cells. The comparison between voltages and currents oscillations along the cycles, obtained with one, two and three cells is presented in Fig. 6.12. The cycles start with the charging process of the cell. Negative currents in this Figure correspond to this process, and positive ones indicate charge extracted from the system (discharging of the cell).

We observe that the total voltage used for charging was roughly three times larger than the one needed in the simple cell setup. The average voltage rise when fresh water enters the stack was about 29 mV, 44 mV, and 65 mV for one, two, and three cells, respectively. Although the voltage elevation increases with the number of cells, it is not strictly proportional to this number. In addition, the charging and discharging currents are very similar in all cases, indicating that even if the charging voltage is three times larger, so is the internal resistance. Hence, both sets of data taken simultaneously suggest that the proposed stack association produces an amount of energy which does not increase as much as expected.

Using the data in Fig. 6.12, we can calculate the energy per cycle in each of the associations, including the single-cell device. Thus, the CDLE stack produces an average of 0.21, 0.78, and 0.76 mJ per cycle, for one, two and three electrode pairs, respectively. Considering the electrode area (3.14×10^{-4} m^2 each), these values correspond to 330, 620, and 400 mJ per m^2 of apparent electrode area. In order to estimate the efficiency of the technique, several possibilities do exist [50]. In this contribution, we choose one based on the comparison between the area of the experimental cycle and the theoretical predictions (section 2.4) obtained for a cycle where the charge transferred in the process equals the experimental one. Fig. 6.13 shows the details: the predicted voltage jump and charge transferred (per

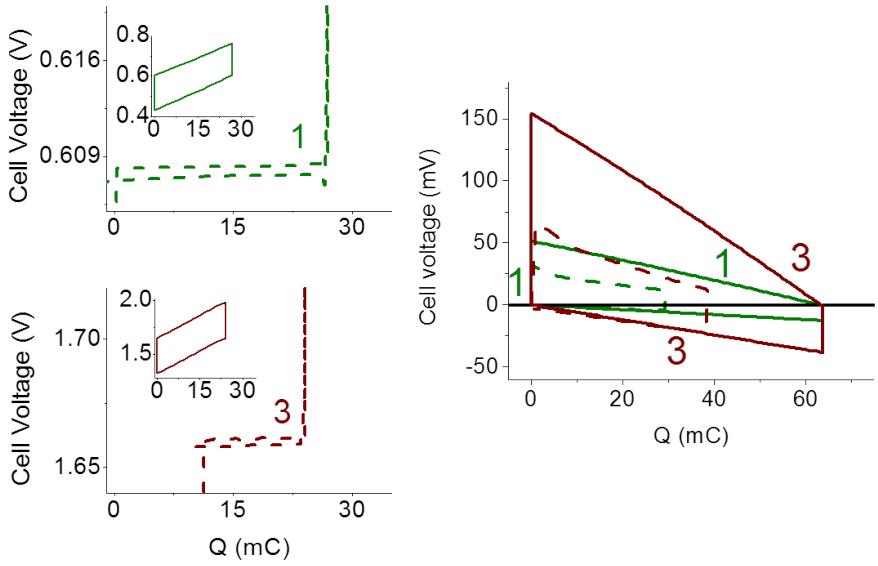

FIGURE 6.13: Left: CDLE cycles for one and three cells. Inset: Theoretical calculations for the same charging voltage and amount of charge transferred. Right: Energy cycles for coated (SE) electrodes. Theoretical (solid lines) and experimental (dashed lines) results. The number of stacked cells is indicated.

unit area of pore) are, respectively, 160 mV and 70 mC/m^2, if the electrode voltage is 300 mV, and the exchanging solutions are 500 and 20 mM NaCl. For these calculations, the carbon film is simulated as a network of cylindrical pores 5 nm in radius. With these data, the energy that could be theoretically obtained amounts to 5.6 mJ per m^2 of pore area. Integration of the current vs. time curves in Fig. 6.12 allows us to determine the exchanged charge, namely, 27.2 mC for a single cell. This means that the electrode area effectively participating in the capmix process is (27.2 mC)/(70 mC/m2), or 0.39 m^2. This is approximately 1 % of the total pore area in a carbon film, considering the specific surface area of Voltea carbon (959 m^2/g) and the amount of carbon per electrode (0.038 g). This reduced use of the available carbon pore surface is quite common in capmix systems: the exchange of solutions does not reach the whole pore surfaces to the same extent. This is confirmed in numerical simulations by Rica et al. [112].

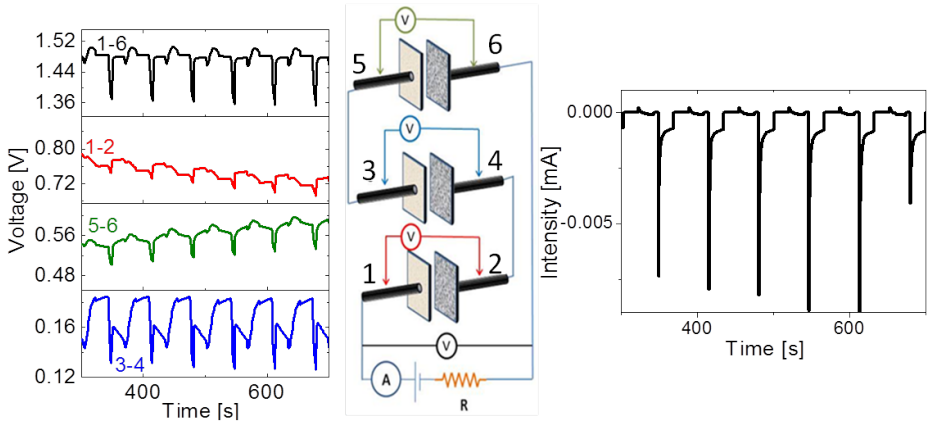

FIGURE 6.14: Voltage (left) and current (right) oscillations during the Capmix cycles. The left panel shows the oscillations of the voltage difference between the indicated electrode pairs.

As Fig. 6.13 shows, the area of the experimental cycle is smaller than that of the theoretical one: the voltage drop in internal and load resistances is not taken into account in the model, and furthermore, the voltage rise is also lower than predicted, due to unavoidable leakage. The amount of energy that might be obtained from one cycle would be 5.6 mJ/m^2 $\times$0.39 m^2, or 2.1 mJ. Referred to the apparent electrode area (discs 1 cm in radius), the result is 6.7 J/m^2. Since our experimental data is 0.333 mJ/m^2, we can conclude that the device allows to obtain 5 % of the energy available for one cell. The calculation for three cells in series is also shown in Fig. 6.13: the prediction in this case is 4.3 J/m^2, and our efficiency would be around 10 %. In this calculation, the work required for the initial charging of the electrodes is not included. It can be estimated to be on the order of 17 J, although the full charging must be performed only once during operation, and hence this requirement of further energy (when divided by the number of cycles) can be made negligible. In addition, in our device we do not use pumps, but valves, and the solutions are fed by gravity. The power required for opening the valves is 12 W, so that a completely autonomous system would require a significant up-scaling.

In order to find an explanation for this behavior, stack#2 (Fig. 3.5b) ap-

peared useful, since it allows for the separate connection of each individual cell to the external circuit. Although this might suppose a larger internal resistance, and it is certainly less compact than stack#1, it offers access to individual measurements. As an example, Fig. 6.14 shows the voltage of each electrode pair (numbered as in Fig. 3.5b) and the total current during successive cycles, after charging with 1.48 V between the outermost electrodes.

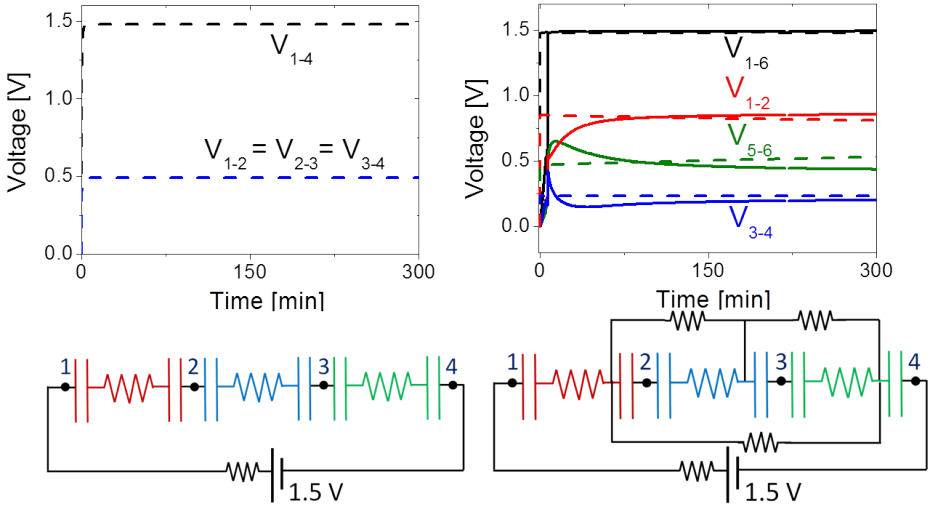

FIGURE 6.15: Time evolution of the voltage of individual capacitors in a series association. Left: Conductive connections exist only between neighbor plates. Right: experimental charging data in stack#2 (solid lines), and simulations (dotted lines) when additional connections are established through external resistors (bottom). The parameters used for the simulation are: C=1 F; R_L=5 Ω; R=100 Ω; R_1=50Ω; R_2=200 Ω; R_3=500 Ω.

It must be noted that the base voltages of each pair are different (Fig. 6.14 left), and do not correspond to the expected value, namely, one third of the overall applied voltage difference. This can be understood by considering the simulation (using LTspice IV, Linear Technology, USA) of the process of charging a series association of capacitors in two cases: the ideal one (conductive connections do only exist between adjacent plates, Fig. 6.15 top) and one in which cells are further connected through external resistors, simulating the conducting path established by the electrolyte solution

(Fig. 6.15 bottom). In the latter case, the stationary voltage of every cell is in good agreement with the simulation results. This calculation indicates that the effect of the conduction between plates of different cells leaves the inner cell (not directly connected to the external circuit) inoperative. Hence, only the capacitors in contact with the charging source contribute to the voltage rise, while the latter is negligible for the internal cell, effectively charged with a low voltage. This limitation appears inherent to the series connection in the CDLE technique.

The fact that the charging voltage is different for each pair has important consequences on the CDLE cycles. As shown in section 2.4, the voltage rise associated to the exchange of salty for fresh water is maximum at intermediate charging voltages. As illustrated in Fig. 6.14, this is precisely what we find: the voltage rises are as indicated in Table 6.4, and they decrease when the effective charging voltage is above 300 mV, roughly, a confirmation that an optimum working voltage exists for CDLE, and that even in stacks, any sub-cell being charged above or below that optimum value will be working out of the best regime.

TABLE 6.4: Charging and rise voltages for the different electrode pairs connected in series as in Fig. 3.5b.

Pair	Charging voltage (mV)	Voltage rise (mV)
1-2	0.761	-5
3-4	0.145	+30
5-6	0.558	+15
1-6	1.460	+40

Both results, namely, the lack of activity in the inner cell and the deviation from the optimum conditions in each of them, are very significant for the design of practical setups based on the CDLE principle: although association in series might increase the potential jumps, such an increase is in reality very limited, and does not compensate for the rise in internal resistance.

6.4.2. Association of polyelectrolyte-coated electrodes

One way of improving on the CDLE method, as already mentioned, is based on using activated carbon films coated with polyelectrolyte layers, with either negative (PSS) or positive (PDACMAC) distributed charges. In Fig. 6.16 we show the voltage of the stack#1 with up to three pairs of films (PSS- PDACMAC// PSS- PDACMAC// PSS- PDADMAC) upon successive exchanges of salty for fresh water and viceversa. As expected, the cell potential (a result of the difference between the respective Donnan and EDL potentials) increases when fresh water enters the inter-electrode spacing and decreases when it is salty water that feeds in. Additionally, it increases with the number of cells in the stack.

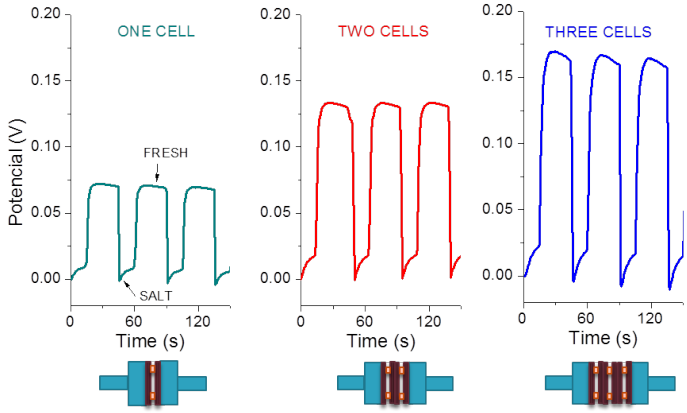

FIGURE 6.16: Open circuit voltage for one, two, and three stacked cells (stack#1, Fig. 3.5) consisting of PSS/PDADMAC coated pairs of electrodes, when salty and fresh solutions are exchanged.

From the practical application point of view, it is also important to consider the behavior of the stack in closed circuit operation, when it is maintained in connection with the external load resistor at all times. The result in this case is most promising, as we can see in the representation of Fig. 6.17. The increase in power available when the electrodes are associated in series is a certainly significant result, ranging from 30 mW/m^2 for one pair of electrodes, to 77 mW/m^2 in the case of using three pairs

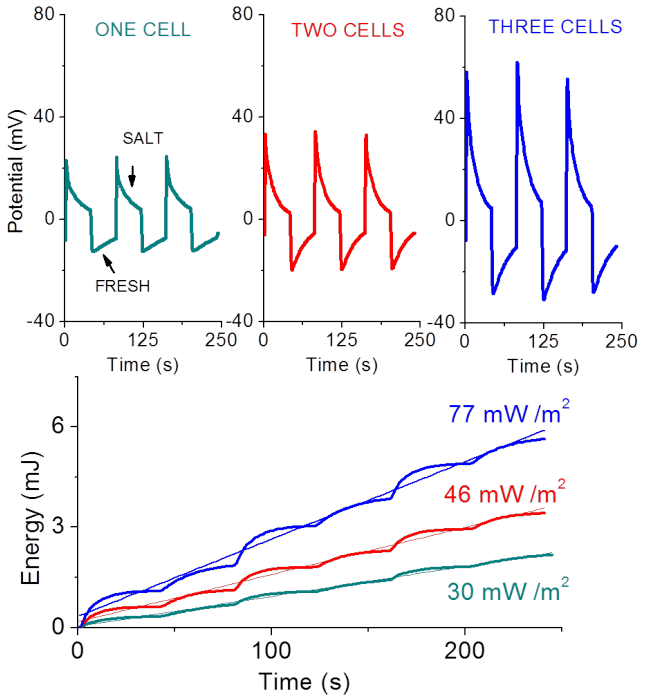

FIGURE 6.17: Top: cell potential cycles in one, two and three cell stacks in closed circuit operation with a 10 Ω load. Bottom: energy vs. time, and average power in each case.

of treated activated carbon films. This positive outcome comes from the fact that the individual capacitors are spontaneously and independently charged by the presence of the polyelectrolyte coating, without the need of connection to an external source and the subsequent coupled charging process.

The SE technique is very suited to series association for increasing the output power, without reducing efficiency significantly.

It may be of interest to analyze, as was done before in the analysis of the CDLE stack, the efficiency of the SE cells by comparing the cycles obtained with those predicted using a model for polyelectrolyte-coated electrodes. This is done in Fig. 6.13 as in the CDLE case, we start from the ex-

perimental data of charge transfer, and use the calculations described in section 5.2. Using electrophoretic mobility data we could estimate the volume charge density of the polyelectrolyte coatings ($\pm$ 6 $\cdot$ 10^6 C/m^3), and the electrokinetic theory for soft particles was used for predicting the voltage-charge profiles in the coated electrodes. The results in Fig. 6.13 confirm that our experimental data in SE cells approach the theoretical predictions, so that the efficiency, evaluated as the ratio between the areas of the measured and predicted cycles amounts to 54 % (single cell), and 40 % (three cells connected). It can be suggested that the SE technique is very suited to series association for increasing the output power, without reducing efficiency significantly.

6.5. Summary and conclusions

In this chapter, we have tackled some issues related to capmix real implementation in order to succeed in optimizing a future capmix device. In the first place, we have presented a study of the effect of using realistic water compositions in CDLE cycles. We have experimentally observed that the main difference in the extracted energy (as compared to NaCl solutions) comes from the presence of multivalent ions. Despite the small amount of multivalent ions in sea and river waters, they contribute with a measurable decrease in the extracted energy. We have presented a model capable of predicting such behavior: multivalent ions produce a decrease in the double layer expansion responsible for the net energy gain in a CDLE cycle. Also, the larger size of these ionic species is responsible for the decrease in the stored charge at the electrodes. These two factors working together bring about a reduction of the extracted energy in spite of the small relative concentrations of the larger, divalent ions.

A further step on the research of the effect of realistic water composition in capmix technologies has been made by the collection of water from the the Gulf of Fonseca (El Salvador). This location has been selected as a region of high salinity water concentration and at the same time, a great abundance of rivers. Open circuit measurements have been performed to study the maximum potential difference between electrodes of

polyelectrolyte-coated activated carbon film for real sea and river waters of this gulf. It can be concluded that even the presence of multivalent ions and dispersed pollutants (mineral particles, bacteria) does not significantly influence this capmix technique as it was predicted before. The reason comes from the heavy rainy season when all river water samples were taken. This fact reduces the ionic content of the river increasing the salinity difference with ocean waters. This would lead to consider the high potential of SE technique in the winter season in Central America due to the variability of water samples composition.

Finally, searching for increased energy and power production in SE and CDLE techniques, we investigate the possibility of associating individual cells (pairs of porous electrodes) in series. Using the CDLE method, it is found that the voltage rise when salt water is substituted by fresh water is roughly a multiple of the rises of individual cells, while the current is the same in all cases. An analysis performed on individual cells demonstrates that the conductive connection between non-adjacent units due to the permeating electrolyte solution leaves only the outermost cells as actually working ones. In contrast, the series association appears very advisable when the technique used is based on poly(electrolyte) coated (or spontaneously charged) electrodes. In such a case, the open circuit voltage effectively increases with the number of cells connected, and, most important, the power produced also increases when a closed circuit configuration, with a load resistor always present, is employed.

7

Conclusions

Conclusions

Here we present the essential contributions obtained from this dissertation. Salinity or blue energy source exists everywhere in nature and it is associated to the release of the Gibbs free energy of a system when two liquids or gases containing different compositions are mixed without chemical reactions. Remarkable advances in fundamental studies, experimental investigations and field demonstrations have been carried out towards finding efficient methods in the past decade. Among all these blue energy methods, capmix techniques, particularly CDLE (capacitive double layer expansion) and SE (soft electrode) technique, have been deeply investigated by both an experimental and a theoretical point of view in this thesis.

The main contribution of this thesis can be summarized as follows:

DLE modeling

We have presented a model for the extracted energy in an ideal cycle of the Externally-Charged-Capacitive-Method. This model is based on the structure of the EDL for a cylindrical pore and takes into account the EDL overlap and the size of the ions (NaCl in this case).

- We have presented a model for the extracted energy in an ideal cycle of the Externally-Charged-Capacitive-Method. This model is based on the structure of the EDL for a cylindrical pore and takes into account the EDL overlap and the size of the ions (NaCl in this case).
- The most significant effects arez observed when the ionic size is considered.
- The extracted energy per unit surface area increases (decreases) with pore size for low (high) potentials.
- The model shows that the ionic size limits the extracted energy that can be obtained with this method to far smaller values than those predicted for point ions.

- In order to obtain the maximum energy, the electrode potential cannot exceed a value of around 200 mV.

Materials and methodology

An analysis has been carried out of the materials and method which are needed for the implementation of the whole capmix process at lab-scale. The main conclusion in this aspects are:

- Extracted energy by CDLE technique can be improved if temperature of the solutions is suitably chosen.
- It is even possible to extract electrical energy from thermal gradients without the need of electromechanical converters.
- The average pore size of activated carbon particles is a determinant quantity. Indeed, optimum CDLE results will be obtained if the carbon used in the electrodes has a significant fraction of mesopore population.
- Significant improvements in efficiency and power density are expected when the technology combining temperature and salinity gradient are further developed.
- Salinity differences beyond the usual 20 mM-500 mM have been tested. It was concluded that these salinity sources could improve extracted power as well as its positive environmental impact.

The soft electrode method

Soft Electrode method is based on the simple deposit of a polyelectrolyte layer on the carbon films. The main difference to CDP is that the membranes are replaced by shells of polyelectrolytes. We have found that:

- SE technique might become an efficient salinity gradient energy method in terms of voltage rise.
- Comparison with membrane-based techniques has shown that, although the energies per cycle are similar, the power is lower in SE.

- It has been found that positive and negative polyelectrolytes adsorb differently on activated carbon.
- PSS seems to adsorb inhomogeneously on the pores of the outermost carbon layers.
- On the contrary, in the case of PDADMAC, we probably have a homogeneous thin layer staying on the surface of the film, which reacts very quickly to salinity changes.
- Further investigation on polymer selection, methods for film treatment and stability of the coating are needed to improve the power output.

Capmix in real world

We analyzed some aspects related to capmix implementation in *real world* conditions. Concretely:

- We have presented a study of the effect of using realistic water compositions in CDLE cycles.
- We have experimentally observed that the main difference in the extracted energy (as compared to NaCl solutions) comes from the presence of multivalent ions.
- A further step on this research was carried out for SE method by the collection of water from the the Gulf of Fonseca (El Salvador).In this case, the presence of multivalent ions and dispersed pollutants (mineral particles, bacteria) does not significantly influence SE technique.
- The increase of energy and power in SE and CDLE technique was investigated by associating individual cells (pairs of porous electrodes) in series.
- It is found that the conductive connection between non-adjacent units due to the permeating electrolyte solution leaves only the outermost cells as actually working ones.

- In contrast, the series association appears very advisable when the technique used is based on poly(electrolyte) coated electrodes. This result present SE as a promising alternative for capmix methods.

To sum up, we conclude that blue energy holds great promise to become an economical and environmental energy resource, available throughout large parts of the world. Nevertheless, the technology to economically harvest this energy has not been developed yet and our work can be considered as a a preliminary result. The electrical work is made available without the use of any kind of electromechanical converters as dynamos or turbines. Finally, this type of energy generation is inherently clean as this process is based on natural mixing processes, which happens anyway in river deltas and estuaries. Neither CO_2 nor thermal contamination will occur. This energy source is renewable as it is based on the hydrological cycle powered by the sun. Hopefully, more investigation will bring about an improvement of the power harvesting.

8

Resumen

8.1. Introducción y objetivos

La producción de energía eléctrica a partir de fuentes renovables supone uno de los retos necesarios para cambiar el actual sistema eléctrico mundial, que perjudica gravemente el medio ambiente de nuestro planeta, provoca desigualdades en la distribución de la energía y es una de las causas importantes del cambio climático. Gran parte de la investigación científica actual se centra en la búsqueda de nuevas fuentes de energía y la optimización de las ya existentes. Aunque la energía solar y eólica lideran en eficiencia las energías renovables, en las últimas décadas otras opciones van tomando relevancia. Entre ellas, la propuesta publicada inicialmente en 1950 [17] y posteriormente en 1970 [16, 18, 39] que plantea cómo la considerable diferencia de salinidad entre el agua de mar y el agua dulce (500 mM y 20 mM, respectivamente) podría usarse en la generación de energía eléctrica. Las fuentes de energía renovable que aprovechan esta diferencia de salinidades se conocen como **energía azul**.

En el caso de la desembocadura de un río, se produce continuamente la mezcla de un cierto volumen de agua con poca salinidad (llamemos c_1 a su concentración de sal) con un volumen mucho mayor de agua salada (concentración c_2). La termodinámica nos dice que la difusión libre experimentada por los iones del agua de mar hacia el volumen de agua de río produce un aumento de entropía (más desorden que en la situación inicial en la que los volúmenes se encontraban separados). Y un aumento de entropía se traduce en una disminución de energía libre, como ocurre para un proceso espontáneo. Puede decirse que los iones del agua de mar pasan de una zona de mayor presión (es la presión osmótica, aproximadamente dada por la expresión de van't Hoff, $p_2 = c_2RT$) a una de menor presión; esta diferencia es del orden de $\Delta p = (c_2 - c_1)RT$, o aproximadamente 10 atm por cada tipo de ion (o alrededor de 20 atm para soluciones de cloruro sódico). Esta presión es equivalente a una columna de agua de 200 m. Por tanto, la energía perdida (que, en parte, queremos utilizar) sería ΔpV o aproximadamente 2 MJ por metro cúbico de agua mezclada. Si todo el caudal del río Guadalquivir (en promedio 164 m^3/s) pudiera aprovecharse para este fin, la potencia disponible sería superior a tres veces la consumi-

da en la ciudad de Granada, la cual está en torno a 100 MW (<www.junta de andalucia.es>). De manera similar, para todo el planeta se estima que la potencia total que se podría extraer mediante estas técnicas alcanzaría 2 TW, que coincide con la demanda eléctrica anual [20].

Para poder extraer esta energía, la investigación actual se centra en la búsqueda de métodos eficientes. Entre ellos, destacan las técnicas que pueden considerarse recíprocas de las de desalinización como la **electrodiálisis inversa** (RED) [40] y la **ósmosis de presión retardada** (PRO) [35]. A pesar de los considerables avances realizados en las técnicas citadas [19, 24, 32] estos son en su mayoría a escala de laboratorio. Además, presentan claros inconvenientes que deben ser resueltos, principalmente en relación con las membranas y su coste, así como la necesidad de utilizar convertidores adicionales, tales como turbinas para producir energía eléctrica de forma efectiva.

Este contexto ofrece oportunidades a tecnologías alternativas, en concreto, las que presentamos en este trabajo, denominadas **técnicas capmix**, destacando de entre ellas esencialmente dos, conocidas como **CDLE** (capacitive energy extraction based on double layer expansion methods) [49, 50] y **CDP** (capacitive energy extraction based on Donnan Potencial) [58, 61]. En la primera, se tiene en cuenta que el potencial eléctrico en la interfase sólido/disolución iónica aumenta, si la carga es constante, al disminuir la fuerza iónica. Esta propiedad es ampliamente conocida en la ciencia de las interfases y sistemas coloidales y es debida a la **expansión de la Doble Capa Eléctrica** (DCE). Su origen es fácil de entender: la mayoría de las sustancias adquieren carga eléctrica cuando se ponen en contacto con un medio polar como el agua, por ejemplo, debido a la disociación de grupos ionizables superficiales. Por ello, las técnicas se basan en el hecho de que la DCE puede acumular una enorme cantidad de carga si el área superficial es suficientemente grande, y, además, su capacidad depende de forma significativa del contenido iónico del medio (véase Fig. 8.1 arriba).

En la técnica CDP (véase Fig. 8.1 abajo), las interfases se cargan sin una fuente de alimentación externa, pues se genera automáticamente una diferencia de potencial entre los electrodos, manifestación de la diferencia de potenciales Donnan asociados a las membranas selectivas de iones de

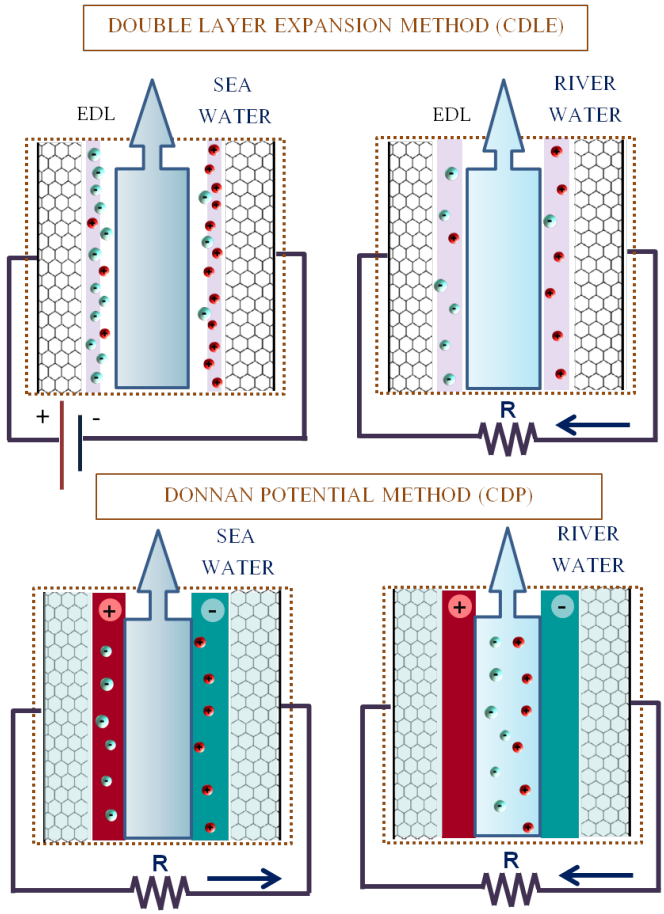

FIGURA 8.1: Esquema ilustrativo del funcionamiento de las técnicas capmix: CDLE (arriba) and CDP (abajo). Las líneas gruesas discontinuas representan las membranas de intercambio iónico.

carga opuesta en cada uno de los electrodos. En principio, el enfoque de CDLE sería más barato y más fácil de implementar debido a la ausencia de membranas. A pesar de esto, los problemas de autodescarga de la celda han impedido un avance real de esta técnica [57].

Recientemente, se ha desarrollado una nueva técnica que combina aspectos de las dos tecnologías Capmix originarias, CDP y CDLE (Fig. 8.2). Esta técnica está basada en el uso de electrodos recubiertos de polielectroli-

tos (polímeros susceptibles de cargarse eléctricamente, por disociación de grupos ionizables en su estructura), que denominamos **electrodos soft o SE** [53, 63]. Puede decirse que SE aprovecha la generación espontánea de potencial, como CDP, pero evitando el uso de las membranas, como CDLE. Se basa, por tanto, en la modificación físico-química de los dos electrodos de carbón activo mediante una capa de polielectrolito, catiónico o aniónico, respectivamente. De esta forma, este método presenta numerosas ventajas pues reduce las pérdidas que presenta el método CDLE, y evita el uso de membranas de intercambio iónico como CDP, siendo por ello mucho más económico.

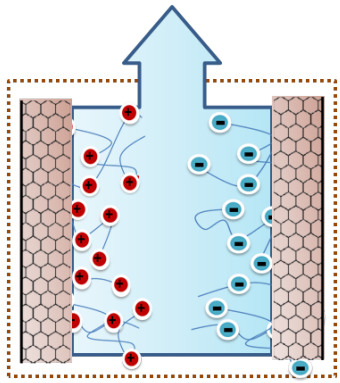

FIGURA 8.2: Esquema ilustrativo de la celda capmix con electrodos recubiertos de polielectrolitos para la técnica de electrodos soft o SE.

Con esta motivación, los objetivos esenciales de esta tesis son los siguientes:

- **Modelización del proceso de extracción de energía por métodos capmix**. Debido a la existencia de un gran número de efectos y la complejidad teórica del fenómeno, es necesario encontrar un modelo que explique el proceso en su totalidad.
- **Optimización de los electrodos, materiales y otros parámetros experimentales** para la mejora del proceso de extracción de energía azul. Se trata de conocer las propiedades de los materiales que pueden afectar en la extracción óptima de la energía y desarrollar electrodos eficientes con respecto a la electrocinética del proceso.

- **Estudio de los electrodos cargados con polielectrolitos** catiónicos y aniónicos, respectivamente (electrodos soft) y su potencialidad como técnicas capmix.
- **Aplicación de las técnicas capmix en contextos reales**. Para ello, se ha estudiado el efecto multi-iónico del agua de mar real. Los iones presentes en el mar son muchos más que el cloruro sódico generalmente estudiado. Además, se ha trabajado en el desarrollo de un stack, analizando un modelo de varias celdas en conexión serie o paralelo.

8.2. Principales resultados

Evaluación teórica de la energía extraída

Los electrodos en su mayoría están formados por un conjunto de micropartículas porosas de manera que dos tamaños de poro están presentes: los macroporos (espacio entre partículas) y los microporos (dentro de las propias partículas). La carga superficial es mucho mayor para los microporos de manera que el electrodo total puede modelarse como suspensión de nanopartículas esféricas, o un haz de poros cilíndricos. Se ha desarrollado un modelo riguroso para el análisis de la estructura de la DCE, y de esta manera, ha sido posible describir las relaciones carga-potencial de los microporos usando el modelo de celda (en caso de esferas) o el cálculo riguroso de la distribución de potencial (en el caso de poros cilíndricos).

El potencial al que se cargan los electrodos puede ser relativamente alto (varios cientos de mV) y el diámetro de los poros de carbón activo suele ser del orden de los nanómetros, de modo que los modelos que suponen bajo potencial e interfases planas no pueden describir con precisión este proceso. Por ello, hemos propuesto que los siguientes aspectos puedan tenerse en cuenta:

- **DCE con interfase no-plana.** Debido a que los poros más abundantes son típicamente de menos de 10 nm, los efectos de la curvatura sobre el perfil de potencial eléctrico serán significativos.

- **Solapamiento de DCE.** Es posible que exista superposición de DCE para el caso de los poros más pequeños y las soluciones menos concentradas.

- **Potenciales elevados de carga**. La extracción de energía será mayor cuando mayor sea la cantidad de carga transferida de forma que es necesario explorar potenciales tan altos como 500-600 mV.

Para la interacción entre los iones, usamos una aproximación de campo medio en la que se tiene en cuenta el volumen excluido por los iones. Así, las ecuación de Poisson se resolverá separadamente en diferentes regiones (en concreto, tres regiones para dos iones). De esta forma, los iones tendrán un radio de máximo acercamiento a la superficie cargada. Esto determina una región libre de carga al comienzo de la capa difusa, y fue por primera vez presentada por Stern y se ha convertido un componente clásico de la electroquímica de la DCE [76].

Los resultados más relevantes obtenidos se refieren al cálculo de la energía extraída por ciclo para las relaciones carga-potencial de dos soluciones distintas, en concreto, 20 y 500 mM. Para cada potencial puede calcularse el área de un ciclo teórico. En la Fig. 8.3 representamos la energía teórica extraída por unidad de área de electrodo para distintos valores de radio de partícula. La conclusión más significativa al utilizar el modelo de volumen excluido es que encontramos que W_s (trabajo específico extraído o por unidad de área de electrodo) no puede exceder de un máximo. Este resultado conduce a un aspecto clave en esta investigación: existe un potencial de carga de óptimo funcionamiento. Dicho de otro modo, como la energía depende de la distancia entre las curvas $\sigma(\Psi)$ para concentraciones de agua dulce y salada, puede afirmarse que, aunque a bajos potenciales W aumenta con el potencial, a potenciales mayores las curvas $\sigma(\Psi)$ se aproximan debido a que las relaciones entre las capacidades se invierten y esto provoca una disminución de la energía extraída. Por consiguiente, teóricamente, existe un potencial óptimo de trabajo obtenido gracias al hecho de considerar el solapamiento de la DCE y el volumen finito de los iones.

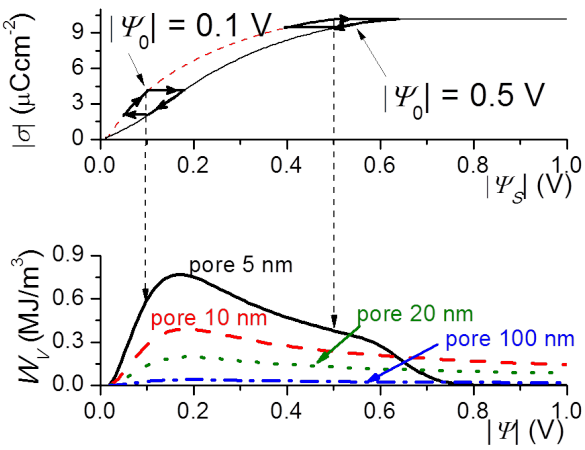

FIGURA 8.3: Arriba: Densidad de carga superficial en función del potencial superficial para R=5 nm. Un ciclo cualquiera está señalado con las flechas. Abajo: Trabajo específico extraído en función del potencial superficial para distintos radios de poro como se indica.

Efecto de la temperatura en la producción de energía mediante cambios de salinidad

Hay muchos procesos industriales donde se usa agua como refrigerante y se devuelve al depósito de agua fría, de modo que se produce una mezcla de fluidos calientes y fríos. El gradiente de temperatura entre ellos puede ser bastante alto en el caso de las plantas de energía térmica, donde para la transferencia del calor se usan embalses. Sin embargo, en todo proceso de refrigeración, se desperdicia energía por la simple mezcla de agua a diferentes temperaturas. En esta apartado mostramos el trabajo realizado para proponer el aprovechamiento de soluciones de agua a diferente temperatura para la producción directa de energía eléctrica. En concreto, mostramos algunos resultados relativos a la aplicación de CDLE con diferencias de temperatura entre las dos soluciones utilizadas en el proceso de intercambio. Se describe un modelo teórico basado en geometría cilíndrica para electrodos microporosos así como el análisis de los resultados experimentales [95].

Las predicciones del modelo se muestran en la Fig. 8.4. Como esperába-

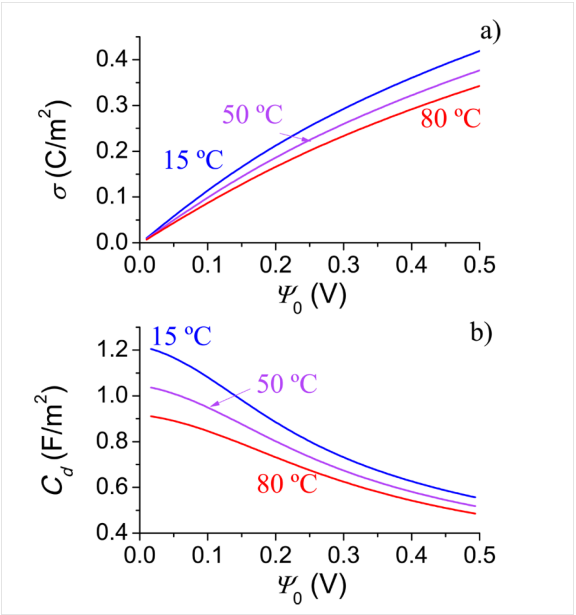

FIGURA 8.4: Densidad de carga superficial (a) y capacidad de la DCE (b) como función del potencial de superficie para las temperaturas que se indican. Concentración iónica 2 M NaCl. El tamaño de poro: 5 nm. Radios iónicos: Na^+ 0.36 nm y Cl^- 0.33 nm.

mos, tanto la densidad de carga superficial como la capacidad de la DCE disminuyen con la temperatura. Esta disminución puede unirse a la que experimenta la capacidad al disminuir la fuerza iónica. De esta manera, podemos usar en lugar de agua dulce en el ciclo CDLE, agua dulce a mayor temperatura. Así, mejoraremos el ciclo CDLE aprovechando la diferencia de temperatura.

Técnica de electrodos soft

La Fig. 8.5 describe los resultados obtenidos por los métodos SE y CDP en los ciclos a circuito abierto. Se representa la evolución de la tensión en la celda cuando se introduce agua salada y posteriormente, agua dulce: en SE (Fig. 8.5a) y CDP (Fig. 8.5b). Se puede concluir a partir de esta figura que el aumento de tensión es similar para ambos casos: alrededor de 120 mV para SE y 140 mV para CDP. Este es un resultado prometedor en términos

de energía extraída. Sin embargo, encontramos una diferencia muy significativa en el tiempo de respuesta, que afectará a la potencia extraída. Como muestra la Fig. 8.5, durante el flujo de agua dulce, SE necesita aproximadamente 200 s para alcanzar el valor de tensión constante, mientras que los electrodos basados en membranas lo alcanzan en menos de 10 segundos. Aunque la cubierta del polímero esté probablemente bien formada, como indica el aumento de tensión, el tiempo de respuesta lento es un inconveniente importante que debe ser corregido para mejorar la potencia extraída. Para entender esta diferencia del tiempo de respuesta que evita que el método SE se convierta en una alternativa equivalente al CDP, realizamos un análisis por separado a circuito abierto de cada electrodo. Estos resultados han proporcionado una interesante visión de cómo funciona la técnica SE [63].

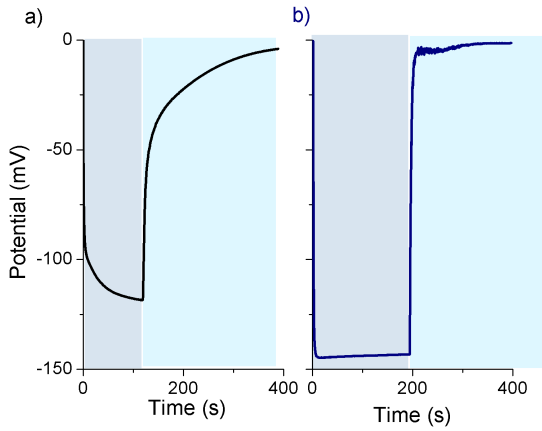

FIGURA 8.5: Evolución temporal de la tensión de celda a circuito abierto para SE (a) y CDP (b) cuando alternativamente introducimos agua salada y agua dulce en la celda de trabajo. Las zonas oscuras: 30 g/L NaCl; sombreado ligero: 1 g/L.

Influencia de disoluciones realistas de agua de mar

En esta sección, presentamos el trabajo realizado para el estudio del efecto de la utilización de composiciones de agua realistas en ciclos CDLE y CDP. Hemos observado experimentalmente que la principal diferencia en

la energía extraída (en comparación con soluciones de NaCl) proviene de la presencia de iones multivalentes. En cuanto a los resultados de la técnica CDLE [108], la Fig. 8.6 muestra la evolución del potencial en sucesivos ciclos CDLE para tres casos: 600mM de NaCl, agua de mar simulada (SSW) y agua de mar real del mediterráneo (MRSW). El agua de mar simulada se realizó siguiendo las composiciones de la literatura [100]. El agua de mar real (MRSW) proviene de la costa de Málaga. Puede verse que la disminución de la subida de potencial cuando se utilizan las aguas de mar, ya sea reales o simuladas, es significativa en comparación con la disolución de NaCl. La Fig. 8.6b muestra la reducción que experimenta tanto el salto de potencial como la carga transferida al usar agua de mar real y simulada. Como consecuencia, la energía extraída se reduce considerablemente (Fig. 8.6c). Por otra parte, hemos elaborado un modelo teórico capaz de predecir este comportamiento, teniendo en cuenta que el dispositivo CDLE consta de dos electrodos de carga opuesta, no simétricas debido al diferente tamaño y concentraciones de sus contraiones. El efecto sobre el trabajo extraído nos lleva a la conclusión que los iones multivalentes producen una disminución de la energía producida a pesar de las pequeñas concentraciones en comparación con los iones monovalentes.

Respecto a la técnicas CDP [118], con el fin de comprender el papel de los iones multivalentes en la producción de energía por intercambio de disolución, analizamos cuidadosamente todo el proceso en un electrodo de carbon cubierto con una membrana. Nuestro estudio incluyó tanto la fase de circuito abierto, cuando se establece el potencial de membrana, como el circuito cerrado, cuando se produce un flujo de corriente a través de una carga externa. Observamos que la presencia de contraiones divalentes en la disolución producía una caída de potencial de membrana, incluso si su concentración era baja, como ocurría para CDLE. El modelo teórico expuesto confirmó que la presencia de iones multivalentes reducía los valores alcanzados por el potencial de membrana, y, como consecuencia, la máxima energía extraída. Además de estas comparaciones, se realizó un estudio de la potencialidad del método SE con aguas de mar y río reales. Con este objetivo, se tomaron aguas del golfo de Fonseca, entrante protegido del océano Pacífico, conformado por un archipiélago localizado al oeste

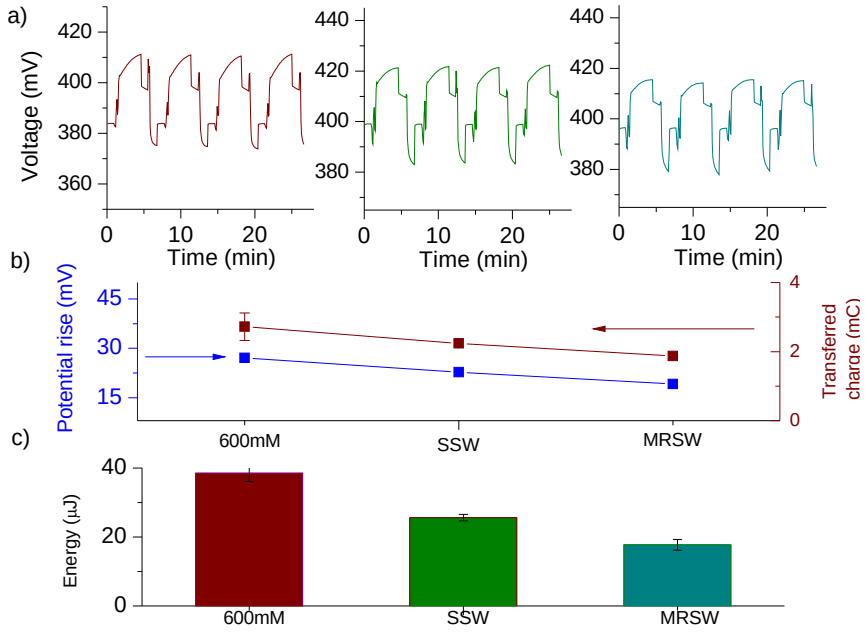

FIGURA 8.6: a) Ejemplos de sucesivos ciclos CDLE en los casos indicados de agua de mar: disolución de 600mM de NaCl, agua de mar simulada (SSW) y agua de mar real (RSW). b) Salto de potencial (eje izquierdo) y carga transferida (eje derecho) para las tres agua saladas estudiadas. c)Energía extraída. En todos los casos, el agua dulce es una solución de 20mM de NaCl.

de Centroamérica, y con una salinidad de 35 g/L en la boca del mismo. Por otra parte, aguas arriba, la salinidad disminuye hasta 1 ó 2 g/L. Estas dos aguas de distinta salinidad fueron probadas en el dispositivo experimental (método SE). La Fig. 8.7 muestra los resultados obtenidos [109]. En primer lugar, observamos un salto de potencial prácticamente igual cuando cambiamos el agua de mar simulada (500 mM de NaCl) por la tomada del Puerto de la Unión. Esto demuestra que el experimento no se vería perjudicado por la existencia de otros iones presentes en el agua de mar como sí ocurría con otros métodos Capmix [108, 118]. Sorprendentemente, observamos cómo al sustituir el agua de río simulada (20 mM NaCl) por agua de río real (Río Rebalse) se produce un aumento de hasta 215 mV. Este hecho se debe a que el agua tomada fue en época de lluvias, por lo que

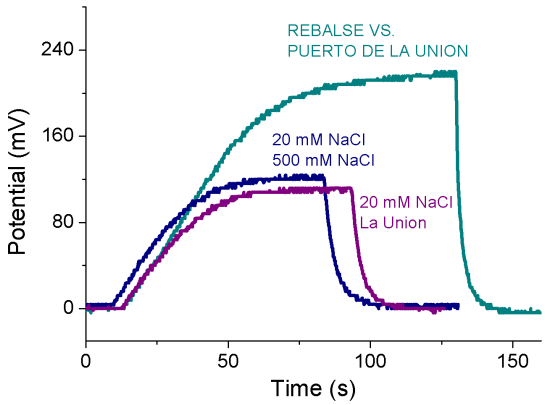

FIGURA 8.7: Medidas a circuito abierto de SE para aguas de mar y río simuladas y reales en función del tiempo.

la salinidad tenía niveles muy bajos debido a la no influencia de las aguas negras. Estas épocas de lluvia intensa beneficiarían los resultados de SE. De esta manera y a partir de este estudio preliminar, se hace necesaria una investigación más profunda de los caudales de los ríos en distintas épocas del año.

Asociación de celdas capacitivas

Hasta hace poco los estudios de energía por gradiente de salinidad de técnicas capmix, se han ceñido al estudio de una sola celda formada por dos electrodos enfrentados. Recientemente, para la técnica CDP, se han hecho avances en la utilización de varias celdas en un mismo dispositivo [60]. Se determinaron las actuaciones de varios pares de electrodos conectados en serie o en paralelo aumentando la potencia lograda en células simples. Además, se estudió el valor de la resistencia interna para serie y paralelo utilizando un modelo de distribución de corriente y mediciones experimentales, concluyendo que la configuración en paralelo es óptima.

En este apartado, con el objetivo de encontrar la configuración óptima de múltiples electrodos para maximizar la producción de energía y potencia

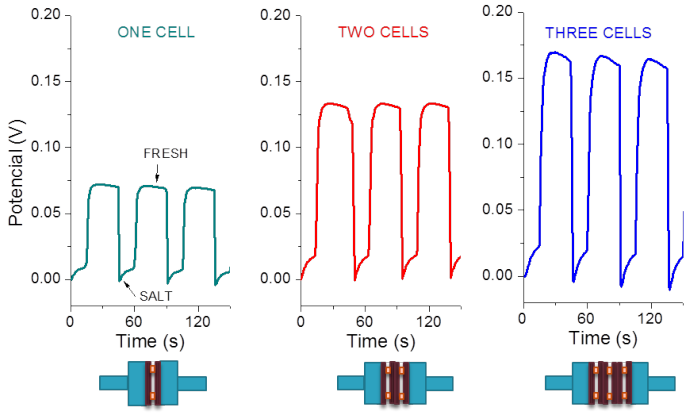

FIGURA 8.8: Medidas a circuito abierto del potencial en función del tiempo para la técnica SE de una, dos y tres celdas conectadas.

y aumentar el potencial obtenido necesario para aplicaciones comerciales, se estudia la propuesta de asociar varias celdas en serie para las técnicas CDLE y la más reciente *electrodos soft* o SE. Para CDLE, se observó que las celdas asociadas no funcionaban al mismpo potencial. De hecho, en el caso de tres celdas, la celda intermedia trabaja a un potencial menor (alrededor de 160 mV en lugar de 500 mV como se esperaría teóricamente), esto produjo una importante disminución en el rendimiento de la configuración en serie. Este efecto se puede entender considerando que todos los pares de supercondensadores formados por la placa de grafito y su doble capa eléctrica (DCE) están conectados a través de resistencias internas, como de hecho ocurre simulando el camino conductor establecido por la solución de electrolito. De esta forma, la tensión de trabajo de cada celda corresponde a la que observamos, donde sólo los condensadores externos son los que contribuyen significativamente con una diferencia de potencial mayor ya que los internos no llegan a cargarse, pues se encuentran conectados a través de la solución.

Cuando se realiza el mismo experimento con la técnica SE, observamos un comportamiento completamente diferente. La Fig. 8.8 muestra los ciclos a circuito abierto de uno, dos y tres pares de celdas conectadas en serie y recubiertas respectivamente con polielectrolitos catiónicos y aniónicos. La

diferencia de potencial cuando conectamos tres celdas corresponde aproximadamente al triple de la de una sola: se pasa de unos 50 mV a 150 mV para tres celdas. Este resultado implica que la conexión a través del electrolito que produce una resistencia interna alta y muchas pérdidas en CDLE, no tiene un efecto tan negativo en la técnica SE, es decir, cuando se recubren los electrodos con polielectrolitos catiónicos y aniónicos [110].

8.3. Conclusiones

Finalmente, presentamos las contribuciones esenciales obtenidas a partir de este trabajo de tesis. La energía azul o energía por diferencia de salinidad aprovecha la energía libre almacenada en la mezcla de aguas con distinta salinidad, como ocurre en la desembocadura de los ríos. Entre las numerosas técnicas existentes con el objetivo de aprovechar esta energía, las llamadas capmix (o de mezcla capacitiva) se caracterizan por permitir la extracción de energía eléctrica directa sin necesidad de procesos intermedios de conversión como turbinas o máquinas térmicas. Concretamente, nuestra tesis se ha centrado en el estudio de dos de ellas: CDLE (basada en la expansión de la doble capa eléctrica) y SE (basada en el uso de electrodos recubiertos de polielectrolitos o electrodos *soft*).

Los principales resultados obtenidos, se resumen a continuación:

Modelado de CDLE

Se ha realizado la modelización de los electrodos capmix mediante un conjunto de poros cilíndricos teniendo en cuenta el solapamiento de la DCE y el tamaño de los iones (NaCl en este caso) y se ha aplicado para la evaluación de la energía extraída mediante la técnica CDLE. Se puede concluir que:

- Los efectos más significativos se observan cuando se considera el tamaño iónico.
- La energía extraída por unidad de superficie aumenta (disminuye) con el tamaño de poro para potenciales bajos (altos).

- El modelo muestra que el tamaño iónico limita la energía extraída que se puede obtener con este método a valores mucho más pequeños que los previstos para los iones puntuales.
- Con el fin de obtener la máxima energía, el potencial de carga no puede exceder un valor de alrededor de 200 mV.

Materiales y metodología

Se ha realizado un análisis de los materiales y métodos necesarios para la implementación de todo el proceso capmix a escala de laboratorio. La conclusión principal de estos aspectos es:

- La energía extraída por la técnica CDLE puede mejorarse si se elige adecuadamente la temperatura de las soluciones.
- Además, es posible extraer energía eléctrica debida a la diferencia de temperatura sin la necesidad de convertidores electromecánicos.
- El tamaño promedio de poro de las partículas de carbón activo resulta ser una cantidad determinante. De hecho, se han obtenido los resultados óptimos para CDLE si el carbono usado en los electrodos tiene una fracción significativa de población de mesoporos.
- Se han probado diferencias de salinidad más allá de los habituales (20 mM-500 mM). Seha concluido que estas fuentes de salinidad podrían mejorar la potencia extraída, así como mejorar su impacto ambiental.

Técnica de electrodos soft

El método de electrodos *soft* se basa en el simple depósito de una capa de polielectrolito sobre las películas de carbono. Hemos encontrado que:

- La técnica SE podría convertirse en un método eficiente de energía por diferencia de salinidad en términos de salto de potencial.
- La comparación con CDP ha demostrado que, aunque las energías por ciclo son similares, la potencia es menor en SE.

- Se ha encontrado que los polielectrolitos positivos y negativos se adsorben de manera diferente sobre el carbón activo.
- PSS parece adsorberse de forma heterogénea sobre los poros de las capas de carbón más externas.
- Por el contrario, el PDADMAC probablemente se deposite en una capa fina homogénea que permanece en la superficie de la lámina reaccionando muy rápidamente a los cambios de salinidad.
- Se necesitan más investigaciones sobre la selección de polímeros, métodos para el tratamiento de las lámina de carbón y estabilidad del recubrimiento para mejorar la potencia extraída.

Aplicaciones capmix en contextos realistas

Finalmente, se ha estudiado la adaptación de las técnicas capmix a contextos reales de implementación. Concretamente:

- Hemos analizado el efecto multi-iónico de disoluciones de mar y río reales.
- A partir de la modelización teórica, se ha concluido que los iones con valencia superior a 1 y de mayor tamaño tienen un papel importante en las relaciones carga-potencial de la DCE y por tanto, en la energía extraída.
- Esta resultado ha sido comprobado experimentalmente para ambas técnicas SE y CDLE.
- Los experimentos realizados para las aguas del Golfo de Fonseca (El Salvador), han demostrado que esta influencia (presencia de iones multivalentes y de contaminantes dispersos) no tiene un efecto tan significativo para la técnica SE.
- Hemos avanzado en el conocimiento de la conexión de distintas celdas capacitivas para aumentar el potencial en un futuro dispositivo comercial.

- Se ha encontrado que debido a la solución de electrolito, existe una conexión conductora entre pares de celdas en serie que perjudica el funcionamiento del ciclo CDLE.
- Por el contrario, esta asociación en serie parece muy aconsejable cuando la técnica utilizada es la de electrodos soft. Este resultado presenta a la técnica SE como una alternativa prometedora para los métodos capmix.

En resumen, la energía azul puede llegar a convertirse en una fuente económica y medioambientalmente sostenible, ya que se basa en procesos naturales de mezcla que tienen lugar en los deltas de los ríos y estuarios y no genera CO_2 ni ningún tipo de contaminación térmica. Sin embargo, la tecnología para obtener esta energía no ha sido desarrollada todavía y nuestro trabajo puede ser considerado como preliminar. Con suerte, más investigación llevará a una mejora de la energía extraída.

Acknowledgments

The research leading to this thesis received funding from the University of Granada (FPU grant), the European Union 7th Framework Programme (FP7/2007-2013) under agreement No. 256868, Junta de Andalucía (Project PE-2008-FQM3993 and PE2012-FQM 694) and Ministerio de Economía y Competitividad of Spain (Project FIS2013-4766-C3-1-R). Further financial support from the Eureka SD Project (agreement number 2013-2591), that is supported by the Erasmus Mundus programme of the European Union is also gratefully acknowledged.

List of Figures

List of Tables

Bibliography

[1] A. K. Reddy, R. H. Williams, and T. B. Johansson, "Energy and major global issues, in energy after rio: Prospects and challenges," *U.N. Development Program (UNDP)*, 1997.

[2] S. Tully, "The human right to access electricity," *The Electricity Journal*, vol. 19, no. 3, pp. 30 – 39, 2006.

[3] "Weo 2015 electricity access database," *International Energy Agency. World Energy Outlook.*, 2015.

[4] R. Karlsson, "Apres paris: Breakthrough innovation as the primary moral obligation of rich countries," *Environ. Sci. Policy*, vol. 63, pp. 170 – 176, 2016.

[5] I. Dincer, "Renewable energy and sustainable development: a crucial review," *Renew. Sustainable Energy Rev.*, vol. 4, no. 2, pp. 157 – 175, 2000.

[6] T. Mueller and A. Passadakis, "Green capitalism and the climate," *Critical Currents*, vol. 6, pp. 54–61, 2009.

[7] J. Cock, "Green capitalism or environmental justice: A critique of the sustainability discourse," *Focus*, vol. 63, pp. 45–51, 2011.

[8] H. Lund, "Renewable energy strategies for sustainable development," *Energy*, vol. 32, no. 6, pp. 912 – 919, 2007.

[9] D. Gielen, F. Boshell, and D. Saygin, "Climate and energy challenges for materials science," *Nat. Mater.*, vol. 15, pp. 117–120, 2013.

[10] O. Ellabban, H. Abu-Rub, and F. Blaabjerg, "Renewable energy resources: Current status, future prospects and their enabling technology," *Renew. Sustainable Energy Rev.*, vol. 39, pp. 748 – 764, 2014.

[11] M. S. Dresselhaus and I. L. Thomas, "Alternative energy technologies," *Nature*, vol. 414, pp. 332–337, 2001.

[12] R. Pelc and R. M. Fujita, "Renewable energy from the ocean," *Marine Policy*, vol. 26, no. 6, pp. 471 – 479, 2002.

[13] Z. Zhou, M. Benbouzid, J. F. Charpentier, F. Scuiller, and T. Tang, "A review of energy storage technologies for marine current energy systems," *Renew. Sustainable Energy Rev.*, vol. 18, pp. 390 – 400, 2013.

[14] M. A. Shields, D. K. Woolf, E. P. Grist, S. A. Kerr, A. Jackson, R. E. Harris, M. C. Bell, R. Beharie, A. Want, E. Osalusi, S. W. Gibb, and J. Side, "Marine renewable energy: The ecological implications of altering the hydrodynamics of the marine environment," *Ocean & Coastal Management*, vol. 54, no. 1, pp. 2 – 9, 2011.

[15] A. T. Jones and W. Finley, "Recent development in salinity gradient power," in *Oceans 2003. Proceedings*, vol. 4, pp. 2284–2287, 2003.

[16] G. L. Wick and W. R. Schmitt, "Prospects for renewable energy from sea," *Marine Technology Society Journal*, vol. 11, no. 5-6, pp. 16–21, 1977.

[17] R. E. Pattle, "Production of electric power by mixing fresh and salt water in the hydroelectric pile," *Nature*, vol. 174, no. 4431, pp. 660–660, 1954.

[18] R. S. Norman, "Water salination - source of energy," *Science*, vol. 186, no. 4161, pp. 350–352, 1974.

[19] G. Z. Ramon, B. J. Feinberg, and E. M. V. Hoek, "Membrane-based production of salinity-gradient power," *Energy Environ. Sci.*, vol. 4, pp. 4423–4434, 2011.

[20] Z. Jia, B. Wang, S. Song, and Y. Fan, "Blue energy: Current technologies for sustainable power generation from water salinity gradient," *Renew. Sustainable Energy Rev.*, vol. 31, pp. 91 – 100, 2014.

[21] J. Kuleszo, C. Kroeze, J. Post, and B. M. Fekete, "The potential of blue energy for reducing emissions of co2 and non-co2 greenhouse gases," *Journal of Integrative Environmental Sciences*, vol. 7, no. S1, pp. 89–96, 2010.

[22] O. Alvarez-Silva and A. F. Osorio, "Salinity gradient energy potential in colombia considering site specific constraints," *Renewable Energy*, vol. 74, pp. 737 – 748, 2015.

[23] P. Stenzel and H. Wagner, "Osmotic power plants: Potential analysis and site criteria.," in *3rd Int Conf Ocean Energy. Proc*, pp. 1–5, 2010.

[24] N. Y. Yip and M. Elimelech, "Comparison of energy efficiency and power density in pressure retarded osmosis and reverse electrodialysis," *Environ. Sci. Technol.*, vol. 48, no. 18, pp. 11002–11012, 2014. PMID: 25157687.

[25] A. Achilli and A. E. Childress, "Pressure retarded osmosis: From the vision of sidney loeb to the first prototype installation. review," *Desalination*, vol. 261, pp. 205 – 211, 2010.

[26] M. Bijmans, O. Burheim, M. Bryjak, A. Delgado, P. Hack, F. Mantegazza, S. Tenisson, and H. Hamelers, "Capmix -deploying capacitors for salt gradient power extraction," *Energy Procedia*, vol. 20, pp. 108 – 115, 2012.

[27] S. Miller, H. Shemer, and R. Semiat, "Energy and environmental issues in desalination," *Desalination*, vol. 366, pp. 2–8, 2015.

[28] S. Roelofs, A. van den Berg, and M. Odijk, "Microfluidic desalination techniques and their potential applications," *Lab Chip*, vol. 15, no. 17, pp. 3428–3438, 2015.

[29] M. Shatat, M. Worall, and S. Riffat, "Opportunities for solar water desalination worldwide: review," *Sustainable cities and society*, vol. 9, pp. 67–80, 2013.

[30] A. Achilli, J. L. Prante, N. T. Hancock, E. B. Maxwell, and A. E. Childress, "Experimental results from ro-pro: A next generation system for low-energy desalination," *Environ. Sci. Technol.*, vol. 48, pp. 6437–6443, 2014.

[31] S. Lin, N. Y. Yip, T. Y. Cath, C. O. Osuji, and M. Elimelech, "Hybrid pressure retarded osmosis–membrane distillation system for power generation from low-grade heat: thermodynamic analysis and energy efficiency," *Environ. Sci. Technol.*, vol. 48, no. 9, pp. 5306–5313, 2014.

[32] B. E. Logan and M. Elimelech, "Membrane-based processes for sustainable power generation using water," *Nature*, vol. 488, pp. 313–319, 2012.

[33] H. Hamelers, O. Schaetzle, J. Paz-García, P. Biesheuvel, and C. Buisman, "Harvesting energy from co2 emissions," *Environ Sci Technol Lett*, vol. 1, no. 1, pp. 31–35, 2013.

[34] J. Paz-Garcia, O. Schaetzle, P. Biesheuvel, and H. Hamelers, "Energy from co2 using capacitive electrodes - a model for energy extraction cycles.," *J. Colloid Interface Sci.*, vol. 418, pp. 200–207, 2014.

[35] S. Loeb, "Osmotic power-plants," *Science*, vol. 189, no. 4203, pp. 654–655, 1975.

[36] J. T. Arena, B. McCloskey, B. D. Freeman, and J. R. McCutcheon, "Surface modification of thin film composite membrane support layers with polydopamine: enabling use of reverse osmosis membranes in pressure retarded osmosis," *J. Membr. Sci.*, vol. 375, no. 1, pp. 55–62, 2011.

[37] L. A. Hoover, J. D. Schiffman, and M. Elimelech, "Nanofibers in thin-film composite membrane support layers: Enabling expanded ap-

plication of forward and pressure retarded osmosis," *Desalination*, vol. 308, pp. 73–81, 2013.

[38] N. Y. Yip, D. Brogioli, H. V. Hamelers, and K. Nijmeijer, "Salinity gradients for sustainable energy: Primer, progress, and prospects," *Environ. Sci. Technol.*, 2016.

[39] J. N. Weinstein and F. B. Leitz, "Electric-power from difference in salinity - dialytic battery," *Science*, vol. 191, no. 4227, pp. 557–559, 1976.

[40] R. E. Lacey, "Energy by reverse electrodialysis," *Ocean Eng.*, vol. 7, no. 1, pp. 1–47, 1980.

[41] P. Długołęcki, K. Nymeijer, S. Metz, and M. Wessling, "Current status of ion exchange membranes for power generation from salinity gradients," *J. Membr. Sci.*, vol. 319, no. 1, pp. 214–222, 2008.

[42] J. G. Hong, B. Zhang, S. Glabman, N. Uzal, X. Dou, H. Zhang, X. Wei, and Y. Chen, "Potential ion exchange membranes and system performance in reverse electrodialysis for power generation: A review," *J. Membr. Sci.*, vol. 486, pp. 71–88, 2015.

[43] O. Schaetzle and C. J. Buisman, "Salinity gradient energy: current state and new trends," *Engineering*, vol. 1, no. 2, pp. 164–166, 2015.

[44] N. Yip and M. Elimelech, "Thermodynamic and energy efficiency analysis of power generation from natural salinity gradients by pressure retarded osmosis," *Environ. Sci. Technol.*, vol. 46, no. 9, pp. 5230–5239, 2012.

[45] J. Veerman, R. De Jong, M. Saakes, S. Metz, and G. Harmsen, "Reverse electrodialysis: Comparison of six commercial membrane pairs on the thermodynamic efficiency and power density," *J. Membr. Sci.*, vol. 343, no. 1, pp. 7–15, 2009.

[46] N. Y. Yip, D. A. Vermaas, K. Nijmeijer, and M. Elimelech, "Thermodynamic, energy efficiency, and power density analysis of reverse

electrodialysis power generation with natural salinity gradients," *Environ. Sci. Technol.*, vol. 48, no. 9, pp. 4925–4936, 2014.

[47] D. A. Rand, "A journey on the electrochemical road to sustainability," *J. Solid State Electrochem.*, vol. 15, no. 7-8, pp. 1579–1622, 2011.

[48] D. Brogioli, "Extracting renewable energy from a salinity difference using a capacitor," *Phys. Rev. Lett.*, vol. 103, p. 058501, July 2009.

[49] D. Brogioli, R. Zhao, and P. M. Biesheuvel, "A prototype cell for extracting energy from a water salinity difference by means of double layer expansion in nanoporous carbon electrodes," *Energy Environ. Sci.*, vol. 4, pp. 772–777, Mar. 2011.

[50] R. A. Rica, R. Ziano, D. Salerno, F. Mantegazza, R. van Roij, and D. Brogioli, "Capacitive mixing for harvesting the free energy of solutions at different concentrations," *Entropy*, vol. 15, no. 4, p. 1388, 2013.

[51] G. R. Iglesias, M. M. Fernández, S. Ahualli, M. L. Jiménez, O. P. Kozynchenko, and A. V. Delgado, "Materials selection for optimum energy production by double layer expansion methods," *J. Power Sources*, vol. 261, pp. 371–377, 2014.

[52] B. B. Sales, M. Saakes, J. W. Post, C. J. N. Buisman, P. M. Biesheuvel, and H. V. M. Hamelers, "Direct power production from a water salinity difference in a membrane-modified supercapacitor flow cell," *Environ. Sci. Technol.*, vol. 44, pp. 5661–5665, 2010.

[53] S. Ahualli, M. Jiménez, M. M. Fernández, G. Iglesias, D. Brogioli, and Á. V. Delgado, "Polyelectrolyte-coated carbons used in the generation of blue energy from salinity differences," *Phys. Chem. Chem. Phys.*, vol. 16, no. 46, pp. 25241–25246, 2014.

[54] M. Jiménez, M. Fernández, S. Ahualli, G. Iglesias, and A. Delgado, "Predictions of the maximum energy extracted from salinity exchange inside porous electrodes," *J. Colloid Interface Sci.*, vol. 402, pp. 340 – 349, 2013.

[55] P. Biesheuvel, Y. Fu, and M. Bazant, "Electrochemistry and capacitive charging of porous electrodes in asymmetric multicomponent electrolytes," *Russ. J. Electrochem.*, vol. 48, pp. 580–592, 2012.

[56] R. A. Rica, D. Brogioli, R. Ziano, D. Salerno, and F. Mantegazza, "Ions transport and adsorption mechanisms in porous electrodes during capacitive-mixing double layer expansion (cdle)," *J. Phys. Chem. C*, vol. 116, no. 32, pp. 16934–16938, 2012.

[57] M. Marino, L. Misuri, M. Jimenez, S. Ahualli, O. Kozynchenko, S. Tennison, M. Bryjak, and D. Brogioli, "Modification of the surface of activated carbon electrodes for capacitive mixing energy extraction from salinity differences," *J. Colloid Interface Sci.*, vol. 436, no. 0, pp. 146 – 153, 2014.

[58] F. Liu, O. Schaetzle, B. B. Sales, M. Saakes, C. J. N. Buisman, and H. V. M. Hamelers, "Effect of additional charging and current density on the performance of capacitive energy extraction based on donnan potential," *Energy Environ. Sci.*, vol. 5, pp. 8642–8650, 2012.

[59] F. Liu, O. Schaetzle, B. B. Sales, M. Saakes, C. J. N. Buisman, and H. V. M. Hamelers, "Effect of additional charging and current density on the performance of capacitive energy extraction based on donnan potential," *Environ. Sci. Technol.*, vol. 5, pp. 8642–8650, Sept. 2012.

[60] F. Liu, T. F. Donkers, R. M. Wagterveld, O. Schaetzle, M. Saakes, C. J. Buisman, and H. V. Hamelers, "Parallel up-scaling of capacitive mixing (capmix) system enhances the specific performance," *Electrochim. Acta*, vol. 187, pp. 104 – 112, 2016.

[61] B. B. Sales, O. S. Burheim, F. Liu, O. Schaetzle, C. J. N. Buisman, and H. V. M. Hamelers, "Impact of wire geometry in energy extraction from salinity differences using capacitive technology," *Environ. Sci. Technol.*, vol. 46, no. 21, pp. 12203–12208, 2012.

[62] O. S. Burheim, F. Liu, B. B. Sales, O. Schaetzle, C. J. N. Buisman, and H. V. M. Hamelers, "Faster time response by the use of wire

electrodes in capacitive salinity gradient energy systems," *J. Phys. Chem. C*, vol. 116, pp. 19203–19210, Sept. 2012.

[63] M. Fernández, R. Wagterveld, S. Ahualli, F. Liu, A. Delgado, and H. Hamelers, "Polyelectrolyte-versus membrane-coated electrodes for energy production by capmix salinity exchange methods," *J. Power Sources*, vol. 302, pp. 387 – 393, 2016.

[64] A. Delgado, *Interfacial Electrokinetics and Electrophoresis*, vol. 106 of *Surfactant Science Series*. New York: CRC Press, 2002.

[65] S. Wall, "The history of electrokinetic phenomena," *Curr. Opin. Colloid Interface Sci.*, vol. 15, no. 3, pp. 119 – 124, 2010.

[66] R. Hunter, *Foundations of Colloid Science*. Oxford: Oxford University Press, 2000.

[67] J. Lyklema, *Fundamentals of Interface and Colloid Science, vol. II: Solid-Liquid Interfaces*. New York: Academic Press, 1995.

[68] J. Masliyah and S. Bhattacharjee, *Electrokinetic and Colloid Transport Phenomena*. Wiley-interscience, newjersey ed., 2006.

[69] R. van Roij, "Statistical thermodynamics of supercapacitors and blue engines," *ArXiv e-prints*, 2012.

[70] C. Merlet, B. Rotenberg, P. A. Madden, P.-L. Taberna, P. Simon, Y. Gogotsi, and M. Salanne, "On the molecular origin of supercapacitance in nanoporous carbon electrodes," *Nat. Mater.*, vol. 11, pp. 306–310, Apr. 2012.

[71] M. Z. Bazant, B. D. Storey, and A. A. Kornyshev, "Double layer in ionic liquids: overscreening versus crowding," *Phys. Rev. Lett.*, vol. 106, p. 046102, Jan 2011.

[72] A. Tanimura, A. Kovalenko, and F. Hirata, "Molecular theory of an electrochemical double layer in a nanoporous carbon supercapacitor," *Chem. Phys. Lett.*, vol. 378, no. 5-6, pp. 638 – 646, 2003.

[73] J. S. Newman and C. W. Tobias, "Theoretical analysis of current distribution in porous electrodes," *J. Electrochem. Soc.*, vol. 109, no. 12, pp. 1183–1191, 1962.

[74] J. Lim, J. D. Whitcomb, J. G. Boyd, and J. Varghese, "Effect of electrode pore geometry modeled using nernst-planck-poisson-modified stern layer model," *Comput. Mech.*, vol. 43, pp. 461–475, Mar. 2009.

[75] Y. Yamada, T. Sasaki, N. Tatsuda, D. Weingarth, K. Yano, and R. Kotz, "A novel model electrode for investigating ion transport inside pores in an electrical double-layer capacitor: Monodispered microporous starburst carbon spheres," *Electrochim. Acta*, vol. 81, pp. 138–148, Oct. 2012.

[76] M. Z. Bazant, M. S. Kilic, B. D. Storey, and A. Ajdari, "Towards an understanding of induced-charge electrokinetics at large applied voltages in concentrated solutions," *Adv. Colloid Interface Sci.*, vol. 152, pp. 48–88, Nov. 2009.

[77] S. Ahualli, M. L. Jiménez, F. Carrique, and A. V. Delgado, "Ac electrokinetics of concentrated suspensions of soft particles," *Langmuir*, vol. 25, no. 4, pp. 1986–1997, 2009.

[78] H. Greberg and R. Kjellander, "Charge inversion in electric double layers and effects of different sizes for counterions and coions rid a-7267-2010," *J. Chem. Phys.*, vol. 108, pp. 2940–2953, Feb. 1998.

[79] J. J. López-García, M. J. Aranda-Rascón, C. Grosse, and J. Horno, "Equilibrium electric double layer of charged spherical colloidal particles: effect of different distances of minimum ion approach to the particle surface," *J. Phys. Chem. B*, vol. 114, pp. 7548–7556, June 2010.

[80] R. Roa, F. Carrique, and E. Ruiz-Reina, "Electric double layer for spherical particles in salt-free concentrated suspensions including ion size effects," *Phys. Chem. Chem. Phys.*, vol. 13, no. 9, pp. 3960–3968, 2011.

[81] M. Plischke and D. Henderson, "Pair correlation-functions and density profiles in the primitive model of the electric double-layer," *J. Chem. Phys.*, vol. 88, pp. 2712–2718, Feb. 1988.

[82] M. C. Henstridge, E. J. Dickinson, and R. G. Compton, "On the estimation of the diffuse double layer of carbon nanotubes using classical theory: Curvature effects on the gouy–chapman limit," *Chem. Phys. Lett.*, vol. 485, no. 1, pp. 167–170, 2010.

[83] T. Goel, C. N. Patra, S. K. Ghosh, and T. Mukherjee, "Effect of ionic size on the structure of cylindrical electric double layers: A systematic study by monte carlo simulations and density functional theory," *J. Phys. Chem. B*, vol. 115, no. 37, pp. 10903–10910, 2011.

[84] G. I. Guerrero-García, E. González-Tovar, M. Lozada-Cassou, and F. D. Guevara-Rodríguez, "The electrical double layer for a fully asymmetric electrolyte around a spherical colloid: An integral equation study," *J. Chem. Phys.*, vol. 123, p. 034703, July 2005.

[85] R. Messina, "Electrostatics in soft matter," *J. Phys.-Condens. Matt.*, vol. 21, p. 113102, May 2009.

[86] P. M. Biesheuvel and M. van Soestbergen, "Counterion volume effects in mixed electrical double layers," *J. Colloid Interface Sci.*, vol. 316, pp. 490–499, Dec. 2007.

[87] Z. Adamczyk and P. Warszynski, "Role of electrostatic interactions in particle adsorption," *Adv. Colloid Interface Sci.*, vol. 63, pp. 41–149, Jan. 1996.

[88] I. Borukhov, "Charge renormalization of cylinders and spheres: Ion size effects," *J. Polymer Sci. Part B-Polymer Phys.*, vol. 42, pp. 3598–3615, Oct. 2004.

[89] M. Endo, T. Takeda, Y. Kim, K. Koshiba, and K. Ishii, "High power electric double layer capacitor (edlc's); from operating principle to pore size control in advanced activated carbons," *Carbon Sci.*, vol. 1, no. 3-4, pp. 117–128, 2003.

[90] D. Rolison and L. Nazar, "Electrochemical energy storage to power the 21st century," *MRS Bull.*, vol. 36, no. 7, pp. 486–493, 2011.

[91] B. Conway, *Electrochemical Supercapacitors: Scientific Fundamentals and Technological Applications*. New York: Kluwer Academic, 1999.

[92] B. E. Conway, W. Pell, and T.-C. Liu, "Diagnostic analyses for mechanisms of self-discharge of electrochemical capacitors and batteries," *J Power Sources*, vol. 65, no. 1, pp. 53 – 59, 1997.

[93] P. M. Biesheuvel, Y. Q. Fu, and M. Z. Bazant, "Diffuse charge and faradaic reactions in porous electrodes," *Phys. Rev. E*, vol. 83, p. 061507, June 2011.

[94] P. M. Biesheuvel and M. Z. Bazant, "Nonlinear dynamics of capacitive charging and desalination by porous electrodes," *Phys. Rev. E*, vol. 81, p. 031502, Mar 2010.

[95] S. A. Ahualli, M. M. Fernández, G. R. Iglesias, Á. V. Delgado, and M. L. Jimenez, "Temperature effects on energy production by salinity exchange," *Environ. Sci. Technol.*, vol. 48, pp. 12378–12385, 2014.

[96] M. Kaus, J. Kowal, and D. U. Sauer, "Modelling the effects of charge redistribution during self-discharge of supercapacitors," *Electrochim. Acta*, vol. 55, p. French Res Agcy, Oct. 2010.

[97] J. Kowal, E. Avaroglu, F. Chamekh, A. S'enfelds, T. Thien, D. Wijaya, and D. U. Sauer, "Detailed analysis of the self-discharge of supercapacitors," *J. Power Sources*, vol. 196, pp. 573–579, Jan. 2011.

[98] G. Iglesias, S. Ahualli, A. Delgado, M. Jimenez, and F. Gonzalez-Caballero, "A device for the measurement of energy by ionic exchange," 2014.

[99] S. Tennison, O. Kozynchenko, V. Strelko, A. Blackburn, A. US Pat. US20040024074 A1, 2004.

[100] J. Mclachlan, "Some considerations of growth of marine algae in artificial media," *Can. J. Microbiol.*, vol. 10, no. 5, pp. 769–782, 1964.

[101] J. E. Barraza, G. I. Mariona, D. N. Pineda, and R. M. Pytkowicz, "Fauna y flora en el golfo de fonseca," *Ministerio de Medio Ambiente y Recursos Naturales de El Salvador*, 2014.

[102] B. Sales, *Capacitive Technology for Energy Extraction from Chemical Potential Differences (ISBN: 978-94-6173-738-0)*. PhD thesis, Univ. Wageningen, The Netherlands, 2013.

[103] E. Chibowski, "Wettability and adhesion, 2nd international symposium on contact angle," Newark, NJ, Jun 21-23, 2000.

[104] E. Chibowski, "On some relations between advancing, receding and young's contact angles," *Adv. Colloid Interface Sci.*, vol. 133, no. 1, pp. 51 – 59, 2007.

[105] Q. Qu, B. Wang, L. Yang, Y. Shi, S. Tian, and Y. Wu, "Study on electrochemical performance of activated carbon in aqueous li2so4, na2so4 and {K2SO4} electrolytes," *Electrochem. Commun.*, vol. 10, no. 10, pp. 1652 – 1655, 2008.

[106] D. Brogioli, R. Ziano, R. A. Rica, D. Salerno, O. Kozynchenko, H. V. M. Hamelers, and F. Mantegazza, "Exploiting the spontaneous potential of the electrodes used in the capacitive mixing technique for the extraction of energy from salinity difference," *Energy Environ. Sci.*, vol. 5, pp. 9870–9880, 2012.

[107] S. Ahualli, *Propiedades electrocinéticas de suspensiones coloidales concentradas*. PhD thesis, University of Granada, 2009.

[108] M. Fernandez, S. Ahualli, G. R. Iglesias, F. Gonzalez-Caballero, A. V. Delgado, and M. Jimenez, "Multi-ionic effects on energy production based on double layer expansion by salinity exchange," *J. Colloid Interface Sci.*, vol. 446, pp. 335 – 344, 2015.

[109] M. M. Fernández, O. O. Flores, G. Iglesias, G. R. Castellano, A. Delgado, and L. Martinez., "New energy sources: blue energy study in central america," *In press*, 2017.

[110] G. R. Iglesias, S. Ahualli, M. M. Fernández, M. L. Jiménez, and Á. V. Delgado, "Stacking of capacitive cells for electrical energy production by salinity exchange," *Journal of Power Sources*, vol. 318, pp. 283–290, 2016.

[111] R. A. Rica, R. Ziano, D. Salerno, F. Mantegazza, and D. Brogioli, "Thermodynamic relation between voltage-concentration dependence and salt adsorption in electrochemical cells," *Phys. Rev. Lett.*, vol. 109, p. 156103, Oct 2012.

[112] R. A. Rica, R. Ziano, D. Salerno, F. Mantegazza, M. Z. Bazant, and D. Brogioli, "Electro-diffusion of ions in porous electrodes for capacitive extraction of renewable energy from salinity differences," *Electrochim. Acta*, vol. 92, no. 0, pp. 304 – 314, 2013.

[113] R. Lin, P.-L. Taberna, S. Fantini, V. Presser, C. R. Pérez, F. Malbosc, N. L. Rupesinghe, K. B. Teo, Y. Gogotsi, and P. Simon, "Capacitive energy storage from- 50 to 100 c using an ionic liquid electrolyte," *J. Phys. Chem. Lett.*, vol. 2, no. 19, pp. 2396–2401, 2011.

[114] R. Palm, H. Kurig, K. Tonurist, A. Janes, and E. Lust, "Is the mixture of 1-ethyl-3-methylimidazolium tetrafluoroborate and 1-butyl-3-methylimidazolium tetrafluoroborate applicable as electrolyte in electrical double layer capacitors?," *Electrochem. Commun.*, vol. 22, no. 0, pp. 203 – 206, 2012.

[115] T.-L. Horng, T.-C. Lin, C. Liu, and B. Eisenberg, "Pnp equations with steric effects: A model of ion flow through channels," *J. Phys. Chem. B*, vol. 116, no. 37, pp. 11422–11441, 2012.

[116] B. Lu and Y. Zhou, "Poisson-nernst-planck equations for simulating biomolecular diffusion-reaction processes ii: size effects on ionic distributions and diffusion-reaction rates," *Biophys. J.*, vol. 100, no. 10, pp. 2475–2485, 2011.

[117] D. R. Kester, I. W. Duedall, D. N. Connors, and R. M. Pytkowicz, "Preparation of artificial seawater," *Limnol. Oceanogr.*, vol. 12, pp. 176–179, 1967.

[118] S. Ahualli, M. M. Fernández, G. Iglesias, M. L. Jiménez, F. Liu, M. Wagterveld, and Á. V. Delgado, "Effect of solution composition on the energy production by capacitive mixing in membrane-electrode assembly," *J. Phys. Chem. C*, vol. 118, no. 29, pp. 15590–15599, 2014.